POLITECNICO DI MILANO

School of Industrial and Information Engineering

Aerospace Science and Technologies Department

Master Degree in Aeronautical Engineering

An Experimental Study of the Interactions with Low-Frequency Instabilities in Hall Thrusters

Academic Supervisor: Prof. Luigi T. DE LUCA (Politecnico di Milano)

Experimental Supervisor: Prof. Mark A. CAPPELLI (Stanford University)

Thesis of:

Fabio RIGHETTI 781989

Academic Year 2013 – 2014
December

Ai miei Nonni
(To my Grandparents)

A planet is the cradle of mind, but one cannot live in a cradle forever.
Il pianeta è la culla della mente, ma non si può vivere eternamente in una culla.
"Планета есть колыбель разума, но нельзя вечно жить в колыбели"
Konstantin E. Tsiolkovsky, Letter written in 1911

Author Note

The author would like to apologize for the poor English used to write this thesis. Hopefully the rather high number of pictures presented will help the reader to better understand some of the parts that would require a higher writing capability to be properly described.

Furthermore, the acknowledgments of this thesis are remarkably vast; for this reason it was chosen to place them at the very end of the document.

Abstract

Abstract (English Version)

Hall Thrusters oscillations have been studied for a long time. The complex dynamics of the plasma formed and accelerated by these devices makes numerical simulations not easy and the physical interpretation of the observed behavior during experiments is still not fully satisfying. More recent is the attempt to interact with the so called low frequency instabilities, characterized by frequencies in the range of tens of kHz; eventually the partial or total dampening of these oscillations throughout active systems is pursued. This thesis aims to expand the interaction capability with low frequency oscillations by the modulation of the magnetic field used in Hall thrusters throughout a different system architecture compared to the previous ones used in past studies. A prototype of the system is thus conceived, described and built; data aquired during a preliminary experimental testing process are then discussed. Two different thrusters and three cathodes have been used during the laboratory experience. While numerous open loop interaction phenomena have been observed proving a successful result for a non ordinary system architecture, the instabilities control performances of the closed loop configuration are still unsatisfactory. It is thus confirmed that the presented interaction strategy is, at least at this date, too complex and not understood enough to be successfully applied for control purpose. On the other hand, the open loop interaction could definitely bring new insight on the dynamics of Hall thrusters. In appendix A the refurbishment and improvement of a modern hollow cathode is reported. The rebuilt cathode opens the possibility of using an existing higher power laboratory Hall Thruster designed to run on Nitrogen, allowing in this way the testing of the described system on this kind of device and other experimental studies as well.

Keywords:
Electric Propulsion, Hall Thruster, Plasma, Magnetic Field Modulation, Hollow Cathode.

Sommario (Italian Version)

I fenomeni oscillatori presenti negli Hall Thruster sono da lungo tempo oggetto di studio. La loro simulazione e l'interpretazione fisica di ciò che viene sperimentalmente osservato è, in alcuni casi, ancora non del tutto soddisfacente a causa della complessa dinamica del plasma presente all'interno di tali propulsori. Più recente è invece il tentativo di interagire con le instabilità aventi frequenze nell'ordine delle decine di kHz, dette instabilità di bassa frequenza, ed eventualmente rimuoverle, o quantomeno attenuarle, attraverso sistemi attivi. Questa tesi vuole estendere attuali le potenzialità d'interazione con tali fenomeni oscillatori attraverso la modulazione del campo magnetico presente nei propulsori ad effetto Hall utilizzando una diversa architettura rispetto alle precedenti. Viene quindi concepito, descritto e realizzato un prototipo di tale sistema che dimostrerà, in parte, la desiderata interazione col propulsore. Segue quindi l'analisi dei dati ottenuti da una preliminare indagine sperimentale condotta su due propulsori Hall affiancati da tre diversi catodi. Nonostante siano numerosi i fenomeni osservati nella configurazione ad anello aperto, i risultati relativi al controllo in anello chiuso delle instabilità descritte restano ancora fortemente limitati. Ciò conferma come tale strategia d'interazione risulti, almeno ad oggi, troppo complessa e non sufficientemente analizzata da un punto di vista teorico, per permetterne una vincente applicazione nello smorzamento attivo delle instabilità di plasma e propulsore. La dimostrata capacità di interazione in anello aperto offre invece una preziosa fonte di nuovi dati sperimentali, la cui analisi potrebbe fornire nuova luce sulla dinamica dei propulsori Hall. In appendice A si descrive il processo di ricondizionamento e miglioramento di un moderno catodo cavo di media potenza che consentirà di utilizzare un esistente propulsore da laboratorio di potenza superiore ed alimentato con propellente non convenzionale, l'azoto, offrendo quindi la possibilità di testare il sistema di interazione sviluppato su tale dispositivo, così come l'opportunità di svolgere altri tipi di indagini sperimentali.

Parole chiave:
Propulsione Elettrica, Hall thruster, Plasma, Modulazione di Campo Magnetico, Catodo cavo.

Contents

Nomenclature

v_{exit}	Propellant exit speed
m_{prop}	Propellant mass on board
m_{dry}	Spacecraft mass without propellant
m_{inert}	Spacecraft mass without propellant and payload
I_{sp}	Specific impulse
T	Thrust
g	Gravitational acceleration
$\boldsymbol{v}$	Particle velocity
e	Elementary charge
$\boldsymbol{F_L}$	Lorentz force
$\boldsymbol{v_{Hall}}$	Electron drift velocity
Z	Atomic specie
μ_0	Vacuum magnetic permeability
μ_r	Relative magnetic permeability
μ	Absolute magnetic permeability
$\boldsymbol{E}$	Electric field
$\boldsymbol{B}$	Magnetic induction field
r_g	Particle gyroradius
q	Particle charge
M_{ion}	Ion mass
V_{acc}	Acceleration Potential
P	Electrical power

n_i	Ion number
n_n	Neutral number
ir	Ionization rate
f	Frequency
L_{iz}	Ionization length
T_e	Electron temperature
Z_i	Ionization number
k_b	Boltzmann constant
T_n	Neutral temperature
η	Efficiency
Ω_i	Current fraction of the *ith*-specie
$\dot{m}$	Mass flow rate
V	Voltage
I	Current
H	Magnetic field
j	Imaginary unit
δ	Loss angle
A	Cross sectional area
ω	Angular velocity
R_m	Magnetic Reluctance
Φ	Magnetic flux
N	Winding turns number
δ_s	Skin depth parameter
ρ	Material resistivity
$\boldsymbol{Z}$	Complex impedance
R	Electrical resistance
Θ	Phase angle
L	Inductance
X	Reactance
C	Capacitance

List of Figures

Estratto della Tesi (Italian language Summary)

Capitolo 1

Introduzione

Il futuro dell'esplorazione spaziale, sia essa intesa con equipaggio umano o senza, risiede senza alcun dubbio nel connubio tra propulsione elettrica ed energia nucleare. La propulsione chimica risulta infatti inadeguata per missioni di lunga durata in cui un elevato livello di ΔV è richiesto; i propulsori al plasma, d'altro canto, pur facendo modestissimo uso di propellente, richiedono un enorme quantitativo di potenza quando un buon livello di spinta è necessario. Una delle più promettenti tecnologie propulsive che soddisfa tali requisiti è costituita dai motori ad effetto Hall, detti *Hall Thruster*. Questi motori ripongono la loro fonte di spinta nell'accelerazione di gas ionizzati attraverso un campo elettrico prodotto grazie all'intrappolamento di elettroni in un campo magnetico opportunamente sagomato, raggiungendo impulsi specifici e durata della vita operativa superiori ai più diffusi motori a ioni. Nonostante questi propulsori abbiano raggiunto uno sviluppo tecnologico sufficiente da consentire un loro impiego nella propulsione di satelliti, la realizzazione di motori capaci di accelerare grossi veicoli spaziali risulta ancora non del tutto accessibile e ancora più incompiuto è il tentativo di acquisire una profonda conoscenza e comprensione dei complessi fenomeni fisici che avvengono all'interno ti tali propulsori. In questa tesi l'attenzione viene posta su uno dei più studiati aspetti che caratterizzano i motori Hall: i moti oscillatori presenti nel propulsore. In particolare si prendono in considerazione le più basse frequenze a cui tali fenomeni hanno luogo e si persegue uno sviluppo fortemente sperimentale di un sistema capace di interagire con tali moti oscillatori agendo sul campo magnetico del motore. Si cerca così di superare alcuni limiti tecnologici incontrati in precedenti applicazioni, verificando la fattibilità di interagire con le fluttuazioni tipiche del plasma generato in questo tipo di propulsori, senza tuttavia ottenere una tangibile capacità di controllo delle stesse, lasciando

intravedere la scarsa e probabilmente non soddisfacente comprensione della fisica alla base dell'opportunità di controllare tali fenomeni attraverso un'opportuna azione tempovariante sul campo magnetico del motore stesso.

Capitolo 2

Oscillazioni a bassa frequenza e strategie d'interazioni negli HET

Questo capitolo non pretende di presentare un'esaustiva panoramica delle oscillazioni tipicamente presenti nei motori Hall, né tantomeno di approfondire la fisica alla base delle fluttuazioni a bassa frequenza, caratterizzate cioè da una frequenza di qualche kHz. S'intende invece presentare una qualitativa descrizione di alcuni di questi fenomeni, con particolare riferimento ad uno dei più intuitivamente accessibili tra essi e che risulta essere, senza alcun dubbio, il cosiddetto *Breathing Mode,* così chiamato a seguito della somiglianza con un fenomeno di inspirazione di gas neutro ed espirazione di plasma da parte del motore stesso. Tale fenomeno risulta essere ben descritto da un modello matematico predatore-preda *(predator-prey)* in cui gli attori sono rappresentati per l'appunto dagli atomi neutri del propellente in ingresso nel canale del propulsore e dagli ioni da essi derivanti, i quali sono poi accelerati ed espulsi a diversi *km/s* dai campi presenti nel motore stesso. Di tale fenomeno si forniscono le equazioni basilari che consentono di costruire modelli numerici relativamente semplici fino a più complesse simulazioni tridimensionali che includono dettagliate dinamiche di ioni ed elettroni presenti nel plasma. In questo capitolo sono inoltre introdotte le due più studiate tipologie d'interazione con i fenomeni oscillatori a bassa frequenza sopra descritti, le quali hanno visto negli anni scorsi una vivace attività di ricerca. Una parte del capitolo è, infatti, dedicata all'interazione e al controllo delle oscillazioni presenti nel plasma e nella corrente di scarica dei propulsori Hall attraverso la modulazione della corrente di scarica stessa, metodica che ha raggiunto un discreto livello di sviluppo grazie all'accurata realizzazione di veloci ed efficaci circuiti elettronici non del tutto diversi da quelli incontrati nei moderni alimentatori, spesso utilizzati nei laboratori di ricerca. La rimanente frazione del capitolo qua descritto è invece dedicata alla presentazione dell'interazione tramite modulazione dei campi magnetici presenti nei motori studiati. Quest'ultima è la strategia scelta per la realizzazione del sistema presentato in questo lavoro di tesi; tale interazione è basata sui numerosi effetti fisici che il campo magnetico produce sulle particelle cariche all'interno del canale del motore ed in particolare in prossimità della sue regione d'uscita.

Capitolo 3

Miglioramento dell'interazione attraverso modulazione del campo magnetico

Si sceglie in questa tesi di approfondire in particolare una di queste modalità d'interazione con i tipici fenomeni oscillatori presenti nei propulsori Hall, la quale fa affidamento sull'opportuna modulazione del campo magnetico necessario al funzionamento di questi motori, cercando di risolvere alcuni degli evidenti limiti attualmente incontrati in questo tipo di applicazione. Sono quindi proposte due architetture per realizzare quanto prima esposto. La prima soluzione tecnica presentata consiste nella riprogettazione dell'intero circuito magnetico con materiali adeguati alla necessità di modulare il campo magnetico, da essi trasportato, a frequenze aventi pari ordine di grandezza di quelle caratteristiche dei moti oscillatori stessi. La seconda architettura prevede invece lo sviluppo di solenoidi ausiliari, privi di nucleo ferromagnetico ed integrati nell'esistente struttura del motore Hall, finalizzati all'interazione con i fenomeni oscillatori sopra descritti e perciò dedicati alla sola modulazione del campo magnetico. Dopo una preliminare analisi tecnico-commerciale si seleziona la seconda come unico possibile candidato per la pratica realizzazione del sistema considerando i vincoli di costo e tempo intrinseci nello sviluppo di questa tesi. Si descrivono quindi più in dettaglio le desiderate caratteristiche di tali solenoidi che evidenziano come l'utilizzo dei tradizionali elettromagneti e relativo circuito magnetico dei propulsori Hall sia lontano dall'ottimale realizzazione di un tale sistema. Una preliminare ma curata sintesi di due diversi modelli di solenoide è descritta sia nelle sue componenti di carattere strettamente pratico sia nella simulazione del campo prodotto con successiva verifica sperimentale. Parte delle differenze presenti tra le due diverse scelte progettuali risulteranno più chiare a seguito della lettura del capitolo successivo, il quarto, riguardante il sottosistema di alimentazione.

Capitolo 4

Realizzazione del sistema di alimentazione per i solenoidi; acquisizione e processamento dei dati

Una volta definiti i principali parametri dei solenoidi che ricoprono il ruolo di attuatori nel sistema di interazione sviluppato e verificata la loro effettiva

impedenza con un *RLC meter*, sono affrontate e discusse in questo capitolo le non banali problematiche associate al sottosistema di alimentazione dei solenoidi stessi. E' infatti richiesto un sistema di alimentazione capace di pilotare carichi induttivi operando in una banda di frequenza del tutto paragonabile con quella utilizzata in applicazioni audio (*20 - 20000 Hz*). Si tenta la sintesi di una rete di *matching*. Dopo una preliminare analisi tale soluzione viene abbandonata a causa della difficoltà di ottenere una banda di frequenze sufficientemente ampia in cui si ottiene effettivamente il fenomeno di *matching*. La necessità inoltre di lavorare con segnali di forma arbitraria, in modo da lasciare aperta la possibilità di un più mirato tentativo di controllo in retroazione delle oscillazione stesse, impone tempi caratteristici dei circuiti presenti nel sistema di alimentazione sufficientemente corti. Un'ulteriore ricerca in letteratura consente di scoprire come un sorprendentemente simile problema è studiato nell'ambito delle applicazioni mediche della risonanza magnetica *(MRI Magnetic Resonance Imaging)*. In tale ambito sono impiegati particolari alimentatori detti *Gradient Amplifier* di cui è fornita una breve e sommaria descrizione. A causa degli elevati costi e della relativa scarsa flessibilità di tali macchine si sceglie di utilizzare un più comune alimentatore capace di amplificare segnali di forma arbitraria, purchè con componenti in frequenza all'interno della banda passante dell'alimentatore stesso, e capace di interfacciarsi con carichi induttivi: un potente amplificatore audio. Si apprende infatti come alcuni di questi alimentatori siano i precursori dei *Gradient Amplifier* e ne approssimino quindi le caratteristiche ricercate. L'acquisizione di alcuni segnali è auspicabile per il monitoraggio del motore durante il suo funzionamento e senza dubbio necessaria per il funzionamento del sistema sviluppato. La medesima banda passante richiesta al sistema di alimentazione è chiaramente necessaria nel sistema di acquisizione e processamento dati. Dopo un iniziale tentativo di realizzazione di un'interfaccia *LabVIEW*, a fronte della non banalità di processare in tempo reale un segnale alle frequenze di interesse (*10 kHz* almeno, considerato il contributo delle armoniche del segnale), si opta per utilizzare un sofisticato oscilloscopio affiancato da una serie di circuiti analogici, parte dei quali commerciali e parte realizzati per l'occasione. Componenti fondamentali di questo sistema sono: gli amplificatori differenziali necessari per la lettura delle oscillazioni nella corrente di scarica del motore, alcuni amplificatori di segnale, un circuito attivo capace di generare in tempo reale la derivata di un segnale in ingresso ed infine l'amplificatore audio precedentemente nominato al cui output è posizionata una *Pearson Probe* utilizzata per controllare l'effettiva forma d'onda in uscita dalla catena descritta. Un generatore di segnali è utilizzato per gli esperimenti in anello aperto. Una sonda di Faraday è inoltre installata e collegata ad un *picoammeter*, e quindi all'oscilloscopio, così da poter campionare una parte della corrente ionica del propulsore.

Capitolo 5

Verifica sperimentale

All'interno di questo capitolo viene descritta l'intera parte applicativa e sperimentale del progetto di tesi che ha occupato la gran parte del tempo necessario per il completamento della tesi stessa. Questa esperienza di laboratorio e con essa tutti i test effettuati sono stati concepiti e condotti presso il laboratorio di fisica dei plasmi dell'Università di Stanford (SPPL, Stanford Plasma Physics Lab) sotto la guida del Professor Mark A. Cappelli. Entrambe le camere a vuoto del laboratorio hanno ospitato le indagini sperimentali; due motori ad effetto Hall e tre catodi sono stati utilizzati. Il primo motore è un Hall thruster anulare da laboratorio con potenza nell'ordine di circa 500W, mentre il secondo è un Hall thruster cilindrico ricostruito e modificato dall'autore e presenta potenza inferiore, dell'ordine del centinaio di watt. I catodi utilizzati sono tangibilmente diversi tra loro: due sono catodi commerciali, un Ion Tech da laboratorio e un *Busek* qualificato spazio, mentre il terzo è un catodo con *emitter* in *Lanthanum Hexaboride* (LaB6), è stato realizzato presso *l'Air Force Institute of Technology*, revisionato e parzialmente modificato dall'autore. Numerosi test sono stati effettuati sia sui motori sopra citati per portarli in uno stato di buon funzionamento, sia, in particolare, sul sistema di interazione con le instabilità di bassa frequenza descritto nei precedenti capitoli. Il motore Z-70 è stato utilizzato abbinato al catodo *Ion Tech* nella primissima fase del progetto. Il CHTr è stato invece utilizzato sia in abbinamento al revisionato catodo con inserto in LaB6, con alimentazione ad argon, presentando oscillazioni a frequenza al di fuori del range operativo dell'amplificatore in dotazione, sia con il catodo Busek ancora con argon ed infine con xenon. Proprio l'ultima configurazione è stata utilizzata sia per i test preliminari dell'intero sistema sia per quelli più avanzati, compreso l'utilizzo di una sonda di Faraday. Una buona capacità di interazione tra motore e sistema è stata riscontrata mostrando la curiosa capacità di poter modificare in parte la frequenza naturale delle oscillazioni del propulsore, così come la possibilità di alterarne la forma d'onda. Tenuto conto di questo interessante fenomeno, sono stati condotti ulteriori test con il tentativo di retro azionare a ciclo chiuso il motore in modo da indagare le possibilità di controllo delle instabilità in esso presenti. La bobina descritta nel capitolo tre, realizzata ed integrata nel motore è stata inizialmente utilizzata in modalità di sensore, come se essa fosse un'antenna, anziché di attuatore, scoprendo così che il segnale catturato rappresentava la derivata della corrente di scarica, come in parte prevedibile. Si è quindi deciso di costruire un circuito per generare tale derivata una volta acquisita la corrente di scarica stessa, per poi amplificarla ed utilizzarla come segnale di eccitazione per il solenoide tornato adesso in configurazione di attuatore. Polarità invariata ed invertita di tale

segnale sono state testate mostrando un diverso effetto sulla corrente di scarica del motore, senza però fornire evidente prova del desiderato effetto di controllo che poteva essere invece prevedibile a livello teorico ed intuitivo. Numerosi sono quindi gli spunti per successive indagini. Una più accurata descrizione teorica dell'interazione tra instabilità e campi magnetici variabili è desiderabile al fine di meglio interpretare i risultati sperimentali ottenuti. Allo stesso tempo una diversa configurazione delle bobine di attuazione merita essere oggetto di studio così come l'aggiunta di ulteriore grado di liberta nella catena di processamento del segnale: un generatore di ritardo che consentirebbe il controllo della fase tra il segnale di controllo delle bobine e la corrente di scarica del motore. Una più sofisticata diagnostica risolta nel tempo potrebbe poi meglio illustrare la relazione tra il comportamento del plasma accelerato dal motore e l'input negli attuatori stessi. Con tali dati sarebbe possibile inoltre generare una funzione di trasferimento dalla notevole utilità nell'abito della simulazione numerica del motore collegato al sistema di interazione sviluppato. Proseguire con lo sviluppo del circuito magnetico del motore completamente rivisitato con materiali adeguati a trasportare campi magnetici rapidamente variabili nel tempo porterebbe certamente ad interessanti risultati, una volte risolte le minori problematiche tecniche e quelle economiche relative a tale strategia. Allontanandosi ulteriormente dalla strada seguita in questo lavoro, l'autore reputa promettente una terza possibilità di interazione con le oscillazioni a bassa frequenza: la modulazione sulla linea di alimentazione del propellente. Ciò permetterebbe il controllo della quantità di atomi neutri iniettati nel canale del motore con tutte le relative conseguenze sulla dinamica predatore-preda descritta in precedenza.

Capitolo 6

Conclusioni

A seguito di un'estesa ricerca in letteratura sulle presenti strategie di interazione con le instabilità di bassa frequenza, caratteristiche delle instabilità incontrate nei propulsori ad effetto Hall, si è intrapresa la realizzazione di un sistema di modulazione del campo magnetico imprescindibilmente presente in questo tipo di motori. Dopo aver analizzato due diverse possibili configurazioni capaci, almeno in teoria, di ottenere quanto descritto, si è deciso di realizzare tale effetto modulante mediante un solenoide, senza nucleo metallico, dedicato a questo specifico scopo. Dopo una preliminare realizzazione di tale tipologia di attuatore su di un Hall thruster anulare, l'attenzione è stata posta su una più curata e completa architettura sviluppata attorno ad un Hall thruster cilindrico revisionato e modificato per l'occasione. Tre diversi catodi sono stati utilizzati,

di cui uno revisionato e anch'esso modificato durante le prove sperimentali e due propellenti gassosi, argon e xenon, hanno trovato impiego durante i numerosi test in camera a vuoto. Particolare interesse ha suscitato lo sviluppo del sistema di alimentazione che ha visto l'utilizzo di un amplificatore audio così come di alcuni circuiti elettronici realizzati per l'occasione. L'analisi dei dati ottenuti, alcuni dei quali raccolti tramite l'ausilio di una sonda di Faraday, permette di mostrare chiaramente come un'interessante interazione tra propulsore, plasma e sistema realizzato consenta di agire su alcuni parametri caratteristici delle oscillazioni studiate, in particolare frequenza, ampiezza e forma d'onda. Una nuova analisi riguardante un preliminare test svolto con il sistema in configurazione di retroazione ad anello chiuso mostra anche in questo caso una curiosa capacità di modificare la forma delle fluttuazioni, ma, nel contempo, una scarsa inclinazione al controllo ed allo smorzamento delle stesse. Ciò, oltre a lasciar pensare che il background teorico in materia sia ancora troppo acerbo per prevedere correttamente una simile interazione, lascia aperta la porta per numerose ulteriori indagini sperimentali sul sistema sviluppato.

Appendice A

Ricondizionamento del catodo cavo

Un esistente catodo cavo con inserto in *Lanthanum Hexaboride* (LaB6) è stato ricondizionato ed in parte modificato. In questa sezione viene brevemente descritto tale processo. Tale catodo, oltre ad essere necessario per l'utilizzo di motori di più alta potenza in alcuni test con propellenti meno nobili, come ad esempio azoto, presenta l'impagabile vantaggio di essere quasi immune dai problemi di avvelenamento da ossigeno o altre sostanze a cui sono invece tanto sensibili i catodi con inserto impregnato di ossido di bario. Il ricondizionamento ha permesso una totale pulizia del dispositivo: in particolare, è stato rimosso mediante leggera sabbiatura lo strato di materiale metallico depositato sulle parti ceramiche facendo così venire a mancare la loro funzione di isolante elettrico; una nuova guarnizione in grafoil è stata inoltre introdotta. Il più rilevante cambiamento nella configurazione del catodo è però sicuramente l'introduzione di un nuovo elemento riscaldante realizzato seguendo una differente tecnica rispetto al precedente. L'esistente e danneggiato filamento riscaldante realizzato con struttura coassiale in tantalo con strato intermedio in allumina offriva un rapporto qualità prezzo non vantaggioso oltre a presentare un notevole rischio di rottura in fase di ordinaria manutenzione ed installazione su motori in allestimento per sessioni di prove in camera a vuoto. Il nuovo filamento riscaldante è realizzato con un singolo filo in tantalo inserito in decine di

cilindretti in allumina che presentano bordi svasati consentendo al componente così assemblato di assumere una forma curvilinea, essenziale per avvolgere il filo sul corpo cilindrico del catodo stesso. Entrambi gli estremi del filamento sono poi portati all'esterno del corpo del catodo consentendo il collegamento con il relativo alimentatore. Tale scelta differisce dalla precedente che prevedeva un solo estremo dell'elemento riscaldante all'esterno del catodo, essendo il ritorno della corrente di alimentazione affidato al corpo centrale del catodo collegato elettricamente al filo riscaldante esclusivamente attraverso contatto garantito dalla componente elastica della deformazione imposta all'avvolgimento una volta spinto al suo interno il corpo centrale del catodo stesso. Durante una delle numerose prove sperimentali il contenitore ed elettrodo esterno del catodo, il *keeper,* è stato danneggiato. Si descrive quindi brevemente anche il processo di lavorazione meccanica che ha consentito di ricostruire l'elemento mantenendo la scelta della grafite come materiale ma aumentando lo spessore delle sue pareti.

Chapter 1

Introduction

1.1 Hall Effect Thrusters

Hall Effect Thrusters (HET) are one of the most successful architectures among the vast category of Electric Propulsion (EP). Developed in the sixties, these devices are becoming more and more popular in station keeping applications after the extensive utilization on Russian spacecraft starting in 1971 [13], in particular after the successful Stationary Plasma Thruster (SPT) series of thruster. After this successful campaign, the United States, which in the meantime focused on ion engines, invested a big effort in HET as well, culminating with the launch of their first thruster, built by Busek, in 2006 [14]. Aboard Earth-orbiting satellites, a propulsion system is indeed necessary to allow for orbital maneuvering and station keeping. In geostationary satellites, ever more precise station keeping is desired to enable a high number of satellites occupying the geostationary without risk of a collision. EP, specifically Hall thrusters, provides a low-thrust and very efficient solution to satisfy the needs of Earth-orbiting satellites. They are suited for orbit transfer mission as well, offering a big propellant mass saving compared to traditional chemical rockets. These thrusters are coaxial plasma accelerators, also called closed drift thrusters, indeed, despite the number of different configurations, an azimuthal drift of electrons is common. Plasma thrusters accelerates an expellant to a v_{exit} speed to produce thrust accordingly the Tsiolkovsky equation, that relates the desired velocity increment ΔV with the already mentioned speed velocity of the jet, the mass of the spacecraft m_{dry} and the mass of the propellant m_{prop} needed to generate the required acceleration:

$$\Delta V = v_{exit}\, ln\left(1 + \frac{m_{prop}}{m_{dry}}\right)$$

where:

$$m_{dry} = m_{inert} + m_{payload}$$

It is easy to understand that in order to have a fuel saving propulsive unit, the accelerated gas should have a very high speed being this the only parameter one can control recalling that the ratio between dry and propellant mass can't assume arbitrary values due to technological reason. High exhaust speeds indeed exponentially decrease the propellant needs. Great effort is being also used to reduce the inert mass of the PPU (Power Processing Unit) necessary for electric propulsion in which the power system is usually a big fraction of the inert mass. In order to achieve such a high specific impulse, HET first ionize a neutral gas (most typically xenon) creating a plasma, which is then accelerated to very high speed, in the order of tens of kilometers per second. A useful index used to classify space propulsion devices is the Specific Impulse that is define as the ratio of thrust to the rate of propellant flow multiplied by the magnitude of the acceleration due to gravity, having then the unit of seconds:

$$I_{sp} = \frac{T}{\dot{m}_{prop} g} = \frac{\dot{m}_{prop} v_{exit}}{\dot{m}_{prop} g} = \frac{v_{exit}}{g}$$

Typical values of specific impulse in electric propulsion systems are:

Engine	Thrust, mN	I_s, s	η_t, %	Propellant	Power, kW
resistojet	$100 - 500$	$200 - 350$	$65 - 90$	H_2, CH_4, NH_3, N_2H_4	$0.5 - 1.5$
arcjet	$200 - 2,000$	$400 - 2000$	$30 - 50$	H_2, N_2, NH_3, N_2H_4	$0.3 - 100$
ion thruster	$0.01 - 200$	$1500 - 5000$	$60 - 80^b$	Xe, Ar, Kr	$0.5 - 2.5$
Hall thruster	$0.01 - 200$	$2000 - 5000$	$30 - 50$	Xe, Ar	$1.5 - 5$
MPD thruster	$0.01 - 20,000$	$2000 - 5000$	$25 - 50$	Xe, Ar, H_2, Li	$1 - 4000$
PPT thruster	$0.05 - 100$	$600 - 2000$	$5 - 10$	$Teflon$	$0.001 - 0.2$
monoprop.[a]	$30 - 100,000$	$200 - 250$	$87 - 97$	N_2H_4	==

[a] included only for comparison.

Figure 1.1: *Main performance parameters of the existing electric propulsive technologies [23].*

The idea of accelerating ion to generate thrust goes back to one hundred years ago when Tsiolkovsky [11] and Goddard [12] proposed this technique. A variety of electric thruster exists. In HET a unique configuration of magnetic and electric field is used in order to achieve such a high velocity of the expellant: a virtual grid negatively charged is created trapping electrons in a crossed electric and magnetic field, creating the Hall current from which the thruster gets his

name. This layer of drifting electrons creates a strong electric field between the exit plane of the thruster and the anode, positioned at the back of the thruster. Basically a spatial E-field is used for ion acceleration and a magnetic field B is used to generate the E-field structure itself (i.e., the virtual grid formed by trapped electrons) and for suppression of electron current generated by the cathode [8]. The Lorentz force

$$\boldsymbol{F_L} = -e\boldsymbol{v} \times \boldsymbol{B}$$

generated on the electrons prevents them from quickly crossing the ionization zone of the thruster, creating indeed a drifting force that, at regime, produces a theoretically steady Hall current drifting at a velocity

$$\boldsymbol{v_{Hall}} = \frac{\boldsymbol{E} \times \boldsymbol{B}}{B^2}$$

After some time the electrons leave the region due to collisional diffusion and fluctuation of the fields. The detailed mechanism of electron transfer across the magnetic field is 50 years later is still in study, being the experimental conductivity typically higher than the theoretically and numerically predicted one. The resulting Hall current is the main ionization mechanism that creates plasma by means of anelastic collisions of electrons with the neutral gas that is injected into the channel.

$$Z + e \leftrightarrow Z^+ + 2e$$

Typical Hall thruster schematics follows, showing the described architecture.

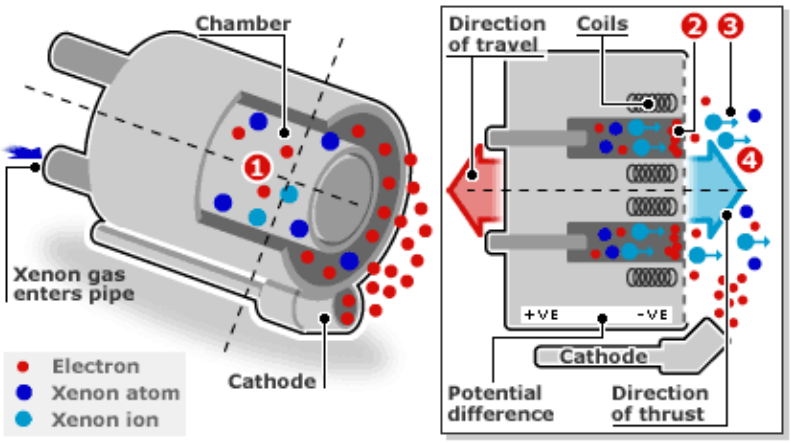

Figure 1.2: *Schematic of an annular Hall Thruster [56].*

Ions experience a force as well while crossing the B field but this effect can be neglected considering that the gyro radius of these kind of particles is much larger compared to the characteristic dimension of the thruster accordingly to this relation:

$$r_g = \frac{m_{vperp}}{qB}$$

where v_{perp} is the velocity perpendicular to the magnetic field B, m is the particles mass, and q is the particle charge. Computing the gyro radius for both electron and ions show how the former is in the order of millimeters and the latter is in the order of meters. The absence of a physical acceleration grid is clearly an advantage compared to the Ion Thruster architecture where its erosion is the main lifetime-limiting factor. Erosion of the walls and cathode are in any case a delicate aspect in the HET [7] but, even if new electrode-less propulsion devices have been proposed [1], to date they still remain at a laboratory research stage. A very interesting feature of HET is also the relative flexibility on the expellant choice: even if xenon is doubtless the most used gas having very low ionization potential, 12.13 eV, and a high mass, other substances may be used. Hall Thrusters running on Argon, Krypton, Iodine, Bismuth, Zinc, Magnesium and other substances have been successfully tested including common very common expellant such as Nitrogen and even Air opening promising applications for the so-called In Situ Resources Utilization (ISRU) [23]. A limiting factor of this class of thruster can be outlined considering the limited typical anode voltages on HET that result in an exit velocity on the order of 30 km/s as already discussed; this value may be not high enough in future application with high Delta V requirements as Interplanetary Missions; in order to achieve higher Isp, an higher anode voltage should be applied requiring as a consequence higher power level obtainable exclusively with nuclear reactors. The developed thrust can be estimated in a very ideal approach using the relation

$$T = I_{ion}\sqrt{\frac{2M_{ion}}{q}V_{acc}}$$

where I_{ion} is the ion current of the beam, M_{ion} the mass of the ion created during the ionization process, q its charge and V_{acc} the acceleration potential that is part of the anode potential. Typical values of the thrust are in the order of mN, though thrusts as high as a few Newtons have been demonstrated by an increasing number of high power Hall thruster [62, 64, 65]. Increasing the efficiency can of course result in a higher thrust, once specific impulse and available power are selected, as shown by the relation:

$$P = \frac{g I_{sp} T}{2\eta}$$

Of course the required power has to be delivered to the thruster from the power system of the spacecraft. Even if solar power has been proposed as a possible source [61, 63], the final hope for future long distance manned missions is placed in the nuclear energy.

1.2 Thesis Overview

This thesis is organized in the following structure. In Chapter 2 a brief introduction to the complex physics of low frequency instabilities in Hall thruster is presented. In the same chapter the most common interaction methods are discussed. Chapter 3 focuses on the description of the technical solutions proposed by the author to partially overcome some of the actual technological limits that restrict the magnetic field modulation from being more widely studied. In the next chapter, Chapter 4, the challenges related to the actuators power system design are discussed. Moreover, on the basis of the theoretical guidelines and measured parameters, the final arrangement is presented. The signal processing system is outlined among with the diagnostics used in the experimental campaign. The laboratory testing of the system is proposed in Chapter 5 and the experimental results are discussed. Finally, some conclusions are summarized in chapter 6. In Appendix A hollow cathodes are briefly described, the refurbishment and improvement process of a Lanthanum Hexaboride cathode is then explained; the testing phase follows.

This thesis has been entirely conducted at the Stanford Plasma Physics Laboratory (SPPL) of Stanford University, Stanford, CA, USA, under the supervision of Prof. Mark A. Cappelli.

Chapter 2

Low-Frequency instabilities in HET and interaction strategy

2.1 Introduction to low frequency oscillations and their origin

Even if mission planning is based on time averaged quantities, the plasma generated by the thrusters presents a definitely time varying nature. Plasma oscillations in a wide band of frequency ranging from 1kHz to GHz have been observed and studied [15, 59]. This chapter does not aim to a complete description of the huge variety of oscillatory phenomena that occurs in HET: the author will try to focus on the low frequency instabilities that are widely studied in this type of thrusters and, in particular, on oscillations that origin from a predator-prey model will be addressed. Many different physical mechanisms are the reasons behind such a huge variety of instabilities, some oscillatory modes are driven by gradients, drift-type instabilities, ionization instabilities, transit rime instabilities and many others resulting in a plasma rich in azimuthal and axial oscillations. Low frequency fluctuations occur in the 1-25 kHz frequency band depending on several parameters including the physical size of the thruster and the circuitry of the. Among the numerous low frequency modes it is possible to identify a rotating spoke mode, a gradient-induced azimuthal oscillation and the so-called breathing mode that is described more in detail in this paragraph. This mode, that is one of the lowest-frequency one but often the largest in the term of magnitude, is indeed ubiquitously in the operation of Hall thrusters and it is mainly driven by ionization instabilities; early Russian literature produced over twenty years ago referred to this mechanism with the name of “instability of location of the ionization zone” [60]. Even if the phenomenon is frequently studied without considering the external circuitry of the thruster, the described instability interacts with the power system forming a complex dynamic system. Several studies focused on this phenomenon revealing by the way that the fundamental physical cause behind the breathing

mode is the ionization instability associated with the irregular propagation of the ionization front in the discharge channel [27-31]. Interaction between such a longitudinal instability and the azimuthal ones has been considered in past studies as well. One of the most common mathematical descriptions relies on a predator-prey model analogy. Even if more complex models exist [30], a simpler zero-D model originally proposed by Fife [29] will be here considered; it can be written considering the conservation equations for neutrals and ions:

$$\frac{\partial n_n}{\partial t} = \frac{n_n v_n}{L} - n_i n_n ir$$

$$\frac{\partial n_i}{\partial t} = -\frac{n_i v_i}{L} + n_i n_n ir$$

where n_i is the ion population, n_n is the neutral population, v_i is the velocity of the ions, v_n is the velocity of the neutrals, L is the length of the ionization zone and ir is the ionization rate that can be modeled in various way with different complexity levels, being in general a function of electron temperature $ir \propto T_e^{1.5}$. In order to derive the first-order dynamic character of the nonlinear system, linear perturbation is taken,

$$n_i = n_{i,0} + \epsilon n_i'$$

$$n_n = n_{n,0} + \epsilon n_n'$$

Considering that $v_n \ll v_i$, and considering the first order of the perturbation it can be shown that the system dynamics can be described with the equation below:

$$\frac{\partial^2 n_i'}{\partial t^2} + ir^2 n_{i,0} n_{n,0} n_i' = 0$$

that represents an undumped harmonic oscillator with frequency

$$f = \frac{1}{2\pi}\frac{\sqrt{v_i v_n}}{L_{iz}}$$

where the ionization zone L_{iz} depends in turn on the ionization rate [66]. Neutrals velocity depends on the propellant that usually enters the thruster channel in a sonic condition, while ion velocity v_i can be modified selecting different discharge potential being, as in ion gridded thruster, a function of the discharge voltage:

$$v_n = \frac{1}{2}\sqrt{\frac{2k_bT_n}{\pi m_n}} \quad and \quad v_i = \sqrt{\frac{2Z_iq_iV_d}{m_i}}$$

where k_b is the Boltzman constant and Z_i is the ionization number of the ion specie having charge q_i. It can be thus noted the close similarity with the Lotka-Volterra (i.e.: predator-prey) model dynamics that describe the dynamic of the population cycles in closed two-species habitats. Inside the accelerator, indeed, neutrals are preys and ions are predators.

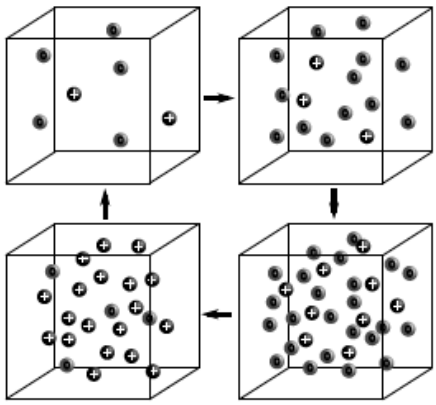

Figure 2.1: *Graphical representation oh the predator-pray cycle, adapted from [67].*

This relation reported above is found in a different description of the system as well, the so-called convective wave model [16]. The model previously described is however greatly simplified and doesn't take into account the variation of the parameters at different thruster conditions as well as a lot of physical phenomena that occur inside plasma and that are often driven by other instabilities mechanisms and the important role of the external circuitry [79]. In more sophisticated numerical simulation, the widening of the ion density distribution can be reproduced as well. As it can be seen be in the figure above, neutrals first fill up the channel resulting in a large population compared to the ion one. Once the neutrals reach the ionization zone, the situation become opposite: the vast majority of neutrals are now ionized by the Hall current. The next step is the acceleration of the new born ions due to the axial electric field inside the channel that is thus empty again and new neutrals will arrive, repeating in this way the cycle. Ionization rate is affected by this process as well: once the burst of ions is formed, the increased number of available electrons increases the ExB drift magnitude resulting in an enhanced ionization rate [68].

2.2 Interaction and control attempt motivation

The described oscillations can be observed as a variation in the intensity of the optical emission of the plasma and indirectly measured as a variation of the current flowing in the anode power supply circuit. Historically, the majority of the discharge current interaction studies in Hall thruster has been performed in order to develop a solid background that could eventually disclose the control capabilities necessary to damp the oscillations. Numerous motivations justify the effort of developing a control system for these fluctuations. In particular since the very first laboratory experiments on closed drift accelerators, it was observed that the regulation of these devices is possible by acting on three parameters: anode discharge voltage, gas mass flow rate and applied magnetic field. In order to obtain high thruster efficiency, no independent regulation of the three mentioned parameters is possible. Selecting indeed a value of the mass flow rate and a discharge voltage, it is possible to generate a function that relates the observed discharge current for different values of the applied magnetic field.

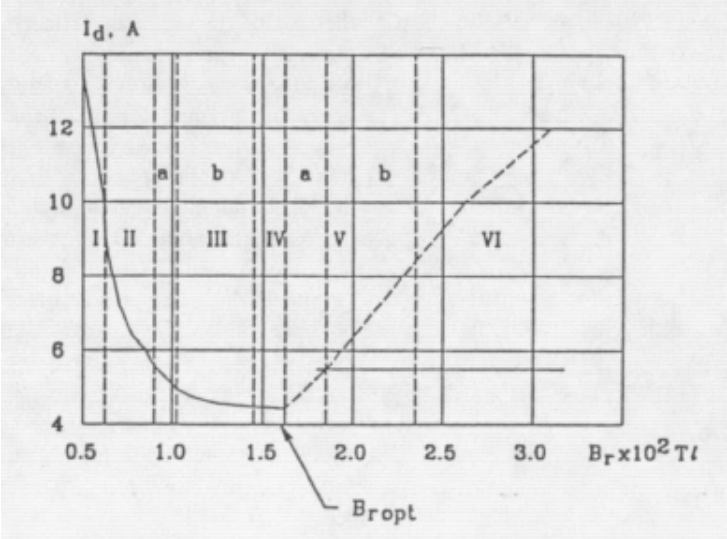

Figure 2.2: *Discharge current as a function of applied magnetic field [60].*

At the minimum of this curve, where the discharge current is at its lowest value, maximum thruster efficiency is reached; amplitude of the oscillations is minimized as well. Unfortunately, in practical application, the thruster is operated at a higher magnetic field because of the fast increase in the magnitude of the discharge current oscillations that occurs on the left branch of the curve compared to the smaller increase in the region of superoptimal magnetic field. A strong fluctuation of the current, besides generating power loss and operational issues in the power system, can disrupt the discharge forcing the thruster to shut

down. It is indeed known that usually higher electromagnets current decrease the risk to enter the minimum zone of the curve where a small perturbation toward the left side of the graph can push the thruster in the highly unstable left branch of the curve itself where the fluctuation in the discharge current can be high enough to shut down the thruster. Operating the thruster at higher B field is thus safer but of course less efficient since the enhanced azimuthal instabilities increase the electron transport resulting in a higher discharge current.
This is by the way not the only target of this research field. Interacting with the thruster means interact with the plasma as well allowing to further study its physics and the system behavior given by the coupling between of the thruster with the plasma itself. The dynamic of such a system can thus be studied more in detail creating a transfer function. A different application is more strictly correlated with laboratory experiments in which stable and regular oscillations are desirable in order to simply and further expand the implementation of some time synchronized diagnostic techniques [2]. An interaction system with the thruster could be used in this case to fine tuning the oscillation frequency or altering the shape of the signal allowing a wider range of studies. Collected data are a precious source of information that can be exploited to further develop numerical models that are, at this time, still unable to fully predict the plasma behavior because of the large number of coupled phenomena. The most attractive use for such a system remains by the way the reduction and damping of the low frequency oscillations that almost always affect the thruster operation. As mentioned above, developing the capability to control the longitudinal low frequency instabilities would allow to operate the thruster in the most efficient operational point without the shut off concern given by the high probability of entering the violent oscillation region. Furthermore, previous experiments [9] performed with a proprietary card by Busek developed to actively control of the magnetic field, even if not satisfactorily working yet, seems to improve the propellant utilization by 2%, being the propellant utilization efficiency defined by Linnel [21] as:

$$\eta_p = \frac{\dot{m}_\iota}{\dot{m}_a} = \frac{M_i I_b}{\dot{m}_a e} \sum_i \frac{\Omega_i}{Z_i}$$

where M_i is the mass of the ion, I_b is the integral beam current, $\dot{m}_a$ is the anode mass flow rate, Ω_i is the current fraction of the *ith* charge species, and Z_i is the charge state of the *ith* species. In any engineering endeavor, higher efficiency and performance are always attractive and this is even truer in the case of rocket propulsion. However depending on the mission profile overall efficiency is not necessary the most important parameter. Controlling the current oscillation requires of course power and this usually leads to a reduction of the magnet current efficiency defined as follow:

$$\eta_{magnet} = \frac{P_d}{P_{tot}} = \frac{1}{1 + \frac{P_{mag}}{P_d}}$$

where P_d is the discharge power, P_{mag} is the magnet power and P_{tot} is the total power [20]. This kind of application results thus attractive for big satellites in which power is not the main issue compared to the precious finite volume of propellant stored on board. Hopefully, next manned missions will be powered by nuclear reactors resulting, likely, in an excess of power as well. Interesting results are related to the plume morphology as well: past researches indicate that a reduction in the divergence angle of the plume is achievable when the oscillations of the discharge current are reduced. High power satellites would be thus able to take advantage of an increased propellant utilization efficiency paired with a reduced divergence angle having usually power in excess. Increased propellant utilization efficiency would allow the satellites to use less propellant for the same ΔV permitting a longer maneuvering lifetime. Oscillations in Hall Thrusters are associated to Electromagnetic Interference as well and a flat operation would be desirable reducing in this way interference with the onboard electronics. Big filters are usually realized and embedded into the PPU (Power Processing Unit) in order to prevent damages to the inner circuitry of the device. As better explained later, additional flexibility compared to this approach would definitely be desirable.
Furthermore past studies [10] indicates that oscillations might contribute to the erosion of the walls of the thruster and thus negatively impact lifetime; hopefully improving the ability of damping these instabilities could improve the lifetime of the thruster, that is right now one of the most limiting factor of electric thrusters. The strong oscillatory regime can be mitigated without using any feedback control by selecting an appropriate set of operating parameters. Feedback suppression adds by the way flexibility; it increases the parameter space in which the Hall thruster can stably operate or operate with higher efficiency. Future high power missions will require clustered propulsive system, where cross talk between each thruster is often an issue. Active interaction systems could reduce this undesired effect as explained in past research [45]. The first approach used to reduce the negative effect created by low frequency oscillations affecting power system relied on passive circuits acting as a filter, as briefly mentioned before. If correctly design a circuit can indeed have a cutoff frequency or, more in general a bandwidth, that prevents some of the frequency content of a signal to reach the device located before the filter itself. The most common filter is a RLC network in which a resistor, an inductor and a capacitor are properly chosen in order to prevent the described fluctuation generated by the thruster on the right reaching the power supply on the left.

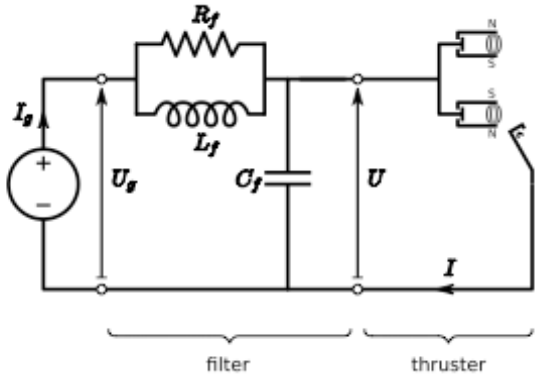

Figure 2.3: *Schematics of a passive filter implemented in HET applications [19].*

A somehow similar solution is adopted in some flight-qualified thruster in which the discharge current line (i.e.: the anode electrical line) is connected in series with the electromagnet of the thruster. Recent effort was put in improving the understanding of this configuration [71]. Indeed, it is still not totally clear if the beneficial effect is given by some sort of weak interaction with the resulting fluctuating magnetic field with the ionization zone, or if the effect is primarily given by the presence of the solenoids that act as a low pass filter. If not properly design indeed, solenoids present high impedance at high frequency as later explained in chapter 4, reducing in this way the AC amplitude of the signal. Of course such a system leaks of flexibility and changing in the oscillating frequency of the thruster will result in a different effect of the filter. The majority of components of the thruster and of its power system effects indeed the fluctuation of the plasma, in particular operating the thruster with different propellants will result in a shift of the frequency. Long-duration operation erosion of thruster component can impact on the nature of the oscillations as well [60] forcing to deal with non constant fluctuation parameters. Frequency of the fluctuation of the discharge current depends also on the expellant gas used, being the ionization length related to the ionization potential of the gas itself. Having the possibility to accelerate different gases is definitely a key feature in future electric propulsion systems that could in this way take advantage of gas produced in different locations (i.e.: in orbit, on a planet, on the moon etc.). The same thruster is then sometimes able to work in different operational point maintaining a fairly high efficient. They can be indeed configured to operate in high thrust mode for orbit maneuvers or high specific impulse mode for station keeping as showed on companies websites [35]. In a laboratory environment, where the setup of an experiment is usually changing really frequently, this is even more important. As mentioned in chapter 5, moving the cathode or simply changing his orientation with respect to the thruster results in a shift of the oscillation frequency. A completely different passive ways to interact and

possibly reduce the amplitude of the low frequency instabilities rely on geometrical adaptation of the thruster wall [31]. Also this solution is clearly not flexible and no extensive life time testing has been conducted.
Because of these reasons active systems are extremely attractive. Of course an active interaction and control system with the thruster and its plasma is much more complex compared to a passive one and the electronics needed to accomplish such a task is without any doubt in larger amount. In the future a larger use of electronics dedicated to the thruster will be considered in any case considering that a monitoring and auto repairing system would be highly desirable for long distance missions. Self-Check could be obtained with a set of gauges whose signals allow execution of prescribed algorithms. In this scenario, an active control system of oscillations seems to have good possibility to be easily integrated and maybe it could participates toward a possible system of self-renovation of the wearied elements as innovatively describes by one of the father of the Hall Thruster, A. Morozov and realized at a concept level many years ago [8].
Because of the numerous reasons mentioned above, active interaction and control strategies have been studied during the last twenty years along with a vigorous research conducted on fusion plasma where great success has been obtained by the use of active control. Numerous interaction strategies exist.

2.3 Active Interaction Strategies review

As explained in the previous section discharge current low frequency oscillations in Hall thruster might affect the power processing unit, shorten the operating life of the device, lower the specific impulse and efficiency and create electromagnetic compatibility with other satellite equipment present on board. A brief description of some of the existing interaction and control techniques implemented on Hall thrusters developed in the past twenty years of research is now provided. Different system architectures have been used involving different physical interaction mechanisms with the plasma. Some of them rely on the customization of the anode electrode in order to implement the modulation of the voltage on it as a function of the anode position allowing on some extent the control of a low frequency azimuthal oscillation: the already mentioned “rotating spoke”. The anode is in this case segmented in order to provide more complete information on the discharge current compared to the total current signal. At the same time this redesign allows to implement a passive control architecture that relies on series resistors connecting each segment of the anode and the power supply, generating, in this way, a voltage drop on the segment that correspond to the front of the azimuthal wave [84]. Past studies indicates great opportunities to interact with a vast class of instabilities using active

control by converting the anode of the thruster in an actuator in a similar way to the one previously mentioned [85].
A different strategy developed more specifically for breathing mode control considers the integration of an electronic control circuit in the anode line in order to directly modulate the discharge current. In this case, active interaction with plasma fluctuations is achieved through the modulation of the discharge current of the thruster. In order to do that, electronic circuits are connected with the anode power supply line; the complexity level of the state of the art of these devices can be rather high. They usually rely on a controller, most frequently a PID controller, and on some kind of fast actuator as a MOSFET. The principle is not different from the passive filters seen before, except that the flexibility is much higher considering that the gains choice is rather broad. A RLC filter can indeed be seen as a fixed gains PID controller:

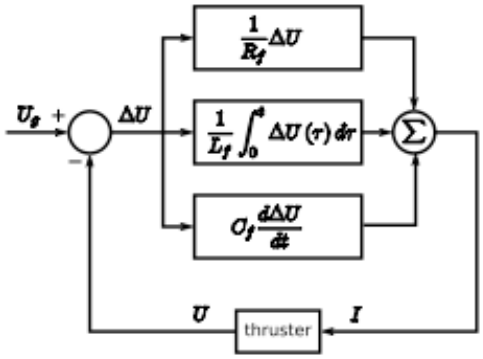

Figure 2.4: *Equivalent current control circuit block diagram [19].*

In the numerical model developed by the main investigator of this technique [70], a dependence of the ionization rate on the discharge voltage was included into the model in order to take into account the effect of the controller [72]. Dependence of the ionization rate *ir* on electron temperature has already been pointed out; considering now that electron temperature responds to changes in the local electric field, and thus in the anode potential V, it is possible to write:

$$\partial ir/_{\partial V} > 0$$

Recalling that plasma density n_i is proportional to the discharge current, as shown with the use of a Faraday probe in chapter 5, proportional control will thus increase the anode potential as soon as n_i decreases in order to increase the ionization rate and repopulate thus the channel with ions.
In the practical implementation, a fast voltage regulator is connected to the anode line producing in this way the voltage modulation that can be written as:

$$V(t) = V_{DC} + V_{AC}(t) = V_{DC} - \left(k_P I_{AC}(t) + k_D \frac{\partial I_{AC}(t)}{\partial t} + k_I \int_0^t I_{AC}(t)dt \right)$$

where gains are positive and the constant part of the voltage is selected depending on the operational point desired, while the time varying part is the output of the PID controller. The mean value of the discharge current is subtracted to the signal before using it as the input for the regulator. It is clear how sampling the discharge current at a sufficiently high frequency, processing it in order to calculate the appropriate output value of the output and then operate an electronic component in order to physically generate the required waveform in few microseconds is definitely not easy. For this reason, a sophisticated digital to analog converter and a fast regulator based on the use of a MOSFET were recently developed allowing the acquisition of interesting data [73]. In order to familiarize with the described interaction technique, some introductive numerical simulations has been done using the Stanford Hall thruster two-dimensional code [83] and introducing a simple proportional feedback loop in the discharge voltage that is now modified at each time step. This configuration is clearly ideal and assumes an almost infinitely fast regulator. One of the plots obtained is reported below.

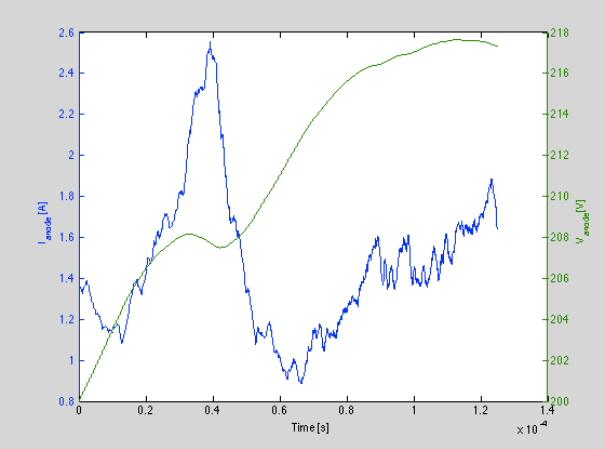

Figure 2.5: *Discharge current simulated with a proportional feedback using Stanford Hall thruster code.*

Even if only two periods of the breathing mode are simulated because of the quite long running time, a damping effect is clearly observable. The capability and maturity of this regulation technic is remarkable. Different ways to interact with the low frequency oscillations have been theorized: magnetic field is probably the most important parameter in this class of plasma accelerator; interesting applications have been demonstrated manipulating this parameter.

Plume divergence has been obtained by optimizing the magnetic field topology [75] as well as interesting thrust steering device as an alternative to traditional heavy and complex gimbal mechanisms [76]. In principle, acting on the magnitude of the magnetic field properly, could open the door to the actively stabilization of some of the low frequency instabilities. In similar way plasma fusion researchers have been successfully used feedback control to mitigate a vast number of instabilities [78].
Some work has been done on the interaction with the breathing mode found in Hall thrusters using the magnetic field modulation as well [45, 48, 81, 82]. Magnetic modulation offers the advantage of keeping the discharge voltage constant, mitigating the possible impact of voltage oscillations on the electric-to-kinetic efficiency, also called thrust efficiency, defined as:

$$\eta = \frac{1}{2}\frac{\langle T \rangle^2}{\dot{m}\,\langle VI \rangle}$$

where $\langle T \rangle$ and $\langle VI \rangle$ are the time-avaraged thrust and discharge power. Relation between ion velocity and discharge potential has already been mentioned. Ion velocity dispersion results thus increased if large anode voltage oscillations are generated by the regulation system or by an external RLC network working close to the resonance frequency. Unfortunately, the physics involved this kind of application is rather complex considering the numerous physical phenomena that can impact the axial electron transport. Electron transport is indeed affected through classical cross-field transport and the anomalous Bohm-type one, respectively $1/B^2$ and $1/B$; a direct relationship between magnetic field and axial electron conductivity exists. An axial drift in now present as well. Other mechanisms are present. Considering indeed a traditional annular Hall thruster and focusing on the exit plane where the magnetic field is mostly radial, the Maxwell-Faraday law should be included in the model. For the mentioned axisymmetric thruster it reduces to:

$$\frac{\partial E_\theta}{\partial x} = -\frac{\partial B_r}{\partial t}$$

The newborn azimuthal electric field generates in turn an axial drift according to the cross product $\boldsymbol{E}\times\boldsymbol{B}$, where B is a function of coil current, while E depends on the time variation of B and so, in turn, on the derivative of the coil current adding an intricate dependence. If a PID regulator is selected, the process variable to be stabilized is the discharge current I and the controlled variable is the current flowing into the coils. In the ideal case, the magnetic permeability of the material remains constant and real-valued in the frequency range of interest and no saturation occurs; in this case, the magnetic field generated by the coil is

proportional to the coil current, $B \propto I_{coils}$, hence the following relation: can be written:

$$B(t) = B_0 + B_{AC}(t) = B_0 - k_{Coils}\left(k_P I_{AC}(t) + k_D \frac{\partial I_{AC}(t)}{\partial t} + k_I \int_0^t I_{AC}(t)dt\right)$$

where k_{Coils} account for the relation between the coil current and the field generated. Unfortunately it will be showed in the next chapter that these hypotheses are too restrictive. B_0 is the DC field used as a bias for the correct operation of the thruster as already discussed. Positive gains should be expected because a discharge current is typically a decreasing function of the magnetic field. More effort should be spent to better understand if this affirmation holds for high frequency modulation of the field as well; increased mobility due to the time and spatial gradient of the fields caused by the modulation, could indeed result in an enhancement of the transport regardless to the sign of the time derivative of the coils current [80]. A schematic of a possible circuitry that is similar to the briefly introduced control architecture is presented below.

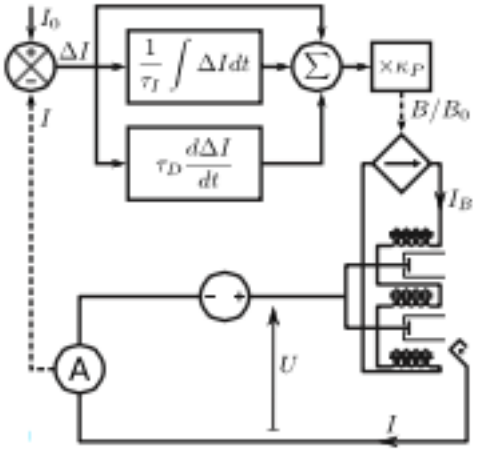

Figure 2.6: *Block diagram of a possible controller based on magnetic field modulation; adapted from [70].*

As for the voltage regulation technique, some numerical simulations were attempted before starting the experimental study. Using the zero dimensional model discussed at the beginning of the section, including a dependence of the ionization rate on the magnetic field value, a feedback loop has been simulated. Different proportional gains were tested and three of them are reported. In particular two of them show a stabilizing effect while the third one is choose on purpose to generate a destabilizing effect.

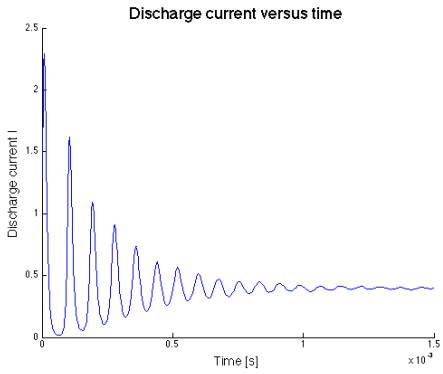

(a) Discharge current; $k_p = -0.145$

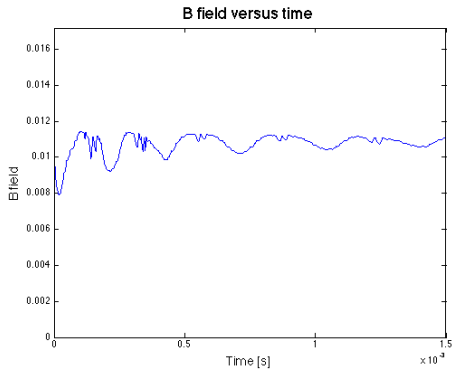

(b) Magnetic field; $k_p = -0.145$

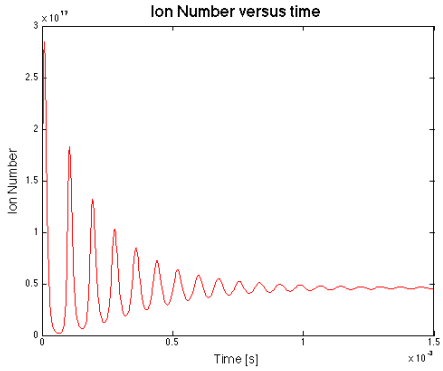

(c) Ion number; $k_p = -0.145$

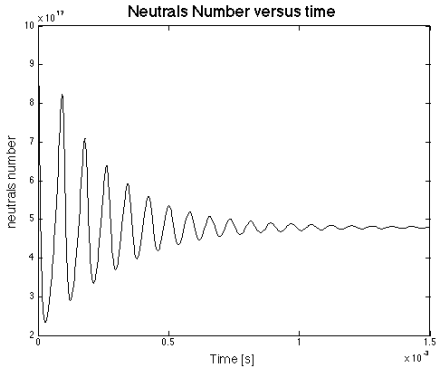

(d) Neutrals number; $k_p = -0.145$

Figure 2.7: *Dampening of the breading mode numerically simulated using Magnetic field modulation feedback with a 0D model; -0.145 proportional gain.*

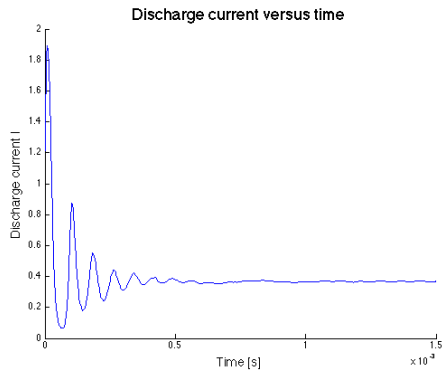

(a) Discharge current; $k_p = -0.4$

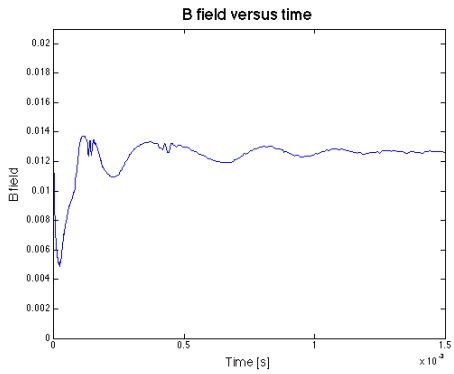

(b) Magnetic field; $k_p = -0.4$

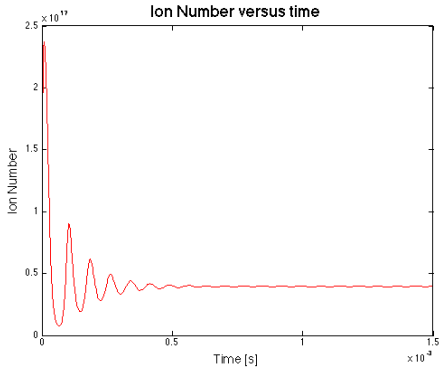

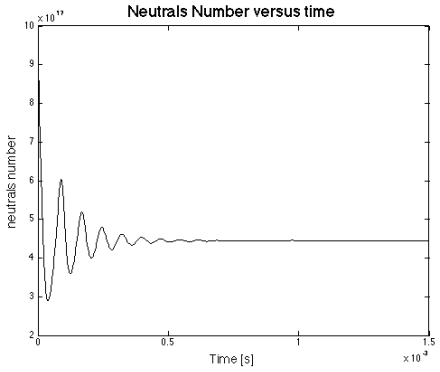

(c) Ion number; $k_p = -0.4$ (d) Neutrals number; $k_p = -0.4$

Figure 2.8: *Dampening of the breading mode numerically simulated using Magnetic field modulation feedback with a 0D model; -0.4 proportional gain.*

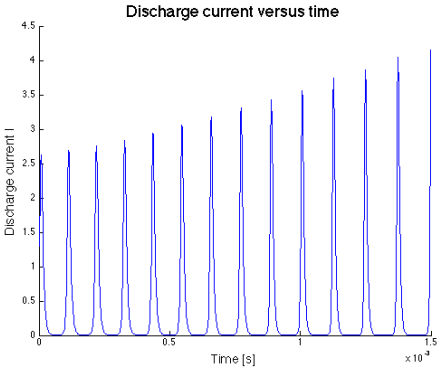

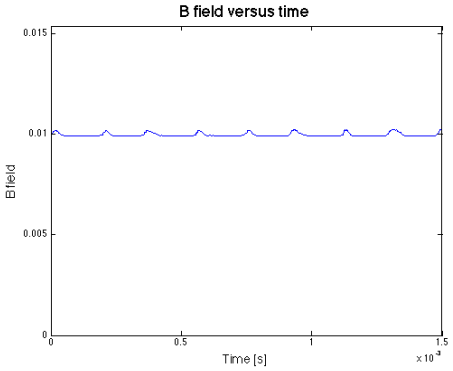

(a) Discharge current; $k_p = -0.4$ (b) Magnetic field; $k_p = -0.4$

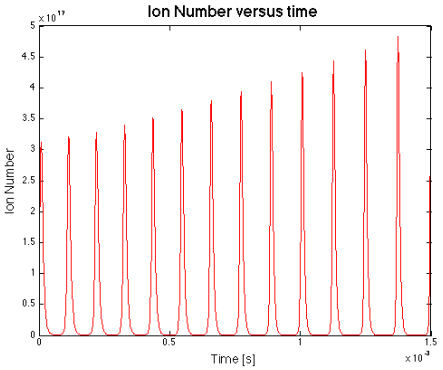

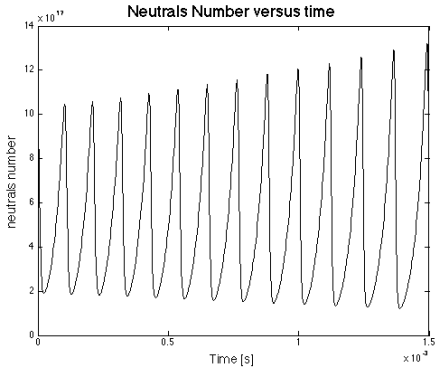

(c) Ion number.; $k_p = -0.4$ (d) Neutrals number; $k_p = -0.4$

Figure 2.9: *Amplification of the breading mode numerically simulated using Magnetic field modulation feedback with a 0D model, +0.01 proportional gain.*

The presented plots show how oscillations can be damped rather quickly when the proper regulator gain is used. Magnetic field impacts indeed on the conductivity: a lower magnetic field is associated with a lower resistivity of the plasma, lowering in this way the electron temperature as well. Ionization rate is thus reduced. When instead magnetic field is increased, ionization rate results higher as showed by the color of the plume during thruster operation with current flowing into the electromagnets. Besides the flexibility provided by an active control system, it has been shown numerically that much greater performance should be expected when implementing such a system, in comparison with traditional passive networks [70]. An interesting plot is reported below:

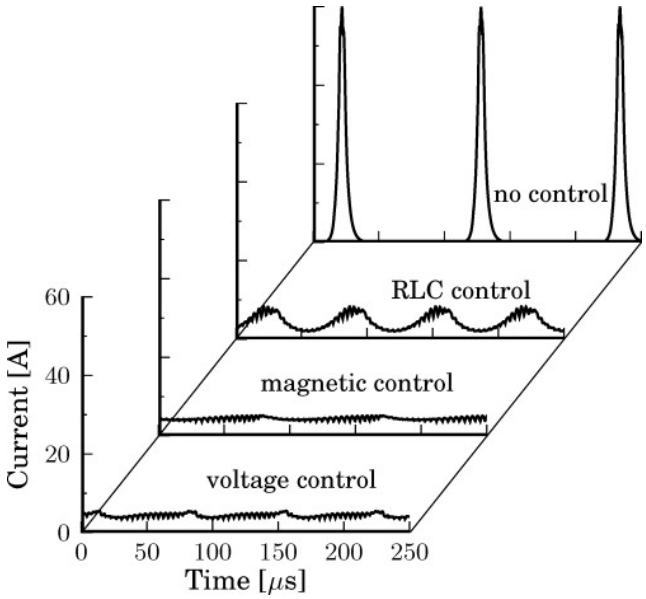

Figure 2.10: *Numerical simulation comparison between the effect of different external circuitry on the discharge current oscillations [70].*

Because of theoretical higher performance of the magnetic control strategy and due to the already quite advanced status of the voltage control strategy one, in addition to a personal interest of the author, the former was selected as a main topic for this thesis.

Chapter 3

Magnetic Field Modulation Interaction Improvement

3.1 Limitations of present B field modulation strategy in HET

Following the works of other researchers [48] in their attempts to interact with and damp the breathing mode oscillation of a cluster of four Hall effect thrusters, a complete redesign of the system was considered aiming to overcome part of the limitations found in previous studies. Working with magnetic fields modulated at some kHz requires indeed a lot of attention, especially if the main aim of the system is not the development of an induction heater. As a note for the reader, it is important to specify that even if from a plasma dynamic standpoint this frequency range is classified as a low frequency one, hence the name low frequency oscillations, from an electric point of view it can be classified as high frequency if compared to traditional AC application. Even if the frequency regime is lower compared to other applications (i.e.: microwaves etc.), it is high enough to create several problems. In previous experiments no dedicated components were used in order to actively modulate the magnetic field: the thruster coils and magnetic circuit have been used without any changing. Even if this approach is extremely attractive since no redesign of the thruster or of new components is required, a lot of drawbacks are present. A detailed description of the physics and the technology behind the high frequency magnetic field science is well beyond the intent of this work. However, some basic concepts and relations will be presented as an encouragement to a better understanding of the topic by way of the vast scientific literature available. The majority of the information used during this work are borrowed from the field of high frequency transformers, in particular, as it will be clearer in the next chapter, from the audio application field. From precedent studies [48], a very sharp decay of the magnetic field generated by typical flight qualified HET's electromagnets powered at various frequencies is observed.

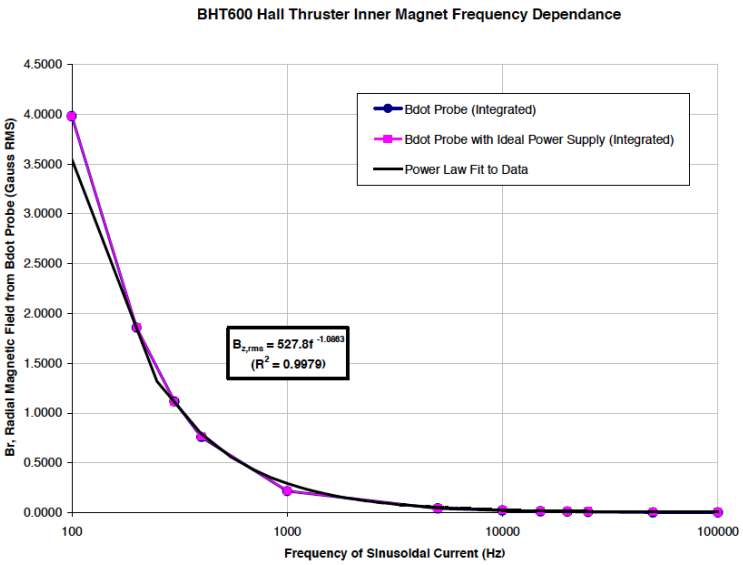

Figure 3.1: *Undesired Decreasing Intensity of the B field with Frequency [48].*

Without any addition information, it is of course not possible to explain with certainty the reason of this decay that brings the magnitude of the filed as low as 1% of its DC value once the 10 kHz range is reached. Never the less, several possible reasons can be identified. A brief discussion on topic follows and, later, a preliminary investigation with magnetic field simulation software will support the previous analysis giving some guidelines in order to improve the discussed strategy.

It is important to give two definitions before proceeding: H is named magnetic field intensity, while B is called magnetic flux density, or induction, even if it is commonly referred to as magnetic field. The relationship between the two parameters is given by:

$$B = \mu H = \mu_r \mu_0 H \quad where \quad H = \frac{N}{l} I_{coil}$$

where $\mu = \mu_r \mu_0$ is the permeability of the material given by the product of the relative permeability, usually tabulated for different magnetic material ranging in a huge interval going as high as a value of 10^6, and the permeability of free space (i.e.: $4\pi \times 10^{-7}\ H/m$, where in this case H refers to the measuring unit of the inductance: Henry). The magnetic field intensity H is then measured in $[A/m]$, while B is measured in Tesla $[T]$.

The most common loss mechanism can now be described. A peculiarity of magnetic materials is the hysteresis effect that strongly impacts the efficiency

and the behavior of the device. A vast literature on topic is easily available. Below, a brief description along with a graph of the phenomenon is reported.

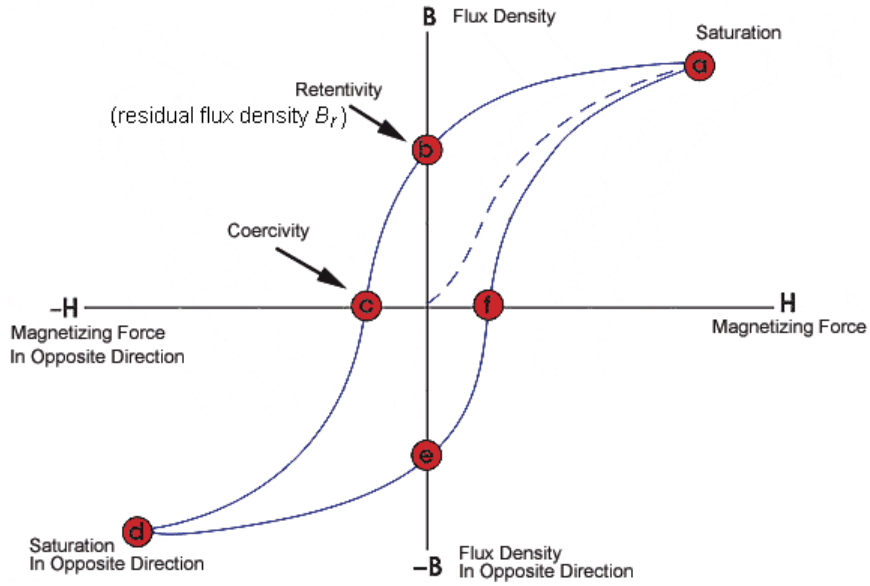

Figure 3.2: *Hysteresis loop [37].*

The relation between H and B is not a function when dealing with non-ideal material; indeed, different values of B are possible for the same value of H, depending on the past of the magnetization process. The most noticeable effect is that once the applied filed is returned to zero, a remaining flux density is still present, even if at the beginning of the process its value was zero as well. A more accurate analysis reveals that the area within the loop is related to the energy lost over a cycle, which is expressed in J/m^3. The consequence is that in order to maintain a low loss level, a narrow hysteresis loop area is required as the following relation suggests.

$$E_{cycle} = \int_0^B H \, dB$$

The associated power is thus directly proportional to the frequency of operation and in order to compute the total power absorbed by the device, the value computed above has to be multiplied by the volume of the material.

$$P_{Hysteresis} \propto f$$

Traditional magnetic materials used in Hall thrusters are not selected on a hysteresis loop area basis, since this is not a design parameter for traditional thrusters in which a DC signal is used to power the coils. It is then clear that a non-customized version of a regular Hall thruster might result quite lossy if high frequency current drives its electromagnets.
Permeability of ferromagnetic material is, in addition, not a simple constant. When frequency is considered, permeability is indeed a complex number, corresponding to the in phase and out of phase response.

$$\mu(\omega) = \frac{B_0}{H_0}\cos\delta - j\frac{B_0}{H_0}sen\delta = \mu'(\omega) - j\mu''(\omega)$$

where j is the imaginary unit. In addition $tan\delta = \mu''/\mu'$ is called the loss tangent and provides a measure of the lost power in the material versus the power that is stored in that. Frequency dependence is probably generated by the phase lag in the motion of magnetic domain walls compared to the applied alternating current flowing into the coils around the core material; different models exist and the molecular details of phenomenon are still studied [34]. Permeability is a function of the current flowing into the coils as well, and so of the value of H, and strongly dependent on temperature.
Moreover an additional loss mechanism is present when dealing with varying magnetic field and it is due to the so-called eddy current, also named Foucault currents. This kind of losses occurs whenever a changing magnetic field is applied to a core material that is electrically conductive, which is unfortunately the most common situation. The established circulating currents produces a magnetic field in the same way of a wire loop creating various phenomena like forces and heating effects. In the ideal case, the power lost due to the eddy currents is proportional to the second power of the frequency.

$$P_{eddy} \propto f^2$$

It is thus clear how a carefully evaluation of the power dissipation mechanisms is mandatory in applications where high frequency magnetic field are used. Several ways to minimize this effect exist and rely on the use of particular kind of core material and design process.
A different type of loss is present in the coil as well: copper losses are indeed present in the electromagnets of the thruster, being localized in the windings resistance, that operates in DC as well, but that increases when dealing with AC signal. The main reason for this behavior is the so-called skin effect. This effect decreases as well the capability of a fast changing magnetic field to penetrate a magnetic material. A more detailed description will be presented later on. A more concise and effective way of understanding the importance of the briefly

described losses mechanisms is obtained using magnetic field simulation software; in this case FEMM was used [69]. In the following plot, a simulation of the magnetic circuit of a thruster similar to the one used in previous studies is shown. The simulation is axisymmetric, it is thus an approximation of the real thruster, and traditional materials are selected for the magnetic circuit (i.e.: soft iron). The first simulation shows the field generated driving the coils at 1 A direct current; the result is compared to a 5 kHz frequency excitation of the electromagnets.

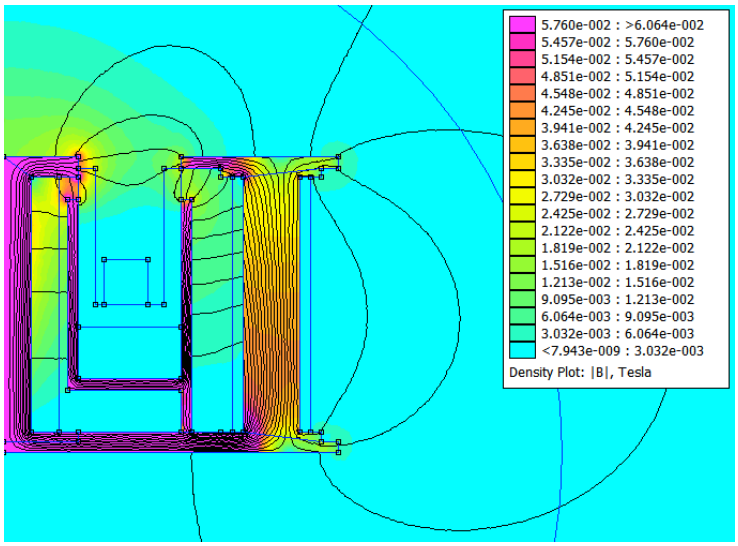

(a) DC simulation of the filed with soft iron core.

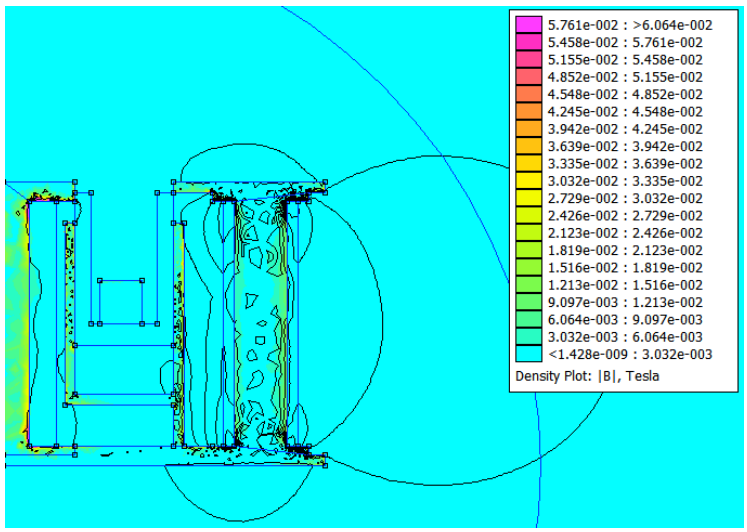

(b) 5 kHz simulation of the filed with soft iron core.

Figure 3.3: *Comparison between DC and 5 kHz current with soft iron core.*

Winding of the solenoid are not shown; comparing the images reported with a section of a traditional annular hall thruster it is clear that the coils are winded around the two main vertical element of the drawings.
It is clear from the simulation that bulky iron core cannot be used with a rapidly changing field. It should be noticed that as a modulation of the magnetic field can impact the discharge current, the opposite effect is true as well. Plasma fluctuations produce oscillations in the magnetic field that is notoriously focused inside and near the magnetic circuit as shown in the previous simulation. In the same way in which there is power dissipation in the magnetic circuit if an AC signal is used to drive the electromagnets as explained above, there could be some power absorption from the surrounding ferromagnetic material when the fluctuation of the field are generated by the plasma itself. This effect is by the way order of magnitude smaller compared to the simulation without plasma showed above. An additional issue related with the conversion of the main coils to a non-DC electromagnet lies into the high inductance of the coils itself as better explained in chapter 4 related to the power system. High inductance implies high impedance in that range of frequency and this means that in order to have a relatively small current flowing through the coils a high voltage is needed. It seems thus preferable using the inner coil only for the control purpose in order to have a lower impedance load. This approach, followed by previous researches [45], generates by the way a different side effect: the outer coil acts as a secondary winding of a transformer giving rise to a time varying voltage at the leads of their power supply. In particular, if the inner coil is built with a low number of turns in order to have a lower inductance and the outer ones in a more conventional way, with a lot of turns requiring a lower current to generate a desired B field, this voltage can reach relatively high values as in a step up transformer. In the previous experiment this issue was clearly not a big one since the material used in the magnetic circuit was not suitable for high frequency application and so the varying component of the field was not subject to good confinement into the magnetic circuit itself, as clearly shown in the simulation above. This last aspect is found in inductive heating as well: neglecting the conductive heat transfer, only the part of the metallic object sitting in the center of the heating coil will became hot, not the rest of the object. This high frequency behavior clearly differ from the well known property of a metallic part that become entirely magnetized when positioned closed to a DC electromagnet or a permanent magnet.
Even neglecting the important aspects previously described, further problems arise analyzing existing solutions that aim to a magnetic field modulation strategy. Past tests on a proprietary card by Busek [9] shows how the active control of the magnet current completely shift the operational mode of the thruster while trying to reduce the RMS of the discharge current itself. With a very low magnetic field the thruster enters the so called glow mode or ball mode;

it is well known that in this regime the discharge current profile is much more flat compared to the high fluctuations observed in the Hall mode, also referred to as the jet mode (i.e., with magnetic field sufficiently high). HET needs to be operated in Hall Mode in order to provide a thrust. The algorithm embedded in the card drives a lower current into the coils of the thruster trying to achieve a quiescent regime forcing the thruster entering in this way the unuseful glow mode. In some cases this strong shifted of the mode is avoided by the presence of large spikes into the discharge current one the transition between Hall mode and glow mode takes place. During this transition electrons generated in the cathode can easily flow to the anode generating a transient RMS high value that drives the card's output at a higher level again; different behavior is obtained changing the working gas. This global trend is manly attributable to the choice of using the main coils as the control one. A better implementation would rely on a zero-mean signal into the interaction coils so that the overall operating parameters of the thruster are not shifted during the active RMS reduction attempt. Increasing in the sampling rate should be desirable as well; being only few Hz the working one of the card tested in previous studies [9].
Two possible improvements to the scenario described above are suggested in the two sections that follow. In the first one, a preliminary redesign of the magnetic circuit of the thruster using high frequency proof techniques is proposed. In the second one a different approach is advanced and further developed and tested in the remaining part of the thesis.
In the next section, the guidelines for the redesign of the magnetic circuit and some characteristics of the revised Hall thruster are outlined.

3.2 Annular HET Magnetic Circuit Integral Redesign

In conventional Hall thrusters the ferromagnetic core of the magnetic circuit is not design for AC operations and they do not perform well under varying magnetic field as already mentioned in the previous section. The first improvement attempt presented in this thesis is then the preliminary redesign of the magnetic circuit of an annular HET that is compatible with a fast varying magnetic field. In the picture below a typical section of this kind of thruster is presented; in particular a magnetic shielding is present and the outer solenoid is coaxial with the channel, as the inner one. Even if this configuration is different from the simpler one selected for the new design and presented later, it is a good way to better understand the simulations presented later, in which an axial symmetric and shielded configuration has been used.

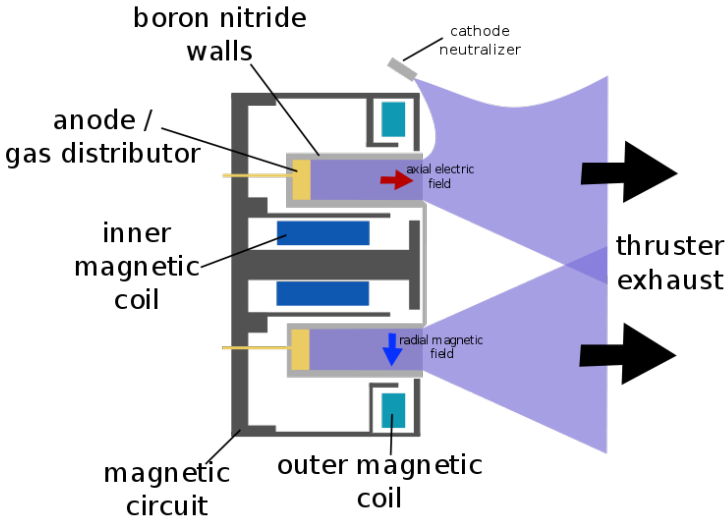

Figure 3.4: *Schematic of a shielded Annular Hall Effect Thruster [5]*

The magnetic circuit geometry is rather similar to the one used in the Z-70 thruster described in chapter 5. The shield, that is best visible around the inner coil, helps to prevent the magnetic field entering the channel in the region close to the anode; this configuration is well known for extending the life of Hall thruster even at high specific impulse operation [88]. As already explained, hysteresis and eddy current losses are two of the main problems to be solved. In the following section a more detailed description of loss mechanisms are presented and the preliminary development of the new design is reported. The first step of this process is the replacement of soft iron, or low carbon steel, commonly used in Hall thruster magnetic circuit with a different material. The number of materials available for high frequency use is enormous and the vast

majority of them have been developed and studied for transformers applications. A detailed description of them and their properties is beyond the scope of this thesis and the reader is invited to check the website of the many companies working in this field. Their catalogs are often a very good source of information and details [36]. As already said a material with a narrow hysteresis loop is needed in order to lower the power dissipated in each cycle of the field. Of course a low coercitivity material is needed in order not to have a magnetic field left once the current flowing in the coils (i.e.: the externally applied field) goes to zero. In order to have low hysteresis loss a low coercitivity is needed. Materials with high coercitivity are called *hard* and are used in permanent magnets; *Alnico* is an example of that kind of material. For the application studied in this work, *soft* magnetic materials are required; *Supermalloy* is a popular low coercitivity material widely used in transformers. Coercitivity is measured in A/m; its value corresponds to the field strength which must be applied in order to bring the remnant magnetic flux to zero and it can varies in a several order of magnitudes range. Remanence is sometimes desired, as in the case of all magnetic recording technologies, including hard disk drives and of course permanent magnets fabrication.
The other key factor is the reduction of the eddy current. This power loss mechanism is minimized by selecting magnetic core materials that have low electrical conductivity and/or by using thin sheets of magnetic material (i.e.: lamination design). Using a material with low conductivity reduce the intensity of the circulating current efficiently. An increase in the resistance of the ferromagnetic core is achieved by alloying the iron with a small amount of silicon; typical values are around 3% that corresponds to an increased resistivity of roughly 4.5×10^{-7} Ωm. The resulting material is often named 'silicon steel' even if no carbon is present in the alloy since it is not desirable in magnetic circuits. This solution is by the way not sufficient. A well-known method to further reduce Eddy current is the laminations of the core. The figure below shows how this idea can be used to reduce the described phenomenon.

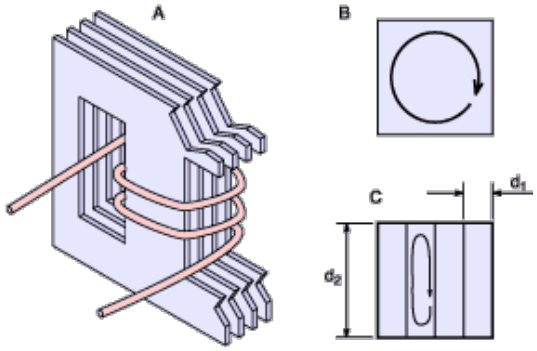

Figure 3.5: *Schematic of laminated transformer core [32].*

Cross section B shows a non-laminated iron core in which there is a large circulating current, while cross section C presents a laminated section that prevents the current forming large loops. In this last case the core is then made of a stack of thin sheets. Schematic A shows only a few laminations but their number is usually much higher. The key feature of these sheets is the insulating oxide layer that covers the surface of the laminates preventing the current from circulating from one lamination across the others. This is equivalent to have a lot of smaller virtual coils, in which virtual windings are formed by the circulating current. It is then clear that the induced voltage is much lower since the change of flux across the surface of these virtual coils is also smaller because of the lamination. Power dissipated is drastically reduced as well since is a proportional to the square of the voltage. A more rigorous analysis allows concluding that eddy current loss is inversely proportional to the square of the number of the laminations.

$$P_{Laminated} = kd^2f^2B_{peak}^2$$

where k depends on the material, d is the thickness of the lamination, f is frequency and B_{peak}^2 is the peak value of the magnetic flux density. This analytical derivation underestimates the dissipation and some semi-empirical relations have been developed [37]. Two main parameters have thus to be chosen: direction of the lamination plane and thickness of the sheets. The direction of the lamination, as already explained, is extremely important since it has to be parallel with the lines of the magnetic field or, in other words, perpendicular to the windings of the coils. The thickness of the sheets is a function of the frequency, the higher the frequency is, the thinner is the sheet that guarantee low power dissipation and in general it depends on the efficiency level desired. A different solution is available if the core is realized using powdered material in which metallic particles are covered by an insulating coating and then glued together. Usually this type of core is obtained by pressing the powders inside molds, since it is not possible machining the described material and it is usually called *iron dust cores*. Modern ferrite materials have low hysteresis and eddy current losses but they can still be significant. Iron losses are in general measured in W/kg and this parameter is usually tabulated in the catalogs.
Numerous materials have been tested using the same software that generates the previously reported magnetic field maps of the thruster at the desired frequency. One interesting result is the following. In this preliminary solution, silicon steel was used. Three percent silicon steel is, without any doubt, the most widely used among all soft magnetic materials due to a good set of properties and relatively low cost. A typical graph showing core losses is presented below; in particular 0,012” (i.e.: about 0,3 mm) thick laminations are considered.

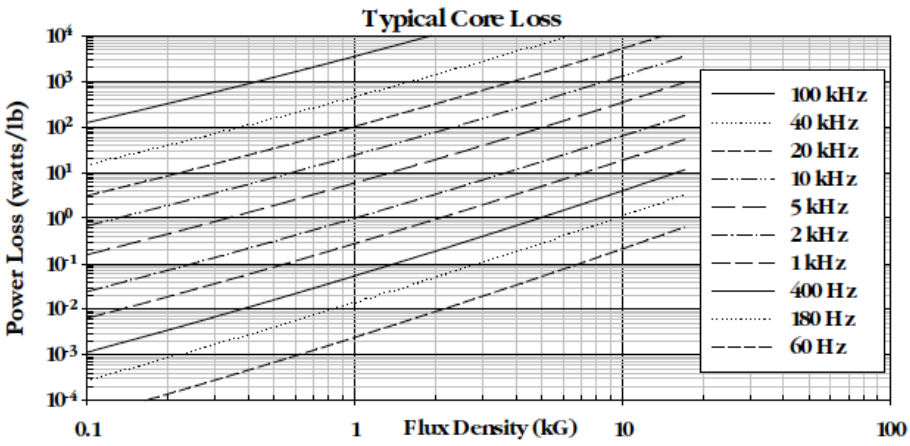

Figure 3.6: *Loss diagram for 0.012" thick laminates silicon steel [36].*

In the following figure, a simulation of the behavior of the core of the thruster at 5 kHz is reported, using M-19 Silicon steel [43]. Note eddy current still largely present on the pure iron anode; in this case a much higher resistance material is not suitable considering that the component has to conduct current. The real anode is by the way hollow reducing almost completely this effect.

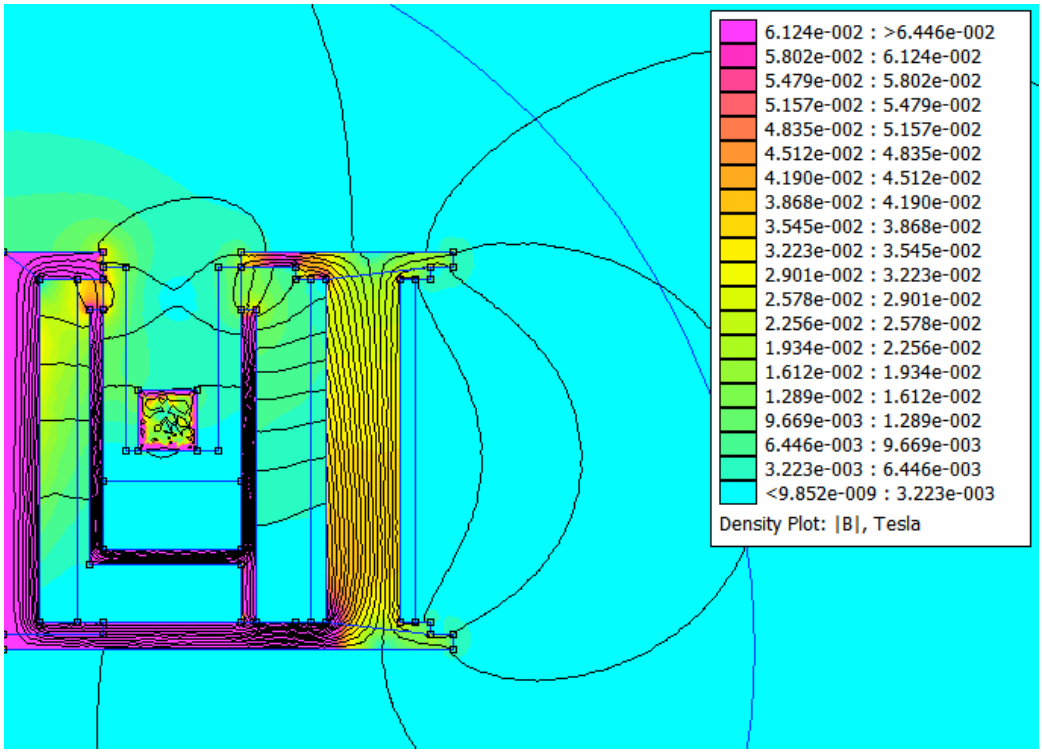

Figure 3.7: *5 kHz simulation using 0.012" thick laminates M-19 Silicon Steel.*

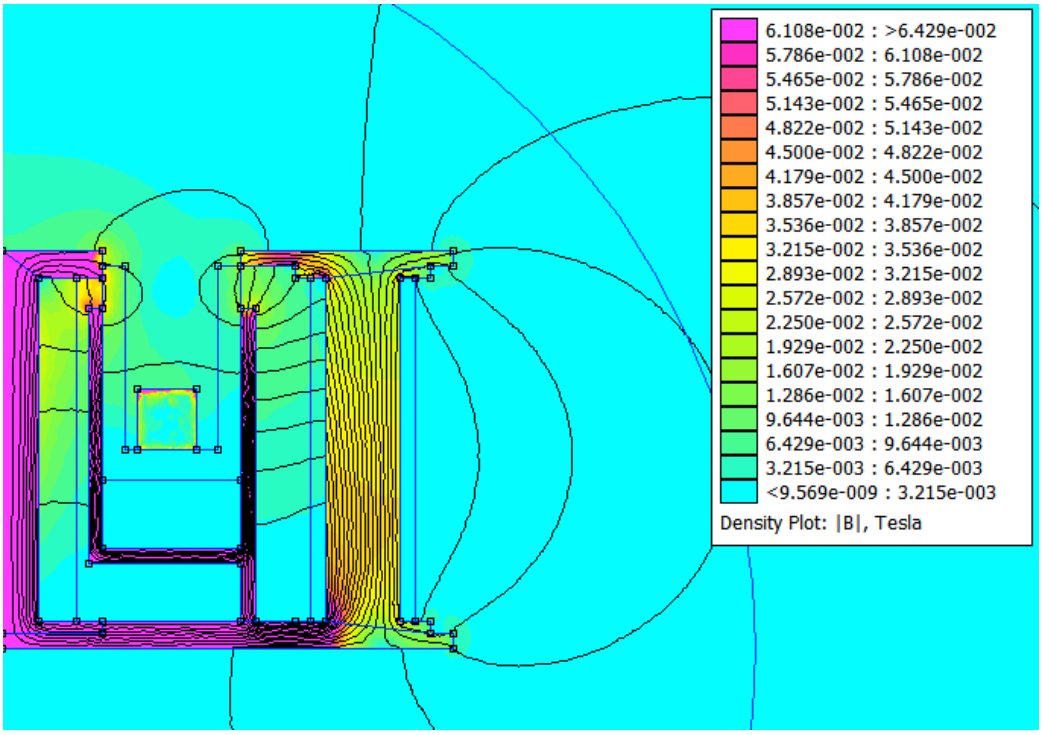

Figure 3.8: *20 kHz simulation with 0.012" thick laminates M-19 Silicon Steel.*

From the plot it is clear that the improvement is already quite high compared to the original situation. After a more detailed literature research, by the way, it was found that for the tens of kHz regime (i.e.: considering higher order harmonics) silicon iron is still too lossy. Lamination with silicon steel material can indeed reduce the losses up to few hundreds of kHz [39]. A much more efficient class of material is the ferrite one that is usually used up to the MHz regime, a brief description follows. Ferrites are ceramic materials made of iron oxides (Fe_2O_4) mixed with different oxides or carbonates; two main groups of ferrite exist, manganese and zinc ferrite (MnZn-ferrite) or nickel and zinc ferrite (NiZn-ferrite). Ferrite cores are used in a wide variety of applications in high frequency power electronics, power inductor, broadband transformer and a lot of other applications. Manganese-zinc is the most common type and they are suitable for application under 2MHz. The presence of metallic oxides reduced eddy currents because of the high resistivity, typically in the order of $10^5\ \Omega m$, thus six order of magnitude higher than iron cores. Relative permeability ranges typically from 40 to 10000 and power loss is in the order of 50 mW/cm^3 at 20 kHz. Further literature research on this material revealed that serious limits related to the working temperature (i.e.: Curies temperature around 150-200°C), temperature gradient and saturation level, about 0.3 T, prevent ferrite to be the best candidate for the new magnetic circuit.

Saturation in particular prevents ferrites to be used in such application, even at laboratory level, unless cross sections are increased in order to reduce the flux. Such a changing in the cross sections can not be integrated easily in an existing thruster without modifying ceramic walls and other components that corresponds to a completely redesign of the thruster. Even if an increase in the cross section of the magnetic circuit components were feasible, the thickness of the front plate of the thruster would be another critical point in which the higher concentration of magnetic field lines could result in saturation of the material again. Moreover, the saturation flux density Bs decreases with temperature. For ferrites, Bs may decrease by a factor of 2 as the temperature increases from 20°C to 90°C [33]. Even if higher temperature can be tolerated by some ferrites, their strong dependence of saturation and permeability on the temperature requires a very accurate design in order to meet the specification needed. Permeability is indeed extremely variable with temperature and a sharp decay is seen over a certain value of temperature.

In order to solve the low saturation issue that affects ferrites, a cobalt iron alloy was selected for further investigation. Iron is often alloyed with cobalt to achieve a high saturation magnetic flux density and indeed it is the peculiar characteristic of this family of alloys. Beyond the clear advantage offered by that, a remarkable high permeability at high magnetic flux follows. They are among the most expensive alloys and for this reason they are used only when a real advantage can derive from their application. Maximum relative permeability is around 15000. Aerospace industry and in space application of cobalt iron is definitely not new [44]: weight can be saved in magnetic circuit considering that a higher magnetic flux can be established before reaching saturation, occurring at 2.4 T, allowing in this way to use smaller cross section components. Hyperco is one of the most popular cobalt iron alloy with an incredible high Curie point above 900° C and the highest magnetic saturation of all soft-magnetic alloys. The low power losses given by the high electrical resistivity of 40 $\mu\Omega cm$, allow this material to be used in 20 kHz application [33]. Unfortunately, after a brief commercial analysis, the difficulty of finding cobalt iron laminates thinner than 0.004" became clear. Considering the frequency range of interest it was decided to account for the possibility of using a material commercialized also in thinner thickness. Nickel iron alloy has been thus considered: Iron is indeed often alloyed with nickel in order to reach a higher permeability. The cost of this alloy is much higher compared to the cost of the silicon steel that was considered at the beginning. The saturation flux is definitely lower than the cobalt iron alloy; permeability is on the contrary much higher. Losses are very low in some of the available species of this alloy; some of them present a rectangular hysteresis diagram whose shape can be altered by heat treatment [40]. Permalloy, with 80% of nickel, has a very high permeability because of this property. A lower concentration of nickel, around 50% as in

Isoperm alloy, produces instead a much higher resistivity in the material allowing application at higher frequency resulting in one half the losses for comparable gauges silicon steel, even if with a lower permeability. Low-nickel alloy is indeed common in audio-frequency applications that are in the range of interest for the interaction with the low frequency instabilities studied in this work. As usual magnetic properties depend on the temperature and material thickness. Very thin sheets of this material are commercially available, up to 0,001" (i.e.: 0,025 mm) and thus it was selected for simulation.

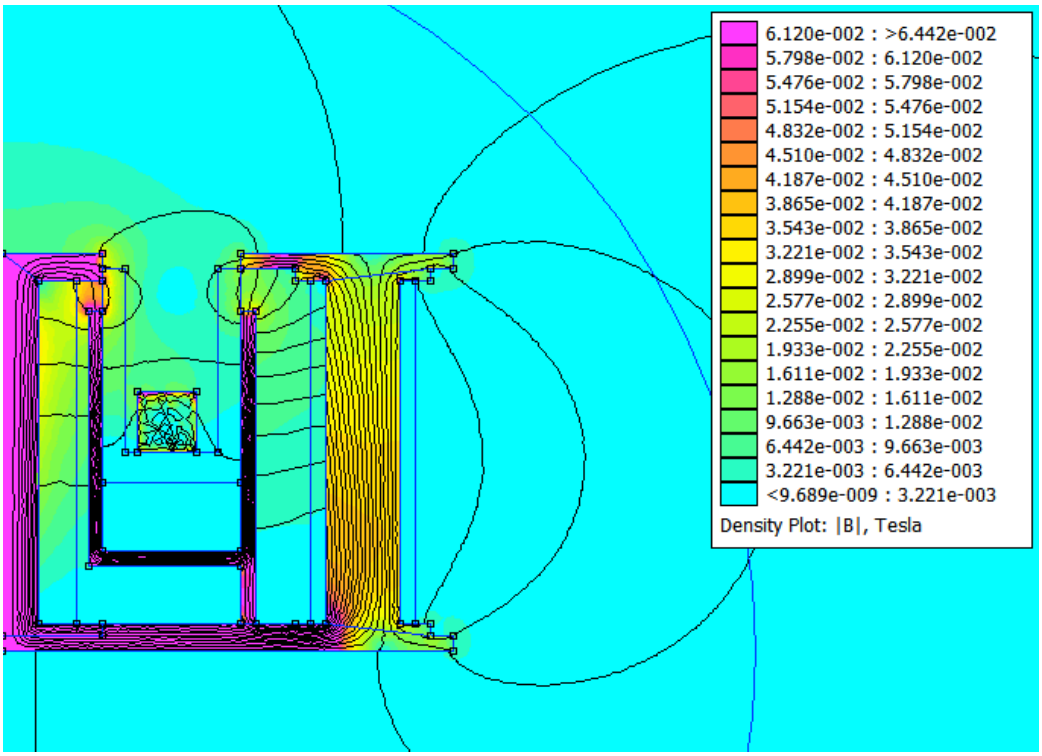

Figure 3.9: *20 kHz simulation using 0.001" thick laminates 50% Ni – 50% Fe.*

As can be seen from the following simulation, the behavior of the material is definitely good up to 20 kHz and above. One of the biggest limiting factors of these laminated materials is the melting temperature of the gluing paste present between each sheet. Even if some experimental compounds can withstand higher temperature, it rarely exceeds 250° C. For this reason an active cooling system for the preliminary laboratory model is necessary, at least for the hottest part of the thruster as in the case of the central rod and the front plate. A last graph on power loss is reported showing the excellent behavior of 0.001" thick laminates made of Ni-Fe alloy.

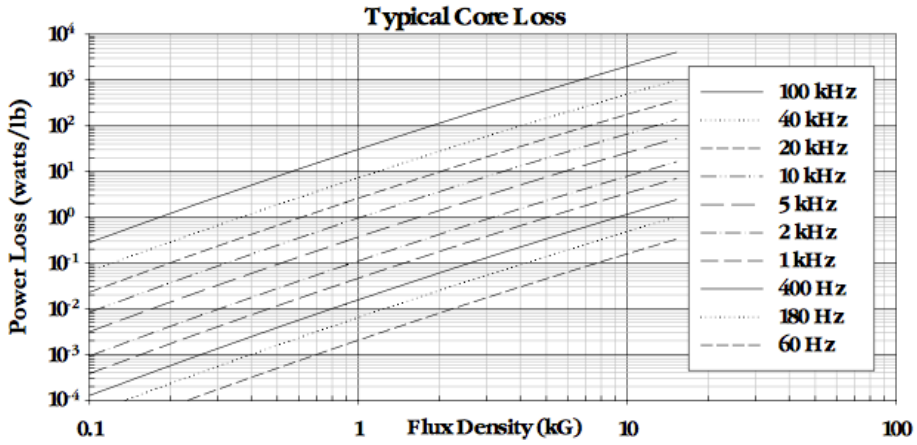

Figure 3.10: *Loss diagram for 0.001" thick laminates 50% Ni – 50% Fe [36].*

Comparing this table with the similar one presented before for silicon steel, it can be noted that power loss is two orders of magnitude lower.
Considering the good overall result of the simulation presented, a preliminary three-dimensional model was realized and commercial analysis performed. For sake of simplicity and cost, an unshielded magnetic circuit has been design.
An overall view of the assembly is shown and some drawings as well.

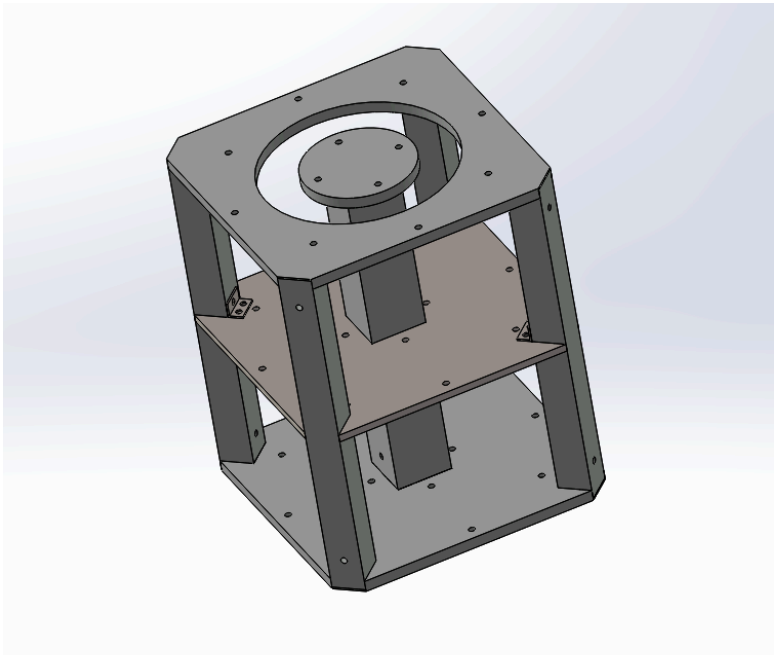

Figure 3.11: *Preliminary 3D High Frequency Magnetic Circuit Model.*

Considering the lower saturation point of this alloy and the already mentioned water cooling circuit probably necessary in order not to reach a too high temperature, it was decided to place the solenoids under the original bottom plate of the thruster (i.e.: the central one in the model above). Extra room in indeed needed to host the cooling pipes and to maximize the cross sectional area of the rods in order to maintain the magnetic flux below saturation limit. With the new arrangements of the electromagnets windings, the bottom plate of the thruster, that is now become the central one, has no more a magnetic role. In the original magnetic circuit, the bottom plate is indeed needed to close the magnetic circuit on the backside of the thruster. This role is now left to the plate at the very end of the circuit, while the intermediate one is only used to hold the anode and the ceramic walls in place. For this reason, no more soft iron is used and non-magnetic stainless steel is choose instead. The holes on the plates and on the vertical elements are necessary for the mounting hardware, except for the intermediate non magnetic plate brackets, not showed for sake of image neatness.
Some drawings are reported below in order to present a more detailed view of the parts contained in the new magnetic circuit assembly except for the intermediate plate that is not crucial in the understanding of the new laminated design. A qualitatively representation of the lamination is shown on the rendering of one external rod; no scale is applied, considering indeed the ratio between rod and single sheet thickness it would result in a not clear representation. No lamination is reported in the technical tables, the direction of the lamination is specified by means of geometrical constrains (i.e.: perpendicular to the holes).

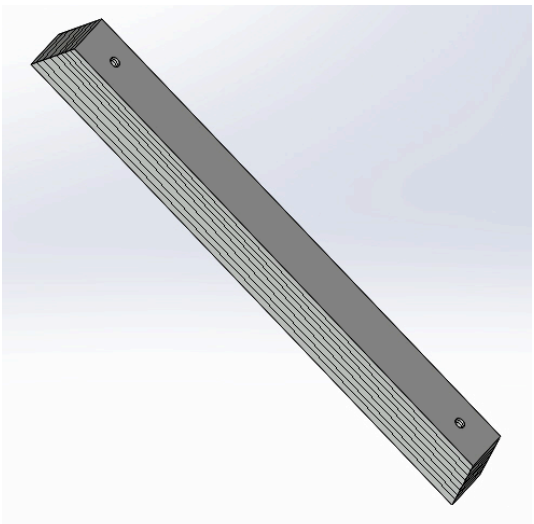

(a) Qualitative representation of the lamination.

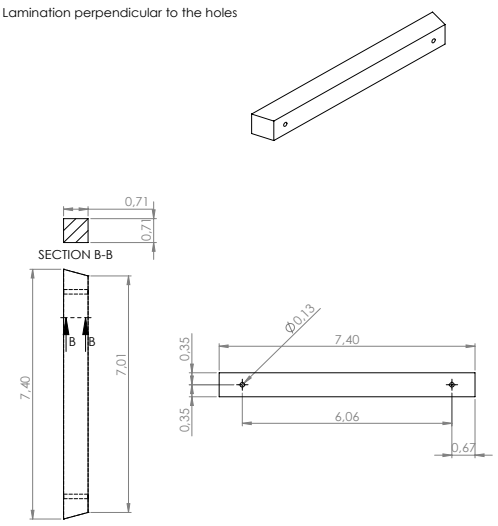

(b) Table of the four outer rods.

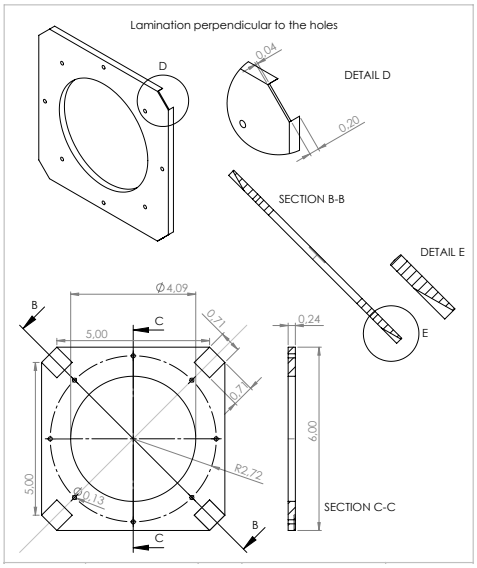

(c) Top outer plate: outer pole piece.

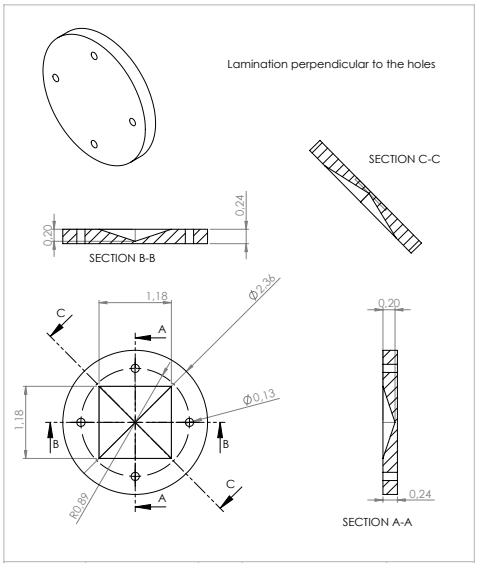

(d) Top inner plate: inner pole piece.

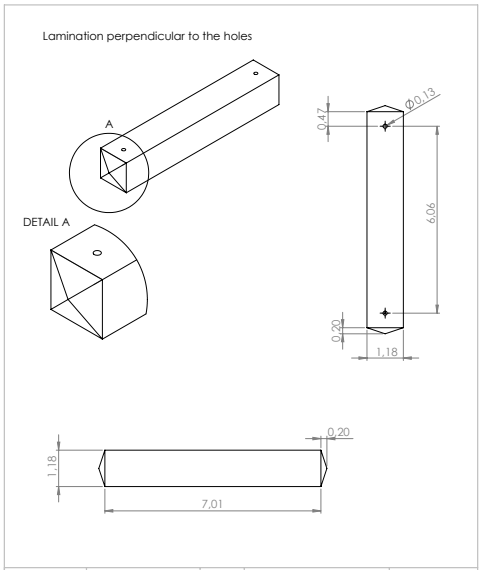

(e) Inner rod; not the pyramidal ends.

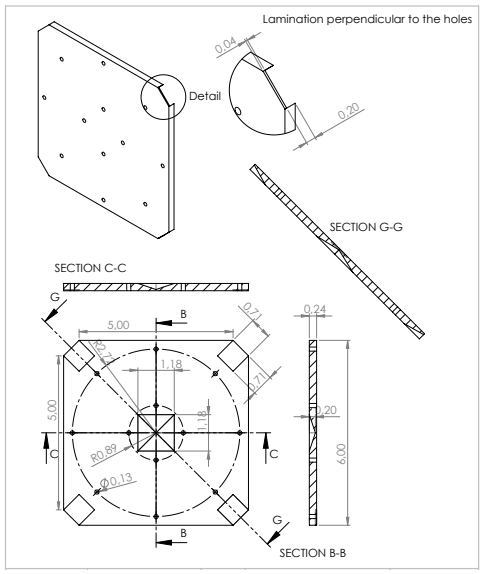

(f) Bottom plate

Figure 3.12: *Drawings of the principal components for the new high frequency magnetic circuit design.*

This design makes the magnetic circuit inevitably longer compared to a more conventional Hall thruster. Besides the increasing in weight, the most important consequence is again related to the magnetic circuit characteristic. An increased length of the core generates indeed a larger reluctance, which is the resistance of

the core to the flow of the magnetic flux measured in $1/Henry$ and that is defined as:

$$R_m = \frac{l_{mpl}}{\mu A} = \frac{NI}{BA}$$

where l_{mpl} is the mean magnetic path length, that is the mean length of the closed path crossed by the magnetic flux, having cross section A. R_m relates the magnetomotive force F with the flux of the magnetic induction B as expressed by the Hopkinson law:

$$F = R_m \Phi$$

As explained before, since μ is a complex number, R_m is complex as well.
Further manipulation gives the following helpful relation:

$$B = \frac{\mu N}{l_{mpl}} I$$

that shows how with an increase of the length of the magnetic field path, a larger current, or number of turns, is necessary in order to obtain the same value of the magnetic field. Reluctance can be defined for an air gap as well. An interesting analogy with electric circuit can be done and a schematic is shown below.

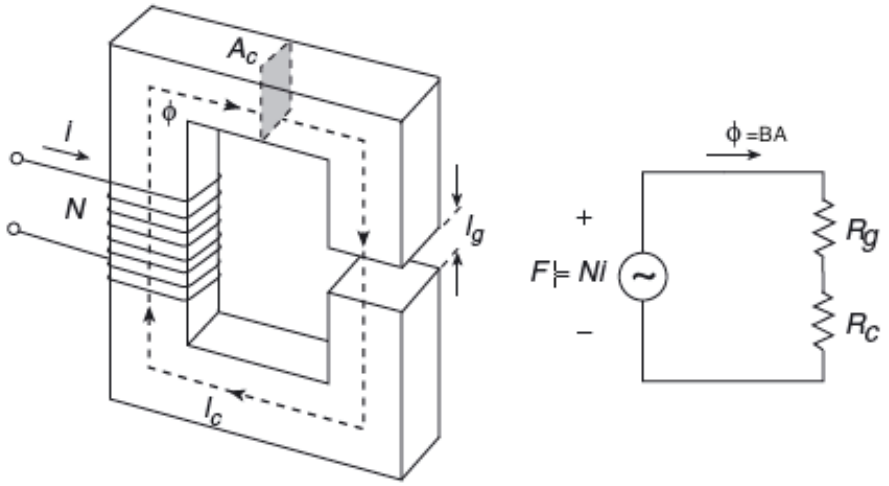

Figure 3.13: *Magnetic circuit and equivalent electric circuit [33].*

Considering that the described redesign is a proof of concept, no great attention was paid on this problem, which was taken into account by simply planning to

drive the electromagnets at a higher current level. It worth notice that even if in principle the problem can be mitigated using a higher permeability material as the previously mentioned permalloy, the big air gap is present, the equivalent permeability of the circuit is much lower that the high value of the metallic core, as expressed by the following relation:

$$\mu_{Equiv} = \frac{\mu_r}{1 + \mu_r \frac{l_{gap}}{l_{core}}}$$

In such a configuration, that is the typical one in the case of Hall thruster, air gap is the only significant contributor to the overall reluctance:

$$\boldsymbol{R_{tot} = R_{core} + R_{gap} = \frac{\frac{l_{core}}{\mu_r} + l_{gap}}{\mu_0 A}}$$

After this very preliminary design process, the commercial analysis started. Unfortunately, no company able to realize the components described was found. Machining difficulties of plates and rods made by stacking very thin sheets turned out to be, apparently, extremely difficult.
Because of this, even is the technical study of such a solution is definitely well promising, the described idea of building a magnetic circuit able to work with high frequency magnetic field was abandoned.

3.3 Auxiliary solenoids

3.3.1 Introduction

Considering the difficulties shown in the previous section where a magnetic core is taken into account, it was decided to develop the actuator for the field modulation in a different way. The strategy followed relies on the use of air-cored solenoids specifically designed for the generation of the varying part of the field. In an air-cored solenoid, indeed, the inductance is not affected by the current that the solenoid carries; the absence of a metallic core prevents harmonics production and the so-called iron losses are not present. This results in a better Q factor with larger efficiency and power handling capability but most important, less distortion, that is a crucial aspect when dealing with modulation purposes. In the following two sections the design process used to develop the solenoids for two different thrusters is described. In particular, basic relations involved in the design of a solenoid are reported in the section below. Considering then the far-from-ideal geometry, a more detailed analysis is carried out numerically. Of course, in the air-cored design some downsides are present. If, for example, a defined inductance value is required, with no high permeability core, more turns of wire are necessary producing larger solenoid with lower self-resonance resonance and higher copper loss (i.e.: more power dissipated and higher temperature of the winding). Even more serious is the problem related to the confinement of the magnetic field. A high permeability core guarantees indeed that the vast majority of the field remains confined inside the material, allowing in this way to reach a high intensity field value also at relative large distance from the winding. This problem will play an important role in the design of the Z-70 auxiliary solenoids as explained later.
A basic theoretical approach is used to conduct a preliminary study of the solenoids design and some simulations are performed as well in order to overcome the numerous simplifying hypothesis of the theoretical approach. Basics relation are reported here as a guideline for the designing process of the solenoid. For an infinite continuous solenoid the following important relation allow computing the magnitude of the magnetic field generated on the axis of the solenoid:

$$B = \mu_0 \mu_r \frac{NI}{l}$$

When a finite solenoid is considered, the math involved in the evaluation of the field is not as easy as before.

One of the most important parameters when dealing with a coil is definitely the inductance. Recalling the definition of magnetic flux through the coil

$$\phi = \iint_S \boldsymbol{B} \cdot d\boldsymbol{s} = \mu_0 \mu_r \frac{NIA}{l}$$

and combining it with the definition of inductance

$$L = \frac{N\phi}{I}$$

allows obtaining the following useful relation

$$L = \mu_0 \mu_r \frac{N^2 A}{l}$$

The inductance of real coils with more complex shapes can be in principle derive from Maxwell equations; in the case of air core coil, inductance is independent of current and is a function of coil geometry and number of turns. A more practical and quick way to estimate the inductance of short, non single layer, and thus non ideal, solenoid is using the many free inductance calculators available on line [38] and then experimentally verified by the several available methods and instruments. In the following sections some of the important loss mechanisms that affects time varying operation of a solenoid will be described as well. For a more detailed description of this kind of losses the author is invited to consult the vast literature that focus on this topic, as the one of reference [47]. A simple Matlab code was developed in order to speed the process of wire length computation of each individual solenoid considering the diameter of the wire, number of turns, inner diameter and length of the solenoid body previously choose. Two different types of solenoids are considered; a preliminary study results in the realization of the solenoids for the annular Hall thruster, while a more detailed approach is used in the design of the cylindrical Hall thruster.

3.3.2 Z-70 annular Hall thruster, auxiliary solenoids development

In the case of the annular Hall thruster two air core solenoids with plain magnet wire were realized. The main steps of the process follow.
The aim of this solenoid is to generate a magnetic field with a radial component with respect to the thruster axis, located at the exit plane of the device as shown

in the three-dimensional model below. Four solenoids are here displayed, but only two of them were used in the preliminary testing of this technical solution.

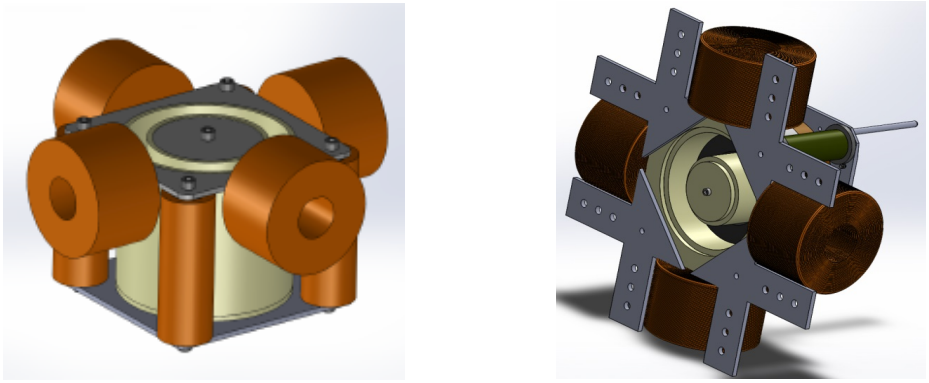

(a) Solenoids and typical Hall thrusters. (b) Z-70 in the quad-solenoid configuration.

Figure 3.14: *3D modeling of the solenoids installed on the thruster.*

Some guidelines were used in order to complete this very first approach to the problem. The desired field strength in the middle of the channel was estimated to be around 20 G and the shape of the line in the region close to the surface perpendicular to the axis of the solenoid possibly not very curved. In order to obtain this the length of the solenoid has to be high enough, so that, along with a high number of layers, almost parallel and less divergent field lines at the exit of the solenoid itself. Moreover a much higher field inside the solenoid has to be realized, about 200 G considering that the intensity of the field rapidly decreases outside the solenoid, more precisely $B_{Air} = 1/d^2$, being d the distance from the exit of the solenoid, along its axis. Thus, Z-70 auxiliary solenoids are realized using a large number of layers made of plain magnet wire for cost and easiness of building, large solid magnet wire is easily plastically deformed so that it holds the desired shape. A summary of the geometrical parameters of the coil is reported in the table below.

Z-70 Coils	
Inner Diameter	25 mm
Length (coil axis)	29 mm
Wire diameter	1,9 mm
Outer diameter	71 mm
Rows	15
Layers	12
Turns	180

Figure 3.15: *Z-70 annular Hall thruster auxiliary coils parameters.*

A two-dimensional simulation of the stationary magnetic field generated by the coil driven with a 6 A DC current is now reported. The following plot shows half of the axial symmetric solenoid; the axial distance between the two solenoids is left empty in order to place the Hall thruster there. The filed lines, only partially showed, are mostly straight at the center of the solenoid where the magnitude of the field is slightly above 200 G and it decreases quickly leaving about 40 G at a distance that corresponds to the center of the channel of the Hall thruster. Experimental measurements will confirm the simulation within good approximation.

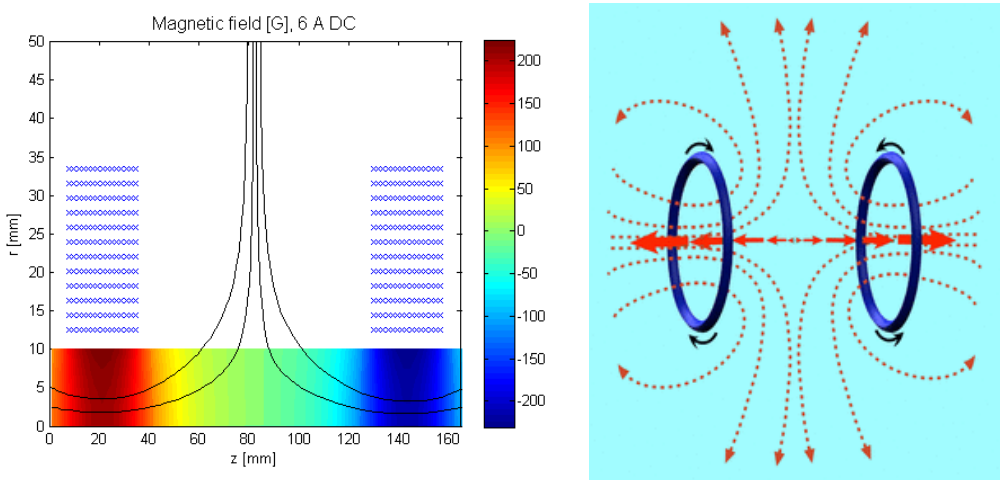

(a) Bidimensional simulation at 6 A. (b) Schematics of the field topography.

Figure 3.16: *Simulation and schematics of the field generated by the Z-70 Coils.*

As already said, plain magnet wire was used to build the solenoids; while for a preliminary DC test the used wire is a good choice, it is definitely not the best one in the non direct current regime. Skin effect indeed forces high frequency currents to the outer surface of a conductor and thus the diameter of the wire should be chosen conformingly with frequency of the signal flowing trough it. Loss mechanisms are indeed present: proximity effect and eddy current and skin effect generate big power losses when a non constant current drive the coil, especially with such a design. A more detailed description of these power loss mechanisms is reported in the following section. Such a high number of turns create some problems in the power system as well if high frequency signals are used to drive the coils, as better explained in the next chapter. Regardless to these considerations, the solenoids were realized considering that a DC test was definitely helpful in order to familiarize with this kind of testing and that a very low frequency was accessible as well. In the pictures below some realization steps are shown; hexagon arrangement was maintain al far as possible.

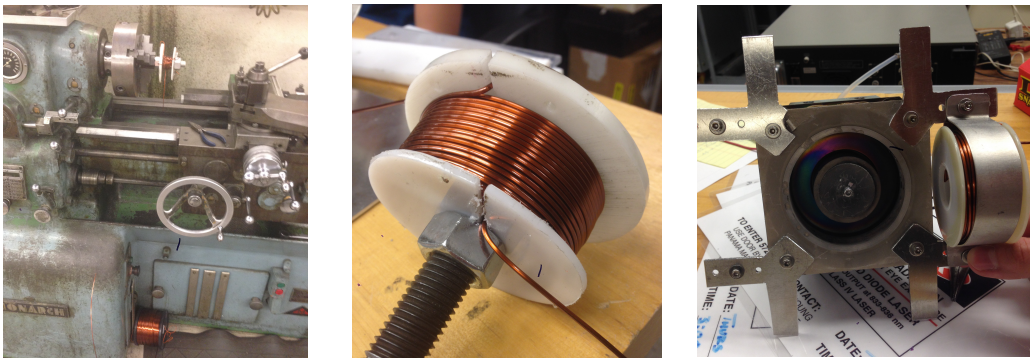

(a) Winding the solenoid. (b) Close up of the coil former (c) Beta-V. coil on the HET

Figure 3.17: *Preliminary solenoid wrapping process.*

AWG 14 wire was used, allowing relative high current to be used; a maximum of 7 A were tested to steadily power the solenoids without reaching the melting temperature of the enamel (i.e.: 240°C). Using a F. W. Bell Gaussmeter (model 4048), the magnetic field generated by the solenoids was measured to roughly map the axial distribution of the field and the linearity of the magnitude of the field with the current. Three distances from the solenoid exit plane were scanned at different DC current level.

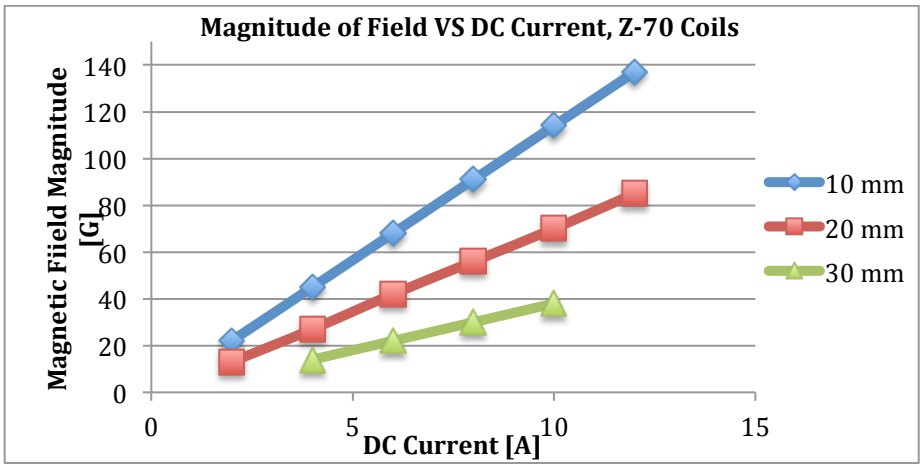

Figure 3.18: *Z-70 annular Hall thruster Auxiliary Solenoids DC characterization.*

As can be seen from the graph, about 6 A DC current is necessary to obtain 20 Gauss in the middle of the channel of the thruster that is at about 30 mm from the exit pane of the solenoid. At 6 A the value of the filed in the core of the solenoid is about 200 Gauss; the field produced is slightly lower in magnitude compared to the calculations.

3.3.3 CHTr cylindrical Hall thruster, auxiliary solenoid development

For the second thruster used in the experimental campaign, a cylindrical Hall thruster, a different design for the air core auxiliary solenoid has been adopted. A much lower inductance was choose using ten times less turns of wires resulting in a field of about 40 G at the center of the coil, with a 10 A DC current. Considering that the use of time varying signal was, the effective value of the dissipated power in the solenoid is still below the limit value that would result in an overheating of the component. More details about the resulting power system will be presented in the next chapter, while the main loss mechanisms are outlined after the description of the coil. The position of the solenoid is different as well: a single coil is indeed wrapped around the discharge channel. In chapter 5 an introduction to the physical mechanism of interaction of such a coil with the oscillating behavior of the thruster if reported. A table with the main geometrical parameters of this coil is reported below along with a simulation of the magnetic field on the axis of the coil generated with 10 A DC current:

CHTr Coil	
Inner Diameter	33 mm
Length (coil axis)	5 mm
Wire diameter	1,9 mm
Outer diameter	45 mm
Rows	2
Layers	7
Turns	14

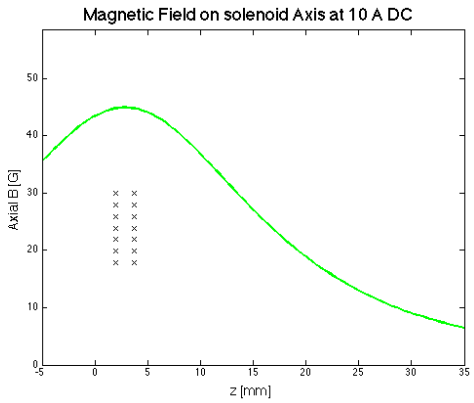

(a) Geometrical characteristics of the coil. (b) Simulation of the magnetic field on the axis.

Figure 3.19: *Geometrical characteristics and filed on the axis simulation for the cylindrical hall thruster auxiliary coil.*

A two-dimensional simulation of the stationary magnetic field generated by the coil driven with a 10 A DC current is reported below. The Matlab code used to simulate the two-dimensional field solves the elliptical integrals that are traditionally connected with the computation of the filed generated by a finite length solenoid. The following plot shows half of the axial symmetric solenoid; the dimensions of the computational domain are comparable to the channel of the cylindrical Hall thruster. The filed lines are mostly straight at the center of the channel and very bended in the region close to the winding. This topography was expected and desired since the diameter of the coil is much larger than the width of the wrapped wire.

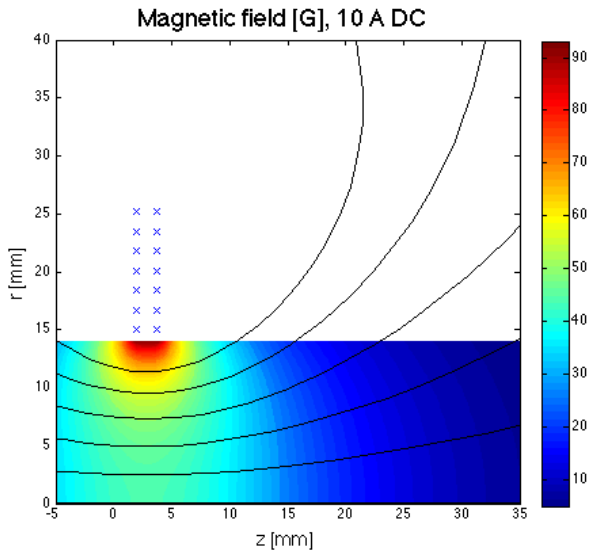

Figure 3.20: *Simulation of the two-dimensional field generated by the coil.*

The peak value of the field on the axis of the solenoid, that coincides with the axis of the thruster, is approximately 45 G at 10 A, while the axial field close to the winding reaches 90 G showing a considerable radial component as planned. The technological and electric characteristics of this coil are also very different compared to the Z-70 ones is needed in order to simplify the power system. A lower inductance coil is indeed realized with great attention to reduce also the loss mechanism inside the solenoid itself. As already said, eddy current creates several problem when dealing with varying magnetic field; one consequence of this phenomenon is the skin effect. For alternating currents, as already said, electrons flowing in the conductor have greater density in the region close to the surface of the wire; this effect causes the resistance to increase with increasing frequency. In order to familiarize with the importance of the phenomenon, it is sufficient to consider that, in a copper wire, at 60 Hz the skin depth is equal to 8,57 mm while at 10 kHz it is 0,65 mm and at 100 kHz it is as low as 0,21 mm. This will cause an apparent increase in the resistance of the coil above the DC value. Unfortunately using a small enough wire able to produce reasonable skin effect losses is not an option. In this case the required number of turn able to produce the desired B field would indeed produce a too high inductance of the solenoid increasing the practical complexity of the power system. In order to solve this problem the use of Litz wire was set. This type of wire strongly attenuates the problem by using multiple strands of copper wire which are individually insulated from each other, resulting in a sufficiently high cross sectional area and, at the same time, in a small enough area of the each single conductor. Later a better description of this interesting kind of wire is outlined.

The current density is thus non-uniform in the section of the conductor resulting larger in the region close to the surface of the wire and creating a higher resistance. The inner portion of the conductor is thus not used, as if the diameter of the wire was decreased. As already discussed, this effect is a function of the frequency the frequency:

$$J = J_o e^{-d/\delta_s} \quad with \quad \delta_s = \sqrt{\frac{\rho}{\pi \mu f}}$$

where J_o is the current density on the surface of the conductor. δ is a parameter that indicates the depth from the surface at which the current density is about 37% (i.e.: $1/e$) of J_o. This depth depends on three parameters: ρ is the resistivity of the material, in this case copper ($\rho = 1{,}73\times10^{-8}\ \Omega\text{m}$), μ that is the magnetic permeability of the conductor and f which is of course the frequency. Considering a circular wire an approximate relation can be easily derived obtaining the following useful relation:

$$R_{skin} \cong \frac{L}{\pi D}\sqrt{\pi \mu \rho f} \propto \sqrt{f}$$

hence the resistance of the wire taking into account the skin effect results proportional to the square root of the frequency, definitely a strong effect.
Skin effect is not the only source of AC losses: proximity effect increases power loss as well. Considering two adjacent conductors carrying alternating signals, the distribution of the current is not homogeneous: in an inductor, for example, were wires lie parallel to one another, the magnetic field of one wire will induce eddy currents in the other wire. These longitudinal currents flow in long and narrow loops in the conductor resulting in two different situations in the two halves of the wire itself. On the side of the wire that is opposite to the first one, main current and eddy one will flow in the same direction, while in the side close to the other wire the two current will flow in opposite directions. The net effect is a redistribution of the current density that results higher in the side facing away from the first wire and lower on the side that faces the first wire. Similarly, current density results in an opposite distribution if the adjacent wires carry currents flowing in opposite directions. The resistance is thus increased considering the focusing effect of the current flowing in the conductor. It is thus desirable not to have a very high number of layers; in some applications crisscross pattern is used in successive layers in order not to have wires lying parallel to one another. Different methods are available to estimate the power loss due to this phenomenon, Dowell and Ferreira being the two best-known ones; but recent improved techniques are available [46]. A quantitative description is by the way beyond the scope of this thesis. As already mentioned, a very good way to lower the power loss associated with the described effects

rely on the use of a special kind of wire called Litz wire, after the German word *Litzendraht,* German for braided/stranded wire or woven wire. This type of wire is widely used for high frequency coils. As already said, it consists of a large number of wires, each of them individually coated in insulating enamel and then stranded together.

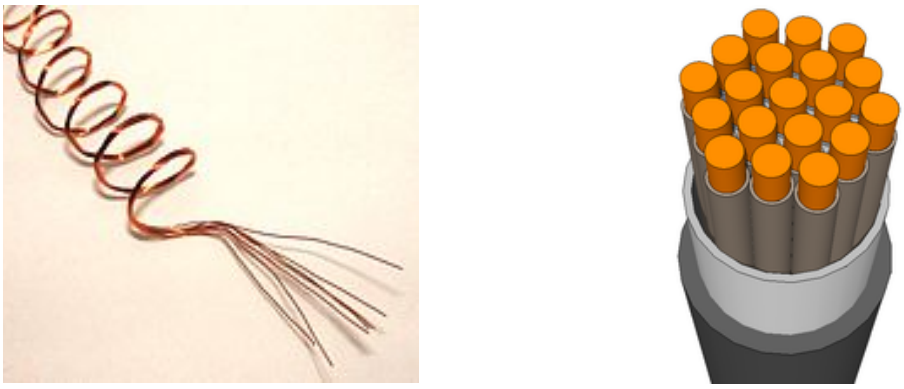

(a) Picture of a 8 strands Litz wire. (b) Typical section of a Litz wire, 3D modeling.

Figure 3.21: *Typical construction geometry of a Litz wire.*

Typical applications for litz wire coils are high frequency transformers, audio equipment, antennas, electronic ballasts, induction cooking equipment, photocopy machines, color monitor tube assemblies and many other high frequency signal and power circuits. The main purpose of such a configuration is to increase the surface area of the conductor in order to reduce the skin effect, which usually causes big resistive losses that arise at high frequency applications and consequently an extra heating source due to resistance losses. This type of wire helps reducing the negative effect of the proximity effect as well. In a winding realized with litz wire, this effect may be sub-divided into internal and outer proximity effect: the internal one takes place within the bundle, while the outer one is related to the other bundles. The twisted or weaved geometry of litz wire ensures that the current is equally distributed in the numerous strands that are in the bundle. In the case of big, multi-bundles litz wire, the disposition of the bundles inside the wire impacts the performance of the conductor. Attention should be paid in choosing the proper insulating material in order to prevent its melting during the operation; both internal power and external radiated heat flux will increase the temperature of the component. After a technical and commercial survey, nylon insulation was selected, considering the relatively high melting temperature, 155° C, and for cost and availability reasons. Thermocouples can be used to track the thermal history of the coil during the testing phase if necessary. A comparison between DC and AC operation temperature can provide AC power losses data as well. In the following table the most commonly used insulations are listed.

Insulation	Recommended Max. Operating Temperature	Advantages	Limitations
Cotton	105°C	• Low cost serving. • Good resistance to abrasion.	• Poor space factor compared to Nylon or Celanese. • Non-solderable.
Nylon	155°C	• Good space factor. • Excellent abrasion resistance. • Solderable.	• Hygroscopic
Dacron® (POLYESTER)	155°C	• Good abrasion resistance. • Solderable. • Slightly higher maximum operating temperature than Nylon.	• Better space factor than Cotton or Glass but poorer space factor than Nylon.
Nomex® (HI-TEMP Aramid)	250°C	• Good space factor. • Good electrical properties at high temperatures.	• Non-solderable. • Higher cost than other fibers.
Glass	260°C	• Good electrical properties at high temperatures.	• Space factor equivalent to Cotton. • Non-solderable.

Figure 3.22: *Most common fiber insulation materials for litz wire [42].*

Once a preliminary operating frequency range has been estimated, a specific type of Litz wire is selected in agreement with the following table.

FREQUENCY	RECM'D WIRE GAUGE	NOM. DIA. OVER COPPER	DC RES. OHMS/M' (MAX)	SINGLE STRAND R_{AC}/R_{DC} "H"
60 HZ to 1 KHZ	28 AWG	.0126	66.37	1.0000
1 KHZ to 10 KHZ	30 AWG	.0100	105.82	1.0000
10 KHZ to 20 KHZ	33 AWG	.0071	211.70	1.0000
20 KHZ to 50 KHZ	36 AWG	.0050	431.90	1.0000
50 KHZ to 100 KHZ	38 AWG	.0040	681.90	1.0000
100 KHZ to 200 KHZ	40 AWG	.0031	1152.3	1.0000
200 KHZ to 350 KHZ	42 AWG	.0025	1801.0	1.0000
350KHZ to 850 KHZ	44 AWG	.0020	2873.0	1.0003
850 KHZ to 1.4 MHZ	46 AWG	.0016	4544.0	1.0003
1.4MHZ to 2.8 MHZ	48 AWG	.0012	7285.0	1.0003

Figure 3.23: *suggested single strand gauge as a function of the frequency range [41].*

AWG 36 was chosen in order to ensure proper operation up to 50 kHz: in this way, even if the fundamental frequency is much lower, possible harmonics present in the signal can flow through the coil without experiencing major attenuation. Finally the number of strands was selected. Equivalent diameter of

the litz wire should be carefully chosen in order to offer a sufficiently large overall cross sectional area and avoid overheating because of a too high current density. Thus an equivalent AWG wire size was selected considering the maximum expected RMS (i.e.: route mean square value) current and the time of operation required for the preliminary testing, recalling the 155° C temperature limit determined by the selected nylon coating. The equivalent cross sectional area of litz wire having different number of strands is reported in the useful table that follows:

Equivalent AWG	Circular Mil Area	Number of Wires	AWG of Wire
RECOMMENDED OPERATING FREQUENCY - 20 KHZ TO 50 KHZ			
30	100	4	36
28	175	7	36
26	250	10	36
24	400	16	36
22	675	27	36
20	1025	41	36
18	1625	65	36
16	2625	105	36
14	4125	165	36
12	6625	265	36
10	10500	420	36
8	16500	660	36
6	26250	1050	36
4	45000	1800	36
2	66500	2660	36
1	84000	3360	36
1/0	108000	4320	36
2/0	135000	5400	36
3/0	171000	6840	36
4/0	211500	8460	36

Figure 3.24: *Common Litz wire types and constructions [41].*

Different Litz Wire typologies are available depending on the number of strands. Increasing the current handling capability will result in a higher number of strands. Equivalent AWG 16 was selected, resulting in a wire containing about 100 strands. Different constructions are possible depending on the number of strands; in the case described above, the easiest stranding architecture is used: type 1 showed in the picture that follows. When this number is higher, the construction of the wire can also consist of multiple bundles in which a number of sub-bundles are stranded together resulting in more and more complex

arrangements presenting a number of individual wires as high as several thousands. The two most common types are shown below.

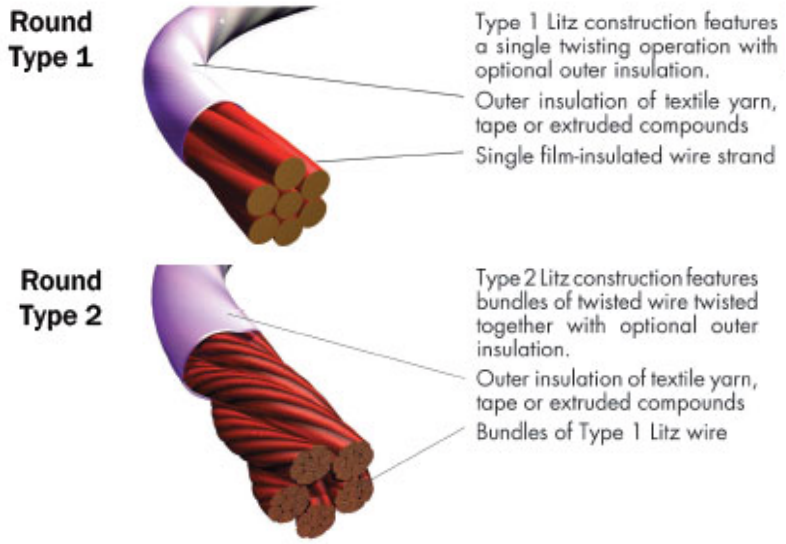

Figure 3.25: *Common Litz wire types [41].*

The smaller constructions of Litz Types 1 and 2 are typically used in High efficiency circuitry (i.e.: high Q factor), such as toroidal coils and transformers. Larger and more complex types of litz wires, not shown, exist and the reader can find more information on the literature. After the described design process, the auxiliary coil was thus built and installed around the thruster channel.

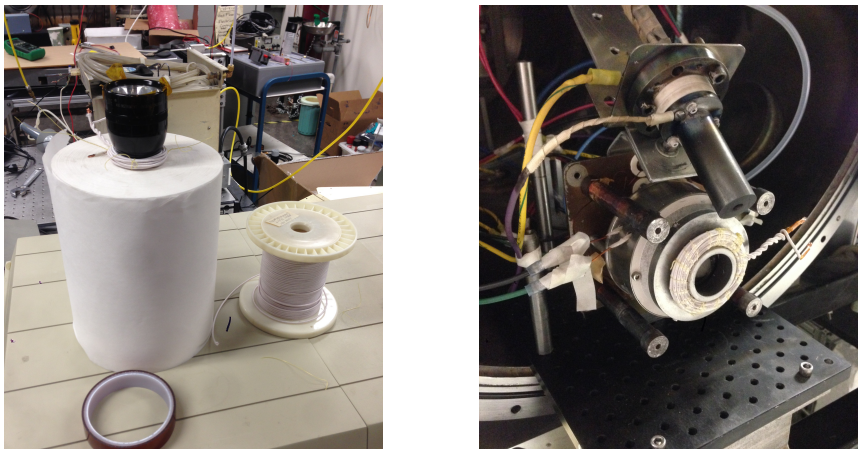

(a) Wrapping the coil with Litz wire. (b) Auxiliary coil installed on the thruster.

Figure 3.26: *Cylindrical Hall Thruster Auxiliary Solenoid realization.*

Chapter 4

Auxiliary solenoids power system and signal processing

4.1 Introduction

In the following section a preliminary analysis of the power and signal processing system is presented. The study of a circuit with inductive loads driven in an arbitrary regime is definitely a topic that requires a careful analysis in particular when an amplification stage is required into the signal processing chain. When dealing with broadband signals this results in an even more challenging problem. The analysis that follows is then a preliminary study that aims to identify the key parameters necessary to realize a prototype of the power and processing unit. All the considerations that follow are carried out under the simplifying assumption of no plasma in the thruster. Once the plasma is on, some of the parameters are of course going to be different since permeability and permittivity of the region around the solenoids are going to be different from the vacuum one. This analysis addresses however a more basic study.

4.2 Impedance of the auxiliary solenoids

After identify the described main limiting factors of the previous studies, some improvements were addressed. The most challenging aspect of designing the power system for the auxiliary solenoids is related to their intrinsic reactive behavior. A sinusoidal signal is assumed in the first part of the following description. In order to choose the best power and control system for the solenoids, their characterization from an electric point of view was conducted. Electromagnets are used to generate magnetic field; these components are able to store energy and eventually give it back. From this peculiarity they are named reactive components that present an interesting behavior from an electric point

of view. For reactive circuits the concept of resistance is generalized and renamed "Impedance" or Z, and it is thus defined as the ratio between voltage and current; unlike resistance it possesses both magnitude and phase. This parameter is indeed a complex number and it can be represented as a vector in a complex plane where the x-axis is real and the y-axis is imaginary. When a circuit is driven in DC, impedance and resistance coincide and the vector lies on the real axis (i.e.: x-axis). The real part of the impedance represents the resistance of the circuit, while the imaginary part is called reactance.

$$\boldsymbol{Z} = \frac{\boldsymbol{V}}{\boldsymbol{I}} = R + jX$$

where j is the imaginary number. The magnitude of the impedance is equal to the ratio between effective value or peak-to-peak value of voltage and current and it is measured in Ohm [Ω]. This parameter fixes the required voltage at the power supply output once the current value need to produce a desired value of magnetic field is determined. Impedance magnitude is defined as follow:

$$|\boldsymbol{Z}| = Z = \sqrt{R^2 + X^2}$$

Phase is an important parameter as well. It is define as follow:

$$\theta = arctan\frac{X}{R}$$

This angle represents the phase shift between voltage and current. It is clear that when this value is high, even if the voltage generated by the power supply is synchronized with the signal generator or with the output of a control circuit, the current will result not in phase with the voltage. The magnetic field generated will thus result not correctly timed with the signal amplified, being the field proportional to the current flowing in the solenoid.
Unfortunately reactance is strictly related to inductance that is in turn correlated to the current level necessary to produce a certain value of magnetic field as already explained in the previous chapter. In a pure inductor (i.e.: an ideal solenoid) the reactance is proportional to the inductance value L, while in a capacitor the relation is different:

$$Z_L = j\omega L \quad and \quad Z_C = \frac{1}{j\omega C}$$

where C is the capacitance value. In a real solenoid, all three elements are combined: resistance, inductance and capacitance. Different models of a real

inductor can be considered depending on the precision required in the simulation of the circuit. In any case, a real inductor is an RLC circuit. Thus, a resonance frequency is present and the relation of the magnitude of the impedance with frequency is not linear as expected in the ideal case. Later on some data showing this trend will be presented. In all the inductors considered, the resonance frequency is above the range of interest. As already pointed out, a high magnitude of the impedance corresponds to a high voltage different at the leads of the solenoid itself in order to reach the current level required.
Assuming not a big difference in the impedance of the coils of the thrusters of similar size, it is clear that using them as an actuator for the magnetic field modulation would result in a difficult load to drive, especially at high frequency, since even a small current value requires a big voltage. Of course the larger the voltage is, the higher slew rate the power supply/amplifier has to be able to handle in order to generate a signal with the required frequency. From previous measurement on the inner electromagnet in a BHT-600 an inductance of almost 100 μH was computed [48]; this value is already large enough to require attention in the power system design that can not be a single power amplifier connected to the load.
Considering the typical current values used to power the electromagnets of the Hall Thrusters, A the Z-70 auxiliary solenoids were designed to produce a relatively strong magnetic field with a reasonable current, few amperes. Unfortunately this results again in a high impedance of the solenoid itself that cause the inductance to vary strongly with the frequency of the signal amplified. A measure of the magnitude of the impedance for a single solenoid is reported below, it uses measured values of voltage and current to calculate the impedance as it varies with frequency.

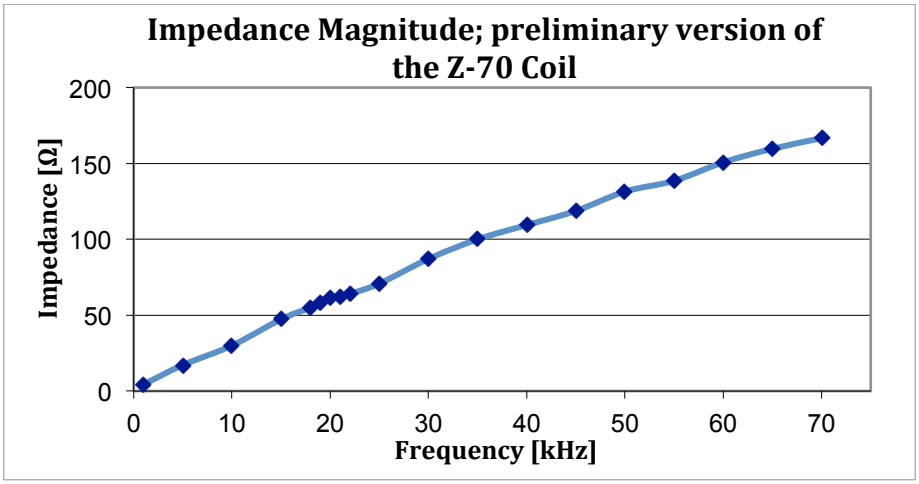

Figure 4.1: *Impedance measurement of the preliminary version of a Z-70 auxiliary solenoid.*

As shown in the graph, the load is mostly reactive; the resistance is indeed represented by the above y-intercept. Considering a frequency range around 15-20 kHz, where the most interesting low frequency oscillations are usually located in the Z-70 Thruster, the value of the reactance is quite large, especially recalling that it was originally planned to use four solenoids. Series connection is indeed recommended in order to be sure that the same current flows through all the solenoids. Parallel connection would result in lower impedance, but it is not guarantee equal partitioning of the current. Difference in the plasma characteristics in the region in front of each solenoid can indeed impact the flowing of the current in a parallel configuration. Plasma affects indeed the inductance of the solenoid and this would results in differenced in the impedance values of the four solenoids with consequent current imbalance. Basics relations for series and parallel impedance are recalled to show how the equivalent impedance can be altered with series or parallel connection.

$$Z_{Serie} = \sum_{i=1}^{N} Z_i \quad and \quad Z_{Parallel} = \sum_{i=1}^{N} \frac{1}{Z_i}$$

From the measurements reported before, the value of the inductance of the coil was deduced using the simple relation, in which parasitic capacitance is neglected:

$$L = \frac{1}{\omega}\sqrt{Z_{TOT}^2 - R^2}$$

The value of L was computed for each point obtaining in this way the following graph:

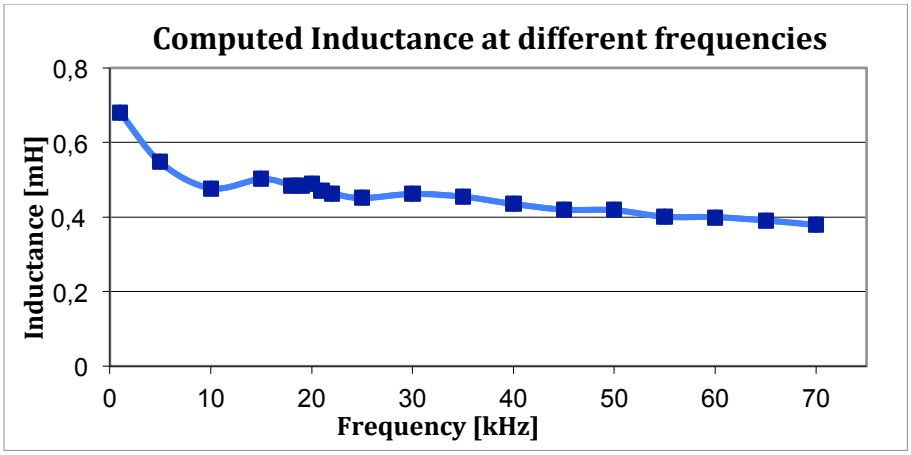

Figure 4.2: preliminary version of Z-70 auxiliary solenoid inductance computed.

Even if a constant value of the inductance was expected, the result is compatible with the strong simplifications assumed. No inter-winding capacitance was considered and moreover a constant value of the resistance (i.e.: real part of the impedance) was assumed. This is definitely not realistic: numerous AC losses mechanisms are indeed present inside the solenoid. Indeed, as already pointed out in chapter 3, skin effect forces electrons to flow closer to the surface of the wire creating in this way a reduces cross section available for the current. In any case, even if some uncertainties are present, a value close to 0.45 mH can be assumed as a rough representation of the preliminary version of the annular Hall thruster coils. This value is high enough to generate difficulties: high inductance coils are more difficult to drive since they require matching networks or other expedients. It is indeed easy to show how a high inductance creates the need of a high voltage in order to make the current varying as showed by the well-known relation that is derived under the assumption of a purely inductive load:

$$V = L\frac{dI}{dt}$$

The relation has the same meaning in the time domain of the definition of the impedance in the frequency domain. Self resonance frequency is important as well: a smooth trend of the impedance is desirable in order to maintain a fairly constant ratio between voltage and current, possibly with a low phase angle in order to assure the best condition for open and closed loop interaction with the thruster. Especially in broadband applications, it is not desirable having the resonance of the coil in the range of interest. In the following graphs, characteristic trend of the impedance of a solenoid over a wide range of frequency, up to 2 MHz, are reported. The peak of the impedance at the resonance is associated with the nature of the coil that can be, in the simplest approach, modeled as an RLC parallel circuit where C and R are the capacitance and resistance of the winding. Computing the impedance of this circuit and further manipulating it brings to the resonance frequency.

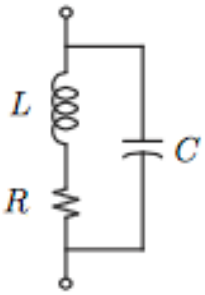

$$\frac{1}{Z} = \frac{1}{j\omega L + R} + j\omega C = \frac{j\omega L + R}{-\omega^2 LC + j\omega RC + 1}$$

that presents a resonant at the following frequency:

$$\omega_0 = \sqrt{\frac{1}{LC} - \left(\frac{R}{L}\right)^2}$$

More precise and numerous measurements were conducted on the two coils realized for the annular Hall thruster connected in series; a modern RLC-meter, model *Agilent E4980A* was used to perform the measurement. The presence of a resonance is clear as shown by the phase graph as well.

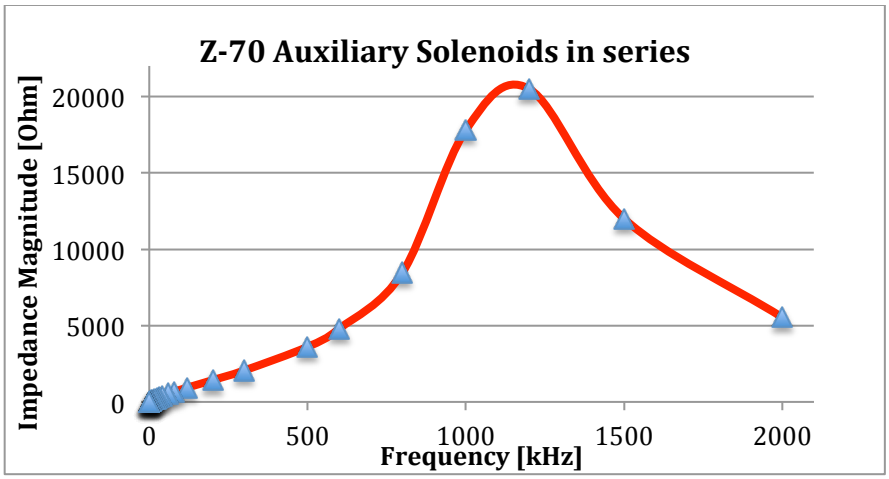

(a) Impedance Magnitude Z-70 Auxiliary solenoids in series.

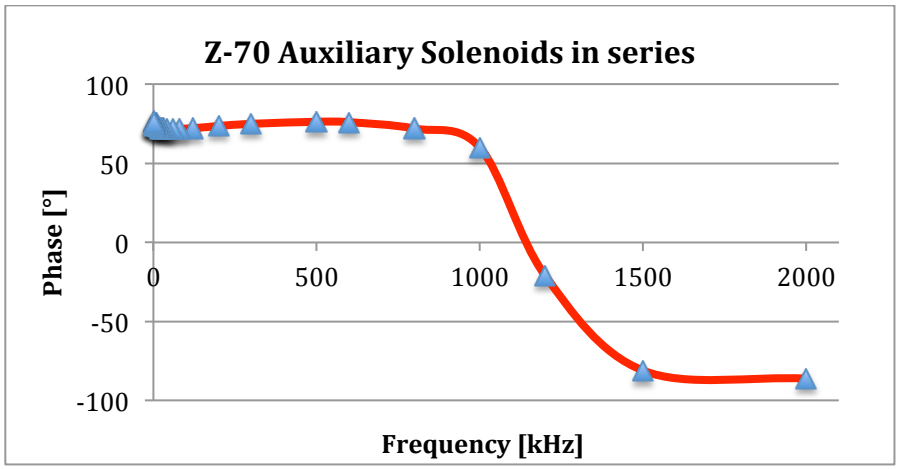

(b) Impedance Phase Z-70 Auxiliary solenoids in series.

Figure 4.3: *Z-70 auxiliary solenoids in series Impedance measurement*.

Even if the resonance is far away from the frequency of interest for the interaction system (i.e.: DC - 40 kHz), the magnitude of the impedance is quickly rising ranging from a value of 10 Ω at 50 Hz to a almost 400 Ω at 40 kHz. Considering the inner electromagnet of a laboratory Hall thruster, the Stanford Hall thruster, the situation is even worst. The iron core increase the impedance value to the kΩ range within the first hundred Hertz of the frequency

axis, showing then a sharp decay because of the parasitic capacitance that makes the phase negative as shown by the following figures.

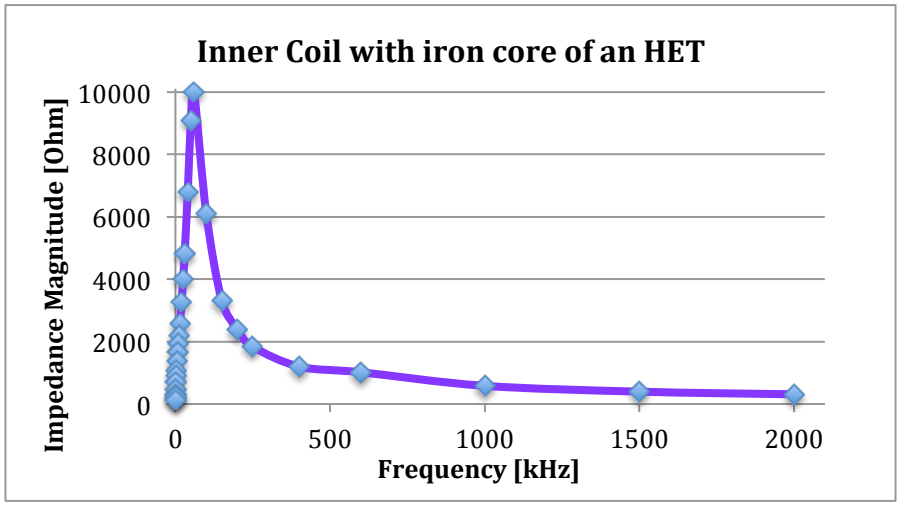

(a) Impedance Magnitude of the SHT inner electromagnet with core.

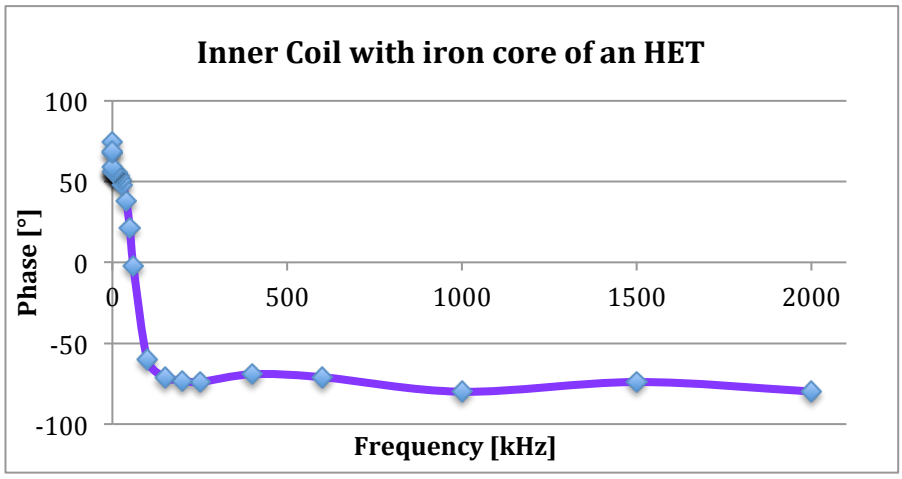

(b) Impedance Phase of the SHT inner electromagnet with core.

Figure 4.4: *SHT inner electromagnet with core, Impedance measurement.*

It is thus clear that, especially with the main electromagnets of the Hall thruster, it is definitely challenging realizing an interaction system, in particular if no broadband matching network is placed in between the power supply and the actuator of the system (i.e.: the electromagnets).
The reported graphs suggest that a different actuator is desirable in order to simplify the choice of the power system. In chapter 3 the auxiliary coil developed for the cylindrical Hall thruster was described and it is now further

characterize from an electric point of view in order to acquire more information that are necessary in the choice of the coil power supply.
The same impedance measurements were conducted on this coil as well. A much lower and smooth curve was expected considering the low number of turns made with litz wire and the absence of an inner metallic core in order not to have heavy distortion of the exciting signal.

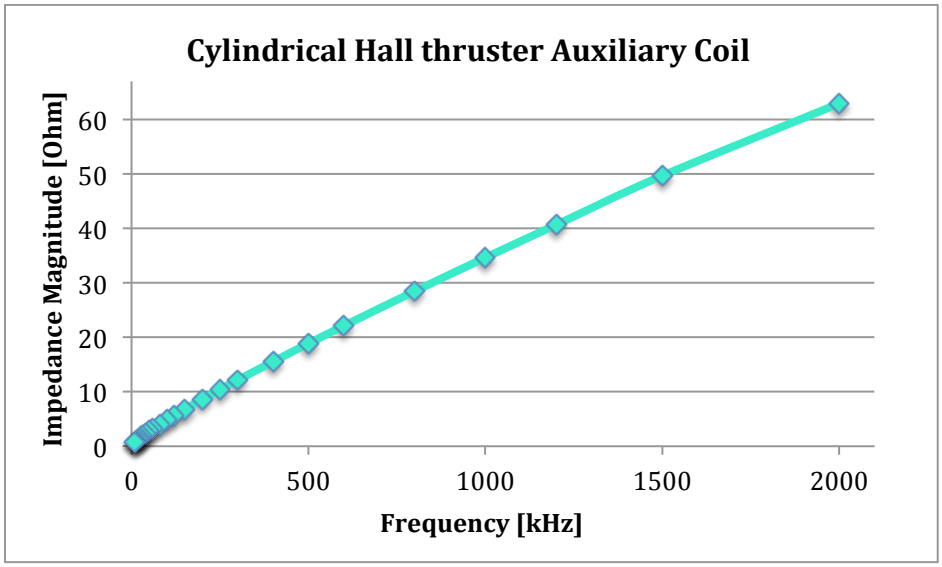

(a) Impedance Magnitude CHT Auxiliary coil.

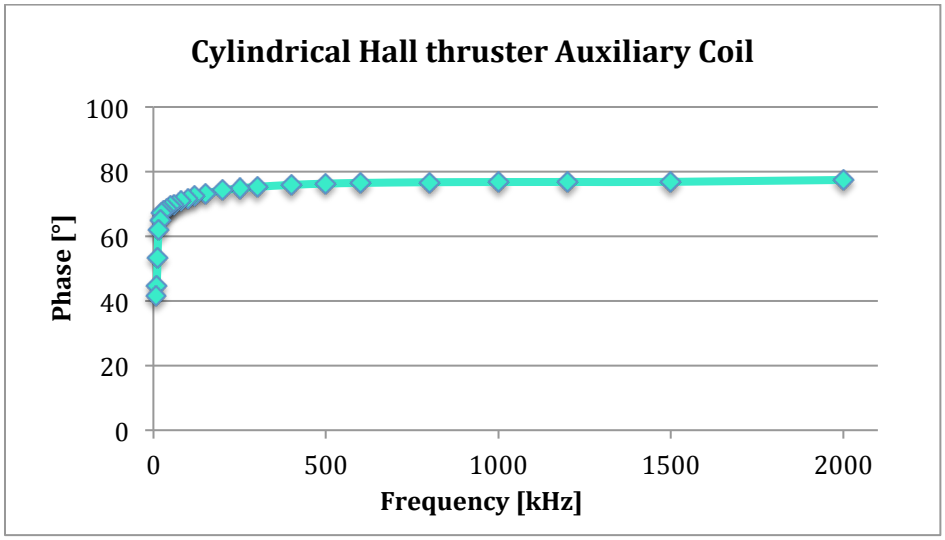

(b) Impedance Phase CHT Auxiliary coil.

Figure 4.5: *Cylindrical Hall thruster auxiliary coil Impedance measurement*.

As more evident in the plotting of the phase where the lowest value is about 40°, frequencies considered for the test are above 4 kHz. Below this value, the RLC meter was showing strong fluctuation in the measured value of the impedance, both magnitude and phase. The data reported are associated with the auxiliary coil already installed in the thruster as shown in chapter 5. The effect of the electrical lines, vacuum chamber feedthrough and, most important, thruster metallic components near the coil is thus included in the measurements. It can be seen that the magnitude of the impedance at the frequency of interest in the case of the Cylindrical Hall thruster, in which the fundamental frequency of the fluctuation used for testing is around 4 kHz, is in the order of few Ohm. This implies that the voltage required to achieve relatively high peak current values, in the order of 20 A, is in the order of some tens of Volt. The result is thus definitely good and from the data presented the auxiliary coil inductance value can be estimated around $10\ \mu H$, very close to the expected value.
A quite high power level is by the way required in order to vary the value of the magnetic filed at kilohertz frequency even if the peak value of the field is pretty low, in the order of tens of Gauss. The reason lies in the property of magnetic field to store energy. It can be shown that the following relation holds:

$$E_{field} = \int_V \frac{1}{2}\boldsymbol{H}\cdot\boldsymbol{B}\,dV$$

Recalling that $\boldsymbol{B} = \mu\boldsymbol{H}$**,** for an ideal and homogeneous filed it can be found that the power required to generate the specified field in a time interval Δt is:

$$P_{field} = \frac{1}{2\mu}VB^2\frac{1}{\Delta t}$$

where *V* is the volume of the region that contains the homogeneously distributed magnetic field of peak value *B*. It can also be showed that this relation is equivalent to the following one, where *V* is now the voltage across the inductor:

$$P_{solenoid}(t) = i(t)V(t) = i(t)L\frac{di(t)}{dt}$$

that is valid for an ideal solenoid having an inductance equal to L. As an example, let's consider a triangular wave at a frequency of 5 kHz. The period of such a frequency is $T = 1/f = 200\ \mu S$; during this time the maximum is reached after a quarter of a period so $\Delta t = 50\ \mu S = 50\times10^{-6}s$. Assuming a filed peak value equal to 50 Gauss and an ideal vacuum volume of $15\ cm^3$, the resulting power is more than $89\ kW$. This energy stored in an air cored or vacuum inductor is much higher compared to the use of a core with high μ. It is

now clear the importance of recovering the energy that is released by the coil while the intensity of the magnetic field is decreasing. Unfortunately with complex waveforms, the frequency content of the excitation signal of the coil can be quite wide; hence the need of a broadband matching network [49]. Considering the complexity level in the design of such a component despite several computed aided tools [50], a power system with embedded circuitry to match the load was desirable.
A more detailed literature research revealed how a very similar problem is faced in a completely different scientific field: Magnetic Resonance Imaging. Inside the machines used in this kind of application, big and peculiar coils are found: they are called gradient coils. These coils are usually made of thin copper sheets laid down on the typical cylindrical surface of MRI machines and they are used to generate a magnetic field that alters a primary field, generating prearranged gradients, hence their name. These gradients are responsible for the variation of protons resonance frequency depending on their position [51]. In order to power the gradient coils, a set of suitable signal, having generally frequency component in the audio frequency range, must be amplified. The signal amplifiers used are powerful machines called Gradient amplifier. The design of these devices is rather complex, partly because of the circuitry dedicated to the matching of the reactive impedance that characterizes the gradient coils. A lot of different gradient amplifier exist, in general they are able to provide very high current, up to hundreds of amps, as well as high voltage, greater than $1\ kV$ in order to assure fast slew rate of the signal flowing through coils whose inductance usually ranges between hundreds of μH and H. The gradient fields have to be indeed modified at frequencies of up to some kHz for fast imaging. These characteristics are obtained using a switching mode power supply core that works at very high switching frequency, in order to amplify the command signal with high fidelity. An embedded matching network handle the reactive power that is the vast majority of the power delivered to the coil, typically, in the biggest machines, $1\ MVA$ versus $50\ kW$ of resistive power. A more detailed description of this kind of signal amplifier can be found in the relative literature as reference [52]. Due to the very high cost and very high knowledge required to buy and operate such a device, it was decided to use a similar device, much less powerful but, in principle, with the same architecture: an audio amplifier.

4.3 Audio Amplifier, Circuit Analysis and Testing.

After a better comprehension of the power sources capable of satisfying the desired requirements, it was decided to use a high power audio amplifier for the preliminary testing of the system. Big audio amplifiers are essentially equivalent to small gradient amplifiers: indeed they offer a large bandwidth (usually 20 Hz

– 20 kHz) with a pronounced or soft decay above that frequency depending on the quality of the device. After an extensive technical and commercial research, a *CE 4000 Crown* Audio amplifier was selected: a 3 kW class I amplifier [54]. Some of the older gradient amplifier came indeed from the same company. This kind of switching mode amplifier can handle reactive loads and they are able to reuse energy returned from the load itself preventing the amplifier to generate that energy again after having dissipated the one entering the device. Audio amplifiers perform at their best with low impedance loads. It is now clearer why litz wire was used. As already said, because of the skin effect, a small diameter of the conductor is required with the connected limit of the current level that can be safely used to drive the coil. Since a low number of turns in needed in order not to have a big impedance, the resulting field would be too weak. That is how litz wire solves the problem, offering at the same time a big cross sectional area allowing large current to flow with a reasonable current density and small diameter of the single strand. Even if a speaker presents typically an impedance with a different shape compared to a plain solenoid [54, 55], audio amplifiers can usually tolerate reactive loads as long as the DC resistance of the load itself is not lower than a certain value, usually 4 o 2 Ω, depending on the unit. Since a low inductance solenoid was selected for the application discussed in order not to deal with a too high voltage across the leads of the load, the number of turns is relatively small as previously presented. Considering that the lower frequency limit of audio amplifiers is usually a couple tens of Hertz, the reactive component of the impedance generated by the coil, at such a low frequency, is almost negligible compared to the minimum required: connecting this load to an audio amplifier would results in a short circuit at very low frequency operation; a series resistor is thus needed. The minimum value of impedance is indeed required in order not drain too much current from the amplifier. This value depends on the device used and on the wiring configuration. A bridged configuration was chosen in order to output the maximum power from the audio amplifier into the single channel represented by the auxiliary coil. In such a configuration, a 4 Ω impedance is required; a resistor was thus introduced in series with the coil. This choice introduces a high power dissipation due to joule effect but assure a safe operation of the amplifier. Part of the power generated by the amplifier is wasted heating the resistor and part of that is used to generate the magnetic field in the coil as the following relation shows:

$$P(t) = V(t)i(t) = \left[L\frac{di(t)}{dt} + Ri(t)\right]i(t)$$

The energy stored in the field is then released by the coil during the part of the cycle in which the magnetic field decreases towards zero.

The resulting circuit was characterize from an impedance point of view using an RLC meter, in the same way that has been described in the previous chapter. The resulting data are plotted in the following graphs.

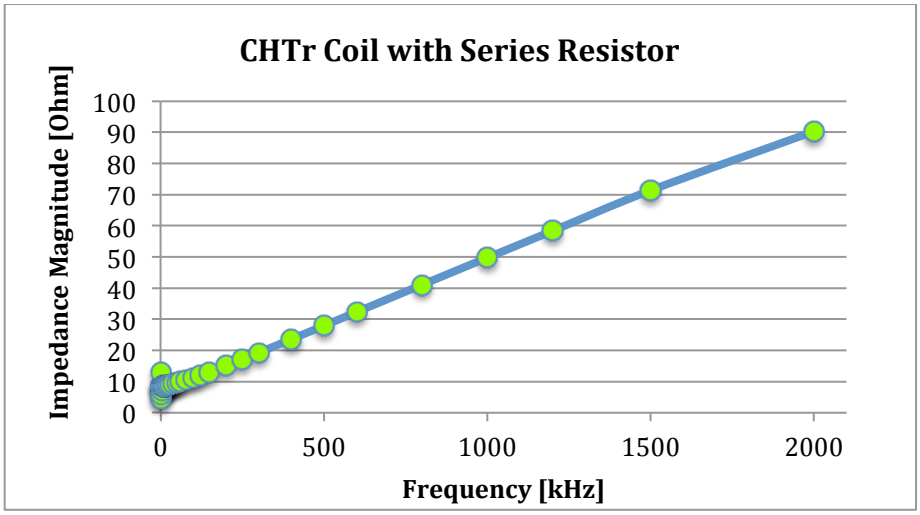

(a) Impedance Magnitude CHT Auxiliary coil and resistor.

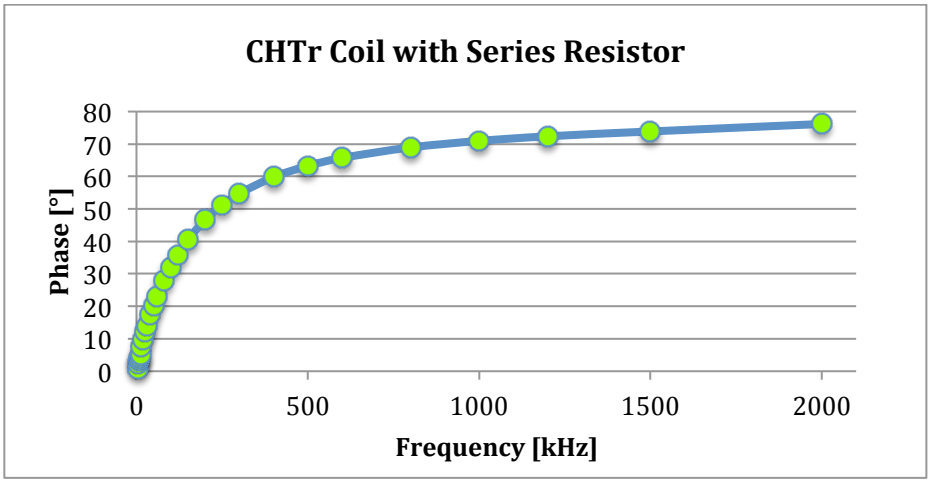

(b) Impedance Phase CHT Auxiliary coil and resistor.

Figure 4.6: *Cylindrical Hall thruster auxiliary coil and series resistor: impedance measurement*.

Slightly higher impedance in the entire range of frequency, including the lower ones, characterizes the new RL circuit as desired, showing in addition a phase that approaches more gradually the asymptotic value. In the next plot a comparison is reported. Plotting on the same graph the two data sets and

comparing the slope of the two lines (i.e.: the one presented before with the one related to the absence of the series resistor in the circuit), it can be deduced that the resistor used is unfortunately not completely non-inductive. A vertical shift of the blue curve was expected but, especially above few hundreds of kHz, the red curve gains height more rapidly compared to the blue one; in other words its derivative is larger.

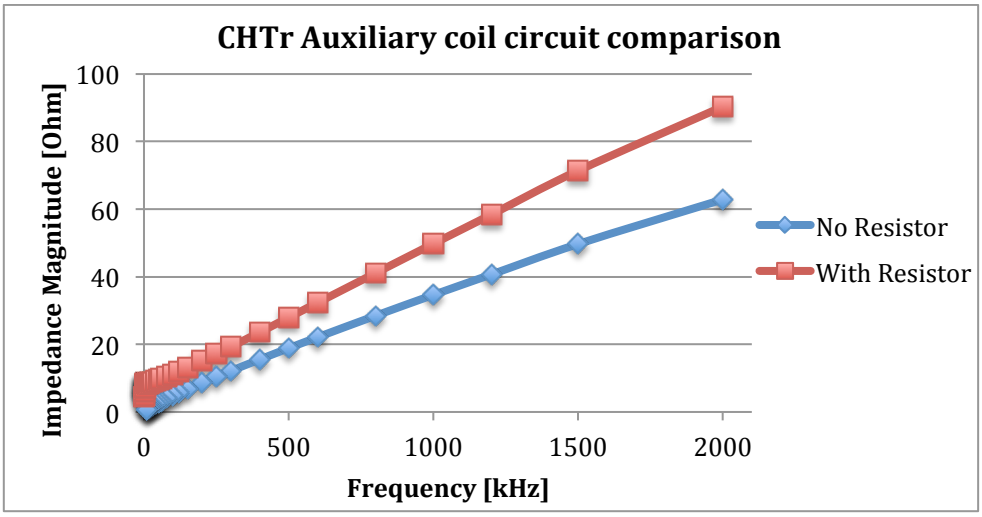

Figure 4.7: *comparison of the impedance with and without resistor in the Cylindrical Hall thruster auxiliary solenoid circuit.*

Focusing on the expected frequency range for the Hall thruster operation that is within 15 kHz as later explained, the impedance magnitude varies between 7 Ω and 9 Ω. In order to extract more power from the audio amplifier the value of the resistor may probably be lowered considering the minimum resistance value required, 4 Ω. In this study, the power outputted from the amplifier was high enough as later reported and the described circuitry was chosen for the final configuration.

After the extensive characterization of the circuit, the power system was tested. The setup and the data taken during the test are described below and summarized in the following two figures. A sinusoidal signal was generated by a signal generator with a peak-to-peak voltage as high as 3 V and it was then amplified by the audio amplified. The resulting current flowing in the circuit connected to the output of the amplifier was sampled using a Pearson probe. The probe used was a *10 to 1* probe able to provide 1 V for a 10 A current, in order to avoid too high voltage on the scope input. The resulting signal is monitored with an oscilloscope and, in the following graph, the peak-to-peak value is plotted as a function of the frequency selected on the signal generator, whose output is sent to the scope as well. Connections between scope, amplifier and

signal generator are made using coaxial cables, while the remaining part of the circuit was wired using litz wire. A wiring diagram is proposed below showing the equipment used during this test.

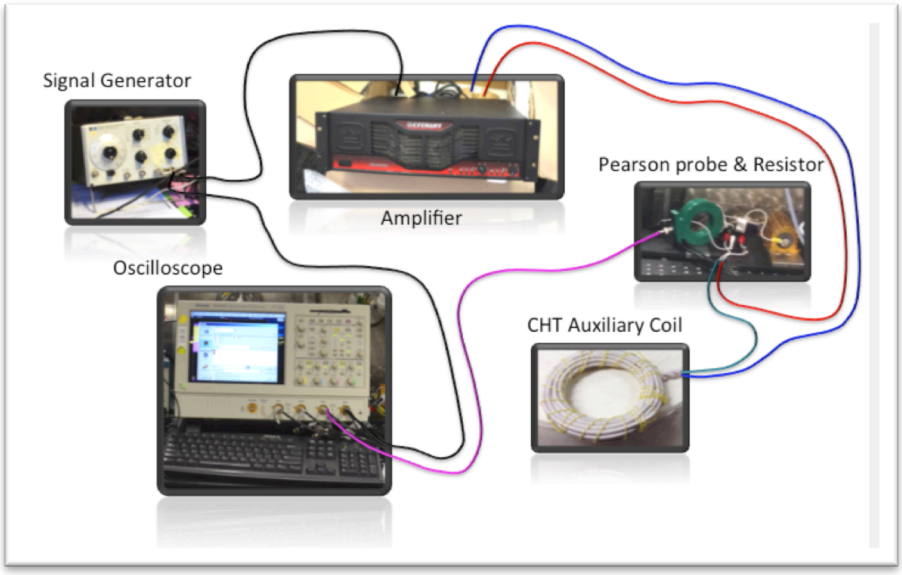

Figure 4.8: *Wiring diagram of the setup used.*

The derived curve showing peak-to-peak value of the current as a function of the selected frequency follows.

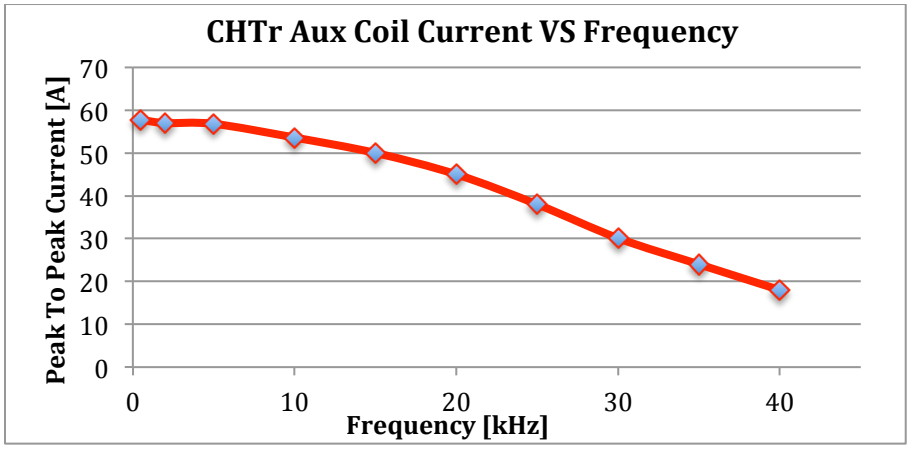

Figure 4.9: *CHTr Coil Characterization, Peak-to-Peak Current as a function of frequency.*

The decreasing trend of the curve can be motivated by two main reasons. As described before, the impedance of the circuit increase with frequency reducing

the current outputted from the audio amplifier that acts as a power supply controlled in voltage mode. A higher resistance would lower the current flowing through the circuit. A decay of the gain of the device is also present at higher frequency, in particular after the upper limit of the audio range that is around 20 kHz. Considering the relatively small decrease of the peak current within the first 20 kHz of the frequency range, approximately 20%, the obtained amplifier performance is definitely acceptable.
Even if the solenoid used for the CHTr does not present any ferromagnetic core, some thruster metallic parts are close to the coil itself as already pointed out during the discussion of the RLC measurements. In order to quantify the influence of the surrounding metallic parts of the thruster on the magnetic field at different frequency, a B-dot probe was used.
This simple device generates a voltage that is proportional to the rate of change of the magnetic filed crossing the inner section of the probe itself. Recalling the basic law of the electromagnetic induction for N loops of wire that experience a variation of the field through it, it is indeed possible to obtained the mentioned dependence.

$$\Delta V = N \oint \boldsymbol{E} \cdot d\boldsymbol{l} = -\frac{d}{dt} \int_A \boldsymbol{B} \cdot \boldsymbol{n} dA$$

It can thus be written that:

$$\Delta V \propto NA \frac{dB}{dt} \propto Bf$$

for a fixed probe geometry. f is the frequency of the sinusoidal excitation current used to drive the coil during this test. In order to quantify the impact of the presence of the metallic parts, the ΔV generated by the probe is monitored with a scope and a large frequency range is scanned. Ideally the peak value of the B field should remain constant for a selected peak value of the excitation signal, regardless to the frequency; thus, plotting the ration $\Delta V / f$ as a function of the frequency itself, it should be possible to verify the pervious statement. As explained in the graph above, by the way, the amplifier used to increase the power of the sinusoidal signal does not present a constant gain. It is thus necessary to further manipulate the acquired data dividing the ratio mentioned above by the value of the current outputted by the audio amplifier at each frequency. It has been indeed already explained that the magnetic field is proportional to the excitation current of the coil. The following plot shows thus the relation reported below, normalized and computed for all the frequencies tested:

$$\frac{\Delta V_{PtP}(f, I_{PtP}(f), materials\ interaction, Bdot\ probe\ parameters)}{f\ I_{PtP}(f)}\ VS\ f$$

The test was performed both with and without the thruster (i.e.: auxiliary coil mounted in the thruster or suspended in air).

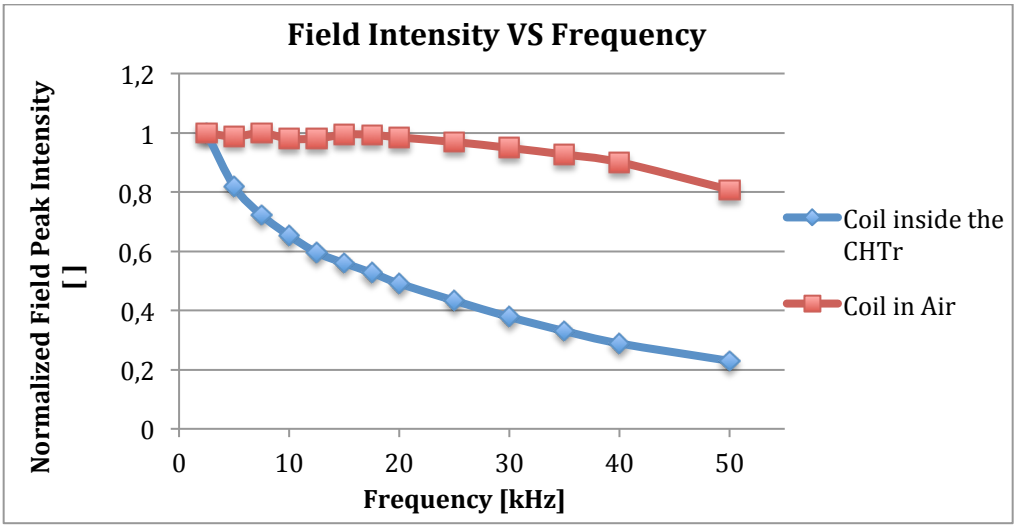

Figure 4.10: *B-dot probe data analysis*.

As it can be seen the situation is far from the ideal one depicted above. In particular, even if no core is present in the solenoid, when the iron components of the thruster are close to it, all the losses mechanisms presented in chapter 3 impact sharply on the amplitude of the magnetic field with the associated decay that increases with frequency.
The situation is much different when the coil is in air: even if a decrease of the peak magnetic field is still observed. It is not clear the reason for this smooth decay. No calibration and frequency characterization of the probe was performed since it was not meant to compute by integration the absolute B field; it is possible that the observed decay associated with the solenoid in air is due to the probe itself even if it is more likely due to some losses in the copper of the coil and of the series resistors that, as already said, where found to be not completely non-inductive. A 20% decay is observed at 50 kHz. In any case, within the 20 kHz range, the air solenoid configuration shows a noteworthy flat behavior meaning that the frequency effect is negligible in the relation that relates the magnetic field with the current of the coil.
Much more lossy is the situation represented by the blue curve associated with the coil inside the thruster. Losses generated by eddy current induced in the metallic elements are clearly visible. Despite the non ideal behavior, the

configuration can be considered a good result: at 20 kHz the 50% of the magnetic field value is still reached in the center of the coil (1.e.: on the thruster axis) and the 65% at 10 kHz. Comparing the reported data with the ones showed at the beginning of chapter 3 obtained in previous studies [48], a big improvement can be observed. In that case, indeed, only the 10% of the DC value of the magnetic filed is detected at the low frequency of 1 kHz while almost no field is found at 10 kHz. A much better result could be achieved if a high frequency compatible magnetic material was used for the metallic parts of the thruster, as already discussed in the previous chapter.
Considering the acceptable resulting behavior of the described system, the setup was used in the experimental campaign with the thruster on as well, as reported in detail in the next chapter. The big and bulky solenoids developed for the annular Hall thruster, the Z-70, will be use mainly in DC and for a few very low frequency, below 100 Hz, experiments without any particular power system, just connecting them to a traditional programmable power supply. With regard to the refurbished cylindrical Hall thruster, CHTr, as already said, the power system presented before will be used for all the open loop tests. Some preliminary closed loop tests will be performed as well adding a component to the power system. In order to better understand the aim of this modified configuration, a brief description of the overall wiring of the setup and of the signal acquisition and processing is now reported.

4.4 Signal acquisition and processing system

As explained in chapter 1 and 2, the magnetic field modulation interaction strategy introduces a time varying component in the magnetic field of the thruster. Two basic options are available, the open loop interaction and the closed loop one. In both cases the discharge current of the thruster has to be sampled in order to monitor the possible variations while modulating the field. Non-inductive shunt resistors are connected in series with the lines where the current waveform has to be monitored, typically the anode line and sometimes the thruster electromagnets line. Voltage across the shunt is then monitored using an oscilloscope. Since both resistor leads are at a non-ground potential, a differential amplifier has to be connected between the shunt and the scope in order to sample the potential difference across the shunt referenced to ground potential. This allows converting the floating signal to a ground-referenced signal that can be displayed safely on any ground-referenced oscilloscope. A commercial high common mode precision differential amplifier has been used, a Tektronix P5200A, along with some home made circuits. A schematic of the thruster and cathode power system follows.

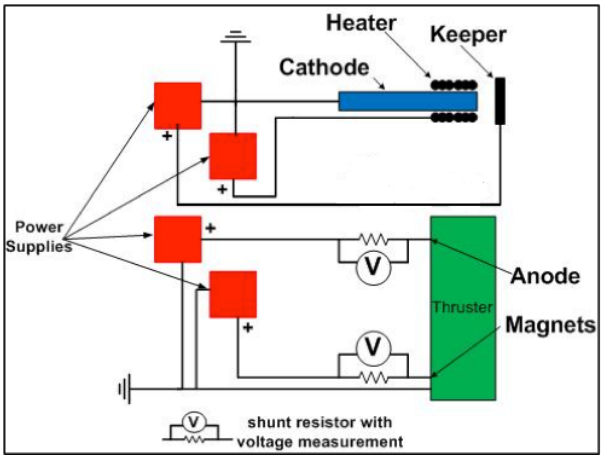

Figure 4.11: *Simplified schematics of the external circuits, adapted from [5].*

The Pearson probe used to monitor the current trace in the auxiliary solenoid circuit described before cannot be used in this case because of the too high mean value of the signal that would saturate the probe.
In the open loop testing, the setup presented above and the solenoid power system described in the previous section are sufficient to conduct the experiment. The scenario is slightly different in the case of the close loop interaction testing where the signal amplified and used to drive the auxiliary solenoid is not outputted by the signal generator anymore. The signal entering the audio amplifier is indeed now correlated to the discharge current trace produced by the thruster. Moreover, as further explained in the next chapter, the coil excitation signal is choose to be proportional to the derivative of the discharge current. In order to realize such signal processing chain, different strategies have been analyzed, including a digital solution based on a LabVIEW interface. After struggling with several implementation issues of such a system, it was decided to realize a more convenient, even if less flexible, active analogic circuit able to derive real time the thruster discharge current sampled by the differential amplifier. A basic schematics of the circuit follows:

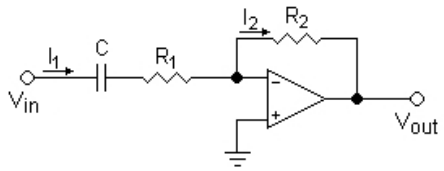

Figure 4.12: *Electrical diagram of the active differentiator circuit.*

This basics circuit is based on the well-known relation between voltage and current across a capacitor:

$$I = C\frac{dV_C}{dt}$$

where C is the capacitance of the capacitor and V_C is the voltage across it. A brief description of the basic principles of such a circuit is now provided. An ideal differentiator circuit will be analyzed: in such a simpler version, no R_1 is present. Recalling the virtual ground effect of the input of the op amp, the same current I considered above will flow through the resistor generating a $V_R = IR$. V_C is then equal to the input voltage of the op amp, while V_R corresponds to the output voltage of the component. As already said, the current across the capacitor is conserved across the resistor; it is thus possible to write the governing equation of the circuit:

$$V_{out} = -RC\frac{dV_{in}}{dt}$$

where the minus sign is given by the op amp. In order to limit the noise amplification, a series resistor is connected with the capacitor. This resistor prevents an excessive amplification of the high frequency components of the signal. It can be showed that the transfer function magnitude of such a circuit is:

$$|G(j\omega)| = \frac{R_2}{R_1}\frac{1}{\sqrt{1+\left(\frac{1}{\omega R_1 C}\right)^2}}$$

It is now clear that at low frequency the traditional transfer function of the inverting differentiator holds: $G(j\omega) = -j\omega RC$; while at higher frequency the gain is constant and equal to: $G(j\omega) = -R_2/R_1$. It is then useful to define the cut off frequency given by:

$$f_{cut} = \frac{1}{2\pi R_1 C}$$

With regard to the ratio between the two resistor is usually good practice to choose a value around 10: $(R_2/R_1) = 10$. Considering that the cut off frequency has to be about ten times higher than the highest frequency component expected to be present in the input signal, the following parameters were chosen:

$$C = 50\,nF; \quad R_1 = 42\Omega; \quad R_2 = 500\Omega.$$

The cut off frequency is thus $f_{cut} = 75\,kHz$.

A picture of the circuit and a screenshot of the produced square wave when a triangular wave is used as an input are presented.

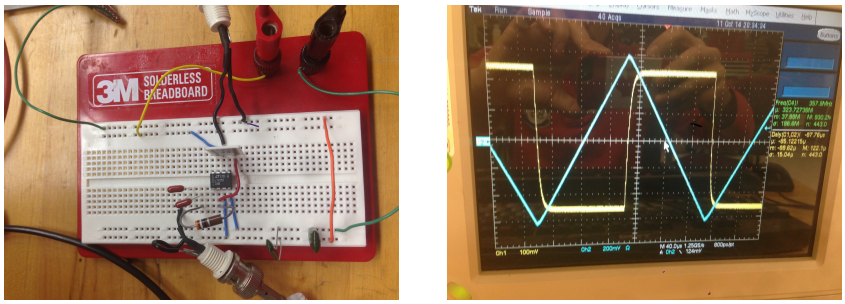

(a) Photograph of the analog differentiator. (b) Input and output test signal.

Figure 4.13: *Analog Differentiator Circuit*.

The output signal had to be amplified before having enough large amplitude to drive the audio amplifier. The low power signal amplifiers were connected after the circuit and before the audio amplifier. The amplification of the signal before the circuit would indeed result in the saturation of the output voltage of the operation amplifier of the circuit. In the last section of chapter 5 the effects generated on the discharge current by the closed loop excitation of the auxiliary coil will be presented. A Faraday probe was used as well to monitor the thruster ion current waveform with and without the auxiliary coil on. A brief description of this kind of probe is reported in the next section.

Faraday Probe:

Faraday probe are often used to measure ion current density in plasma, they are referred as ion probes as well. Several types of Faraday probes exist; a guarded, planar nude Faraday probe was used to measure the beam current density, this probe was built by former researchers at Stanford. The principle and the implementation of this kind of probe is rather simple, nevertheless accurate ion current measurement are difficult to conduct. In the experiment described in this thesis attention was mostly focused on the fluctuation of the ion current.

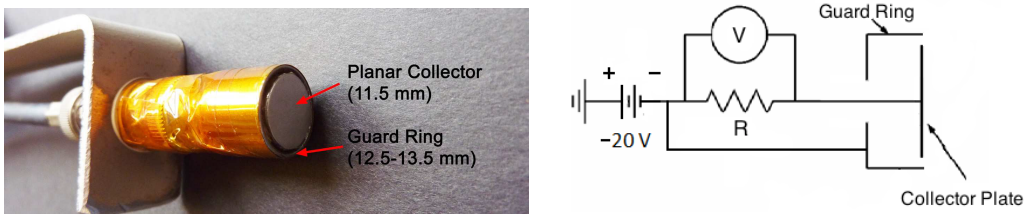

(a) Photograph of the used Faraday probe. (b) Schematics of the probe's circuit.

Figure 4.14: *Faraday probe and wiring diagram*.

Both the outer guard and the inner collector are biased below plasma potential to ensure that electrons contained in the beam are repelled and at the same time to create a relatively flat and uniform sheath over the collector. *-20 V* bias was used, preventing them to be collected by the probe. In that case, indeed, the total beam current would be near zero being the beam quasi neutral. The ions impacting the plate of the probe generate a current into the circuit since electrons are attracted to the plate itself to neutralize the incoming ions. The collector plate is then connected with a resistor so that current flowing can be calculated measuring the voltage drop across the resistor itself, using again a differential amplifier, with the well-known relation $I=\Delta V/R$. Ion current density can be derived from this value using the following formula:

$$j = \frac{V * 1000}{RA}$$

where V is the voltage, R is the value of the resistor, A is the area of the aperture and j is the current density in mA/cm^2. The main disadvantage of this probe configuration is that low-energy ions, typically produced by charge-exchange collisions (CEX), can be attracted by the probe, resulting in some cases in a higher ion current value [22].
To mitigate this effect other configurations of Faraday probe can be used such as collimated, gridded and magnetically shielded probes. As already mentioned, the main goal of this measurement is the acquisition of the fluctuating trace of the ion beam current. This data can provide useful information since the relation between the discharge current and the ion beam current is a function of the thruster magnetic field. Faraday probe data are usually helpful to estimate the total ion current ejected by the thruster as well, performing a scan of the plume with a rotational stage and integrating then the current density over the full hemisphere.
This kind of test was however not carried out, the angular scan being limited by the configuration and geometry of the small vacuum chamber and not of primarily importance for the study presented in this thesis. A different electrical layout was tested as well. The probe can indeed be connected to a picoammeter that allows a direct reading of the current generated by the probe. The picoammeter was then connected to the scope in order to visualize and record not only a mean value but also the entire signal generated by the Faraday probe. In chapter 5 some data collected by the probe will be presented.

Chapter 5

Testing

5.1 Laboratory Description

At the SPPL there are two labs equipped with systems able to perform testing on electric thrusters of various power levels. The characteristic apparatus present in these labs is the vacuum facility: two vacuum chambers of different size are indeed available for testing thruster in a very low-pressure environment in order to simulate space condition. Higher power thrusters ($P > 200\,W$) can be operated in the larger vacuum chamber: this vacuum facility consists of a stainless-steel chamber 1.25 m in diameter and 4 m long it is T-shaped, with two 1m long arms extending to the cooling shrouds. The overall volume of the chamber is approximately 6.25 m^3. The base pressure in the facility before thruster operation is approximately 4×10^{-5} Pa and during typical thrust measurements is approximately 3×10^{-4} Pa, measured using an ionization gauge uncorrected for xenon. High vacuum is accomplished using a two-stage cryogenic cooling system. A Polycold refrigeration system provides the primary cooling (achieving temperatures of 150 K), and a cryogenic helium cooling system (CVI model number TM1200) comprises the second stage (achieving temperatures of about 14 K). The Polycold provides a close-loop circulation of a proprietary mixture of refrigerants. The cryopumps are backed by a $0{,}5\ m^3/s$ mechanical pump and blower. If necessary a turbomolecular pump is available as an intermediate pumping stage. In order to enhance the efficient use of this chamber, a 1,5 m gate valve has been installed to isolate the test section from the cryopumps; in this way, the cryopumps can remain operational with the gate valve closed while adjustments are made in the test-section. Once any changes have been made and the chamber door closed, the turbo pump is used to reduce the test-section pressure. The gate valve is then opened to expose the cryopumps and reduce the test section to operational pressures. Maximum pumping speed is 4000 l/s of xenon equivalent to 28 sccm.

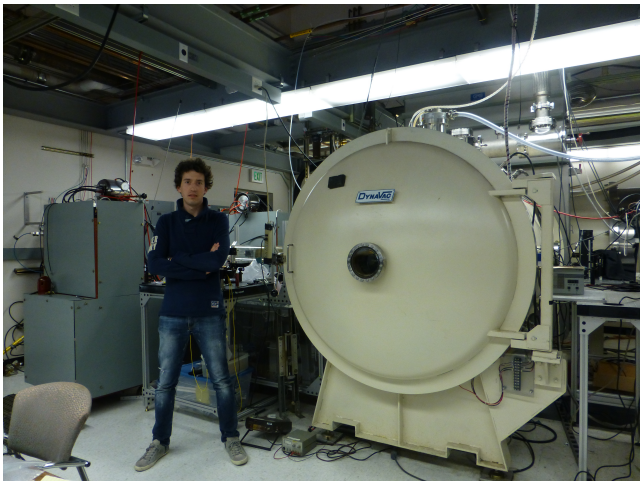

Figure 5.1: *Photograph of the exterior of the Stanford large high-vacuum facility.*

Smaller Thrusters can be operated in the smaller vacuum chamber taking advantage of the higher flexibility that this facility offers (i.e., shorter pumping procedure, easier troubleshooting etc.) This test facility consists of a non-magnetic stainless steel chamber approximately 0,6 m in diameter and 1,2 m in length. The chamber is pumped by a single 50 cm diameter cryopump (CVI-TM500) backed by the same pumps used for the larger chamber. The base pressure of the facility is approximately 10-5 Torr, as measured by an ionization gauge, uncorrected for xenon. Thruster testing at xenon flow rates of 10 sccm results in chamber background pressure of approximately 10-4 Torr.

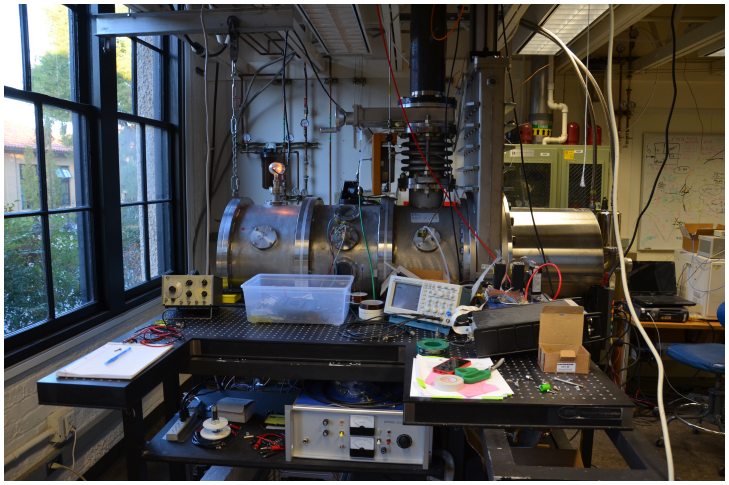

Figure 5.2: *Photograph of the exterior of the Stanford small high-vacuum facility.*

5.2 Plasma sources: Hall Thrusters and Cathodes

5.2.1 Introduction to Hall Thrusters and Cathodes used

A general description of the Thrusters used in this work follows. Two Hall Thrusters were utilized: the Z-70 and the CHTr (both are laboratory thrusters), the first being an annular HET and the second a cylindrical HET as its name suggests. Both of them have wall made out of as boron nitride (BN) even if in laboratory thrusters' alumina (AL_2O_3) is often used for cost reason. These dielectric materials have a low sputtering yield and relatively low secondary electron emission coefficients under xenon ion bombardment. No HET can work without a neutralizer. Three different cathodes where used during this testing campaign: two commercial hollow cathodes, an Ion Tech HCN-252 and a Busek BHC-1500, and a laboratory one AFITr with a Lanthanum Hexaboride (LaB6) emitter.
Even if some operational points are presented and values for mass flow rates, voltages and currents used in the testing are reported, it is important to stress how HET are sensitive to all the surrounding components of the setup. As an example it is worth considering how cathode's position influences the behavior of the thruster for a chosen set of operational parameters [18].
Regardless to the thruster used, the startup procedure presents similar steps. After the multiple hours pumping procedure is complete and the chamber pressure is low enough it is possible to start the heating of the cathode flowing some gas through it. The details of the heating process are different for each cathode and they are a function of the time the cathode was exposed to air for as well, in particular with impregnated insert cathodes that are much more sensitive to poisoning compared to LaB6 cathode. After a long exposure to air, in the order of one day, it is good practice going through a conditioning process that can require some as long as few hours; during this time interval the heater current is slowly increased up to a maximum value that is again varying with the type of cathode, but usually ranging from 6 to 12 A. Once the ramp up process is completed and the mass flow is adjusted to the proper one, again, different for each cathode and ranging from 1 to 10 sccm for the cathodes used in these tests, the cathode keeper's voltage is set to 600 V. At this point, depending on the cathode used, it is necessary to turn on the anode power supply as well and flow some gas through the anode in order to help the cathode start. From now on all the settings are very thruster dependent and the reader can find further details in the next paragraphs. Even if argon was used in some test to check the proper operation of one of the two thrusters used, the xenon tests will be discussed more in detail. Indeed, xenon is still the predominant expellant in HET application and the vast majority of the available data acquired in laboratory

tests is based on experiments running on xenon. During all tests the thruster was allowed to stabilize before taking any data: a drift in the operation point is indeed frequently observed before reaching the final stabilization of the thruster.

5.2.2 Z-70, Annular Hall Effect Thruster

The Z-70 was designed and built at Stanford University and is shown in Figure 5.3, it has a coaxial channel that measures 21 mm in length and 15,75 mm in width with a mean channel radius of $r_m = 28{,}7\,mm$. Wall material is Boron Nitride. This Thruster was operated exclusively with the Ion Tech cathode, being too powerful for the Busek cathode and considering that the AFIT one was still under refurbishment. The thruster is design to run around 450 W with a discharge voltage of 300 V and a discharge current of 1,5 A but it is important to stress that in many experiments the operating point is different, since in many tests, operating at the best efficient point is not the main goal for the experiment itself. This kind of annular HET operates accordingly to the most common radial B field topology as shown in the following picture and described in chapter 1.

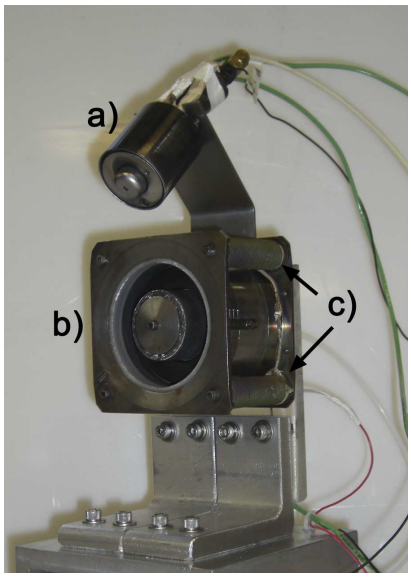

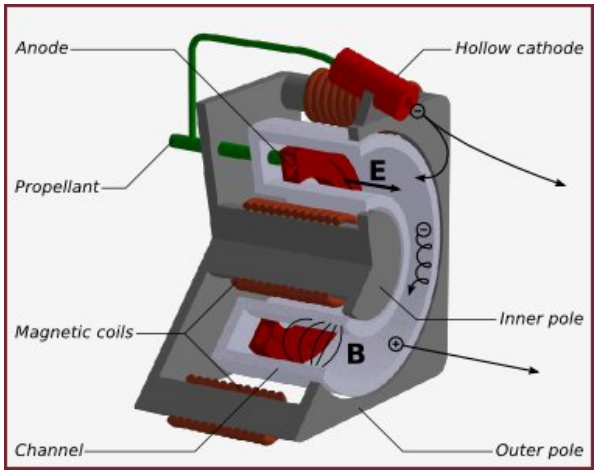

(a) Photograph of the Z-70: a) cathode, b) thruster, c) electromagnets. (b) Section of a typical annular HET. [17]

Figure 5.3: *Z70 Hall Effect Thruster*.

Two MKS model 180A precision mass flow controllers, calibrated for xenon 0-10 sccm for cathode and 0-50 sccm for anode controlled via MKS Type 247

four-channel readout were used in the gas feed system. Commercial power supplies were used to power the cathode heater, cathode keeper, and electromagnets. The unit used to power the anode can output 300 V and 5,5 A.

5.2.3 CHTr, refurbished Cylindrical Hall Thruster

The CHT was also designed and built at Stanford University, but has been refurbished and modified by the author, hence the suffix *r* and the resulting acronym CHTr. This thruster absorbs less power compared to the annular one previously described. A schematic is shown below along with a picture of the thruster. In the configuration used, the thruster has an inner electromagnet and four outer solenoids similar to the ones used in the Z-70. The different configuration reported in the schematics is possible; a different magnetic topology is in this case achieved: a cusp is formed close to the thruster exit plane. A vast literature is available for this less common, interesting type of Hall thruster, particularly suited for low power applications [86].

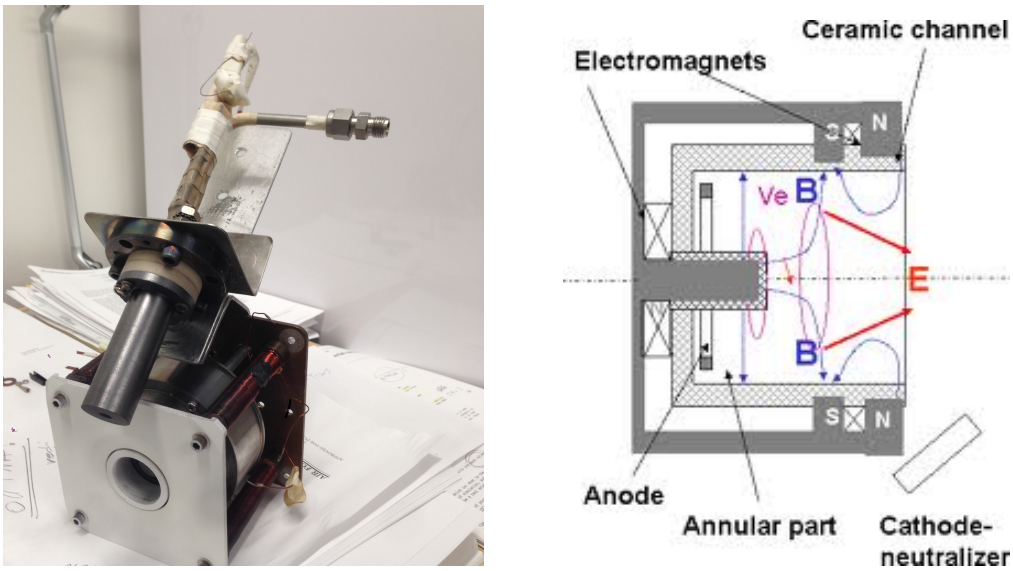

(a) Photograph of the CHTr with AFITr Cathode. (b) Section of a typical CHT [86].
Figure 5.4: *CHTr Hall Effect Thruster*.

The gas feed system includes a 0-100 sccm mass flow controller for the anode and a 0-10sccm controller for the cathode. The commercial anode discharge power supply can provide up to 600 V and 1,7 A. Separate commercial power supplies were used to power electromagnets, cathode heater and cathode keeper.

5.3 Preliminary testing using Z-70 HET and Ion Tech Cathode

5.3.1 Z-70, Annular HET Operational Points

The first test was performed using the Z-70 Hall thruster. As usual before installing any additional components, it is necessary to run the thruster to check that everything is working properly. Cathodes and electrical connections are often a source of problems, and this is even more important when dealing with laboratory components compared to commercial devices that are in general more reliable but much more expensive and more delicate. Some discharge current traces are later presented as an example of the common waveform generated by this kind of plasma accelerators.

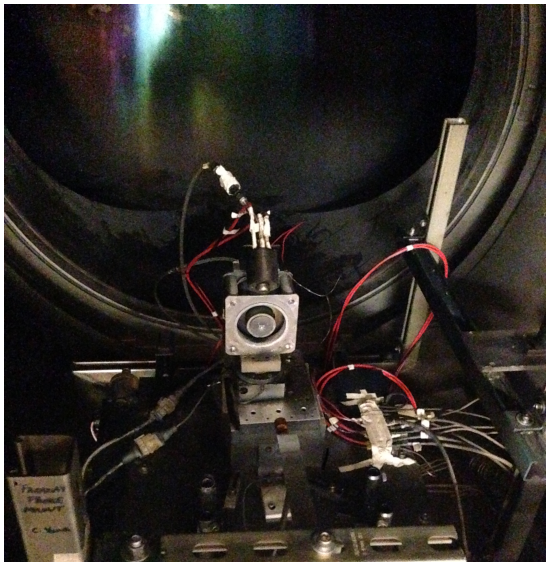

Figure 5.5: *Z-70 Thruster installed inside the vacuum chamber with Ion Tech Cathode mounted in tilted configuration.*

The thruster was thus tested and some operational points where identified and characterized. Even if the extreme limits of stable operation of the thruster are not so shifting from one test to another, the specific operating point and the associated oscillating behavior is definitely sensible to the configuration of the setup. Temperature of the thruster is also important and indeed the devise is always left warming up before doing specific tests on it. Some of the different modes that were found on this thruster are reported below; the four graphs and table are catalogued as Figure 5.6.

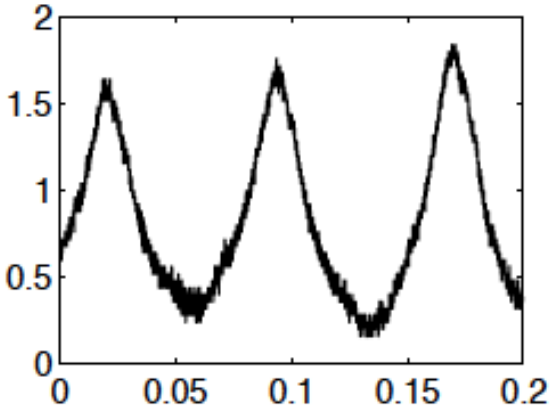

Anode mass flow rate [sccm]	Anode Voltage [V]	Discharge Current [A]	Frequency [kHz]	Thruster Coils Current [A]
20	300	1,98	13,5	0,64

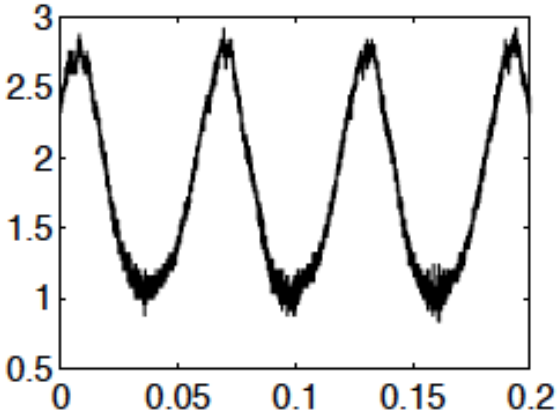

Anode mass flow rate [sccm]	Anode Voltage [V]	Discharge Current [A]	Frequency [kHz]	Thruster Coils Current [A]
15	300	0,84	16	0,73

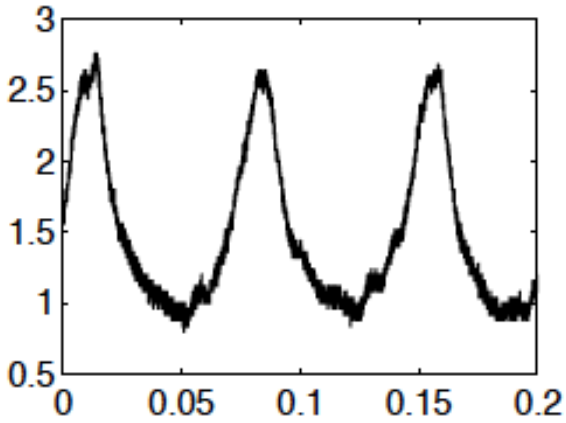

Anode mass flow rate [sccm]	Anode Voltage [V]	Discharge Current [A]	Frequency [kHz]	Thruster Coils Current [A]
20	300	1,55	14	0,66

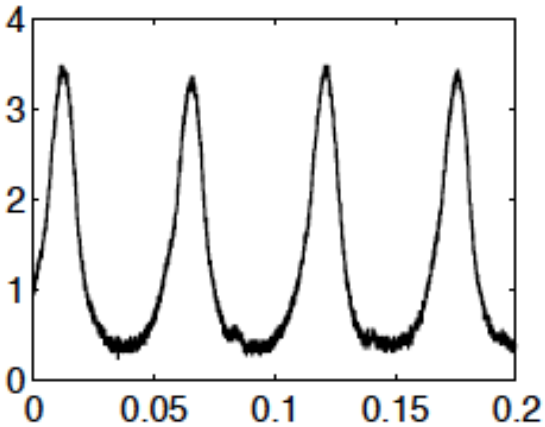

Anode mass flow rate [sccm]	Anode Voltage [V]	Discharge Current [A]	Frequency [kHz]	Thruster Coils Current [A]
20	300	1,25	19	1,17

5.3.2 Preliminary testing on Z-70 with auxiliary solenoids

A proof of concept trial was then conducted using the Z-70 Hall Thruster and two solenoids powered mainly using DC current, but with sinusoidal waveform as well. The frequency used in the second part of this preliminary test was by the way very low (below *100 Hz*). This choice was made for two main reasons: first of all this very first test was performed to familiarize with the sensibility of the thruster to an auxiliary magnetic field. Furthermore the coils used in this preliminary test, described in chapter 3, are definitely not optimized for the sinusoidal operation as already pointed out in chapter 4 and the power supply used in this setup, although able to be controlled and used as powerful signal generator is meant to work mainly in DC and indeed its slew rate doesn't allow to reach higher frequencies. On top of this only two solenoids were mounted even if for sake of symmetry four of them would have been desirable. This simpler configuration was selected for simplicity: the use of four solenoids would have required indeed relocation of the cathode. The mounting plate and respective hardware for the solenoids were coated, as in the case of the front plate of the thruster, with a boron nitride spray helping the prevention of charge accumulation increasing electrical as well as thermal insulation. Sputtering is reduced as well. The images below show the thruster running without and then with the regular magnetic field of the thruster, but with no current into the two auxiliary solenoids.

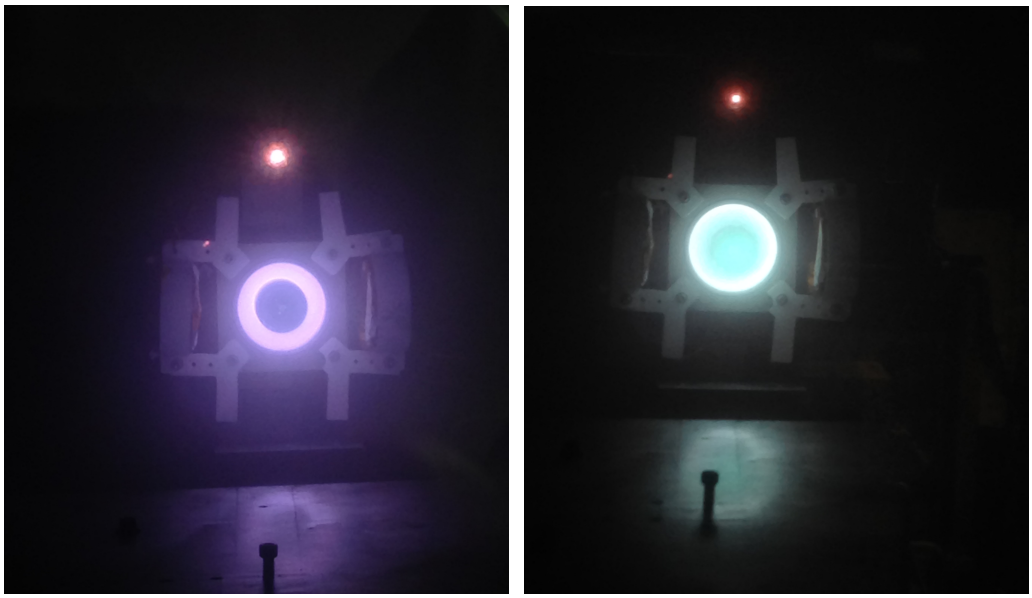

(a) Z-70 running in glow mode w/o B field. (b) Z-70 running with B field.

Figure 5.7: *Z-70 with two solenoids mounted*.

Despite the very rough and invasive configuration described in chapter 3, the operation of the thruster was not tangibly affected by the presence of the two solenoids. After the good functioning of the thruster was proved, a preliminary testing powering with DC current the two external solenoids was conducted. In the power spectral density graphs that follow, the position of the cathode is different compared to the one in the picture of the thruster installed in the chamber, it is indeed not angled: the axis of the cathode is parallel to the axis of the thruster. This choice is definitely not the optimal one and it was adopted in order not to modify the configuration necessary for previous studies; after prolonged cathode ignition difficulties, this configuration was finally abandoned. Attention is focused on a very low frequency oscillation mode whose first harmonic is located around *2 kHz,* as shown in the semilogarithmic power spectrum of the signal below.

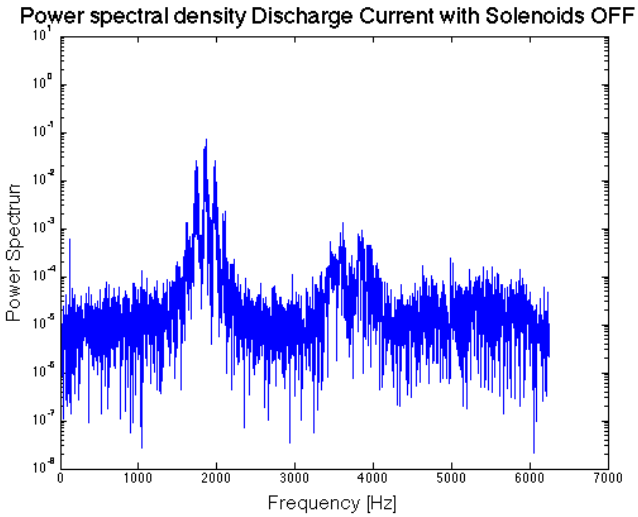

Figure 5.8: *Power spectrum of the Z-70 Discharge Current with no current in the auxiliary solenoids.*

The following semilogarithmic power spectral density graphs show how powering the auxiliary solenoids tangibly impacts on the discharge current. Different current levels are tested: 3A, 6A, 7A, 8A. In addition, both polarities were tested, but spectrum analyses were performed only with auxiliary solenoids in a configuration such that the produced magnetic field adds to the existing one, instead of subtracting to it.

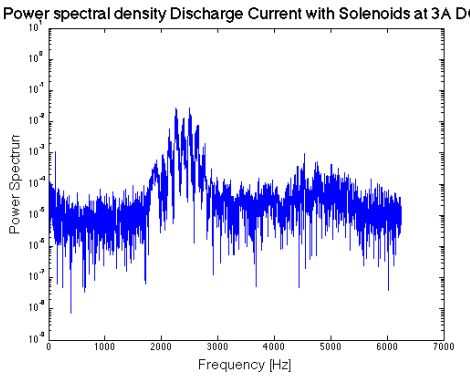

(a) Auxiliary Solenoids powered at 3 A.

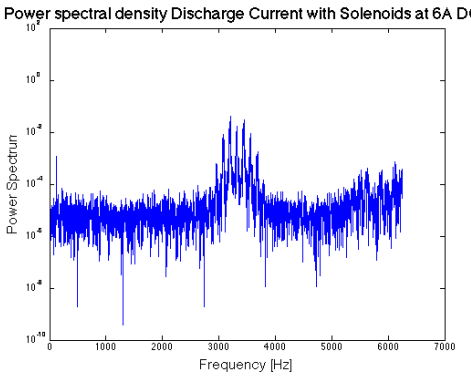

(b) Auxiliary Solenoids powered at 6 A.

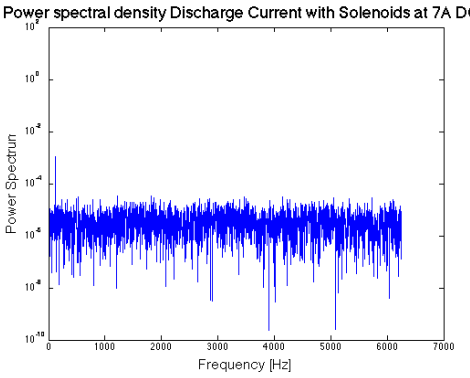

(c) Auxiliary Solenoids powered at 7 A.

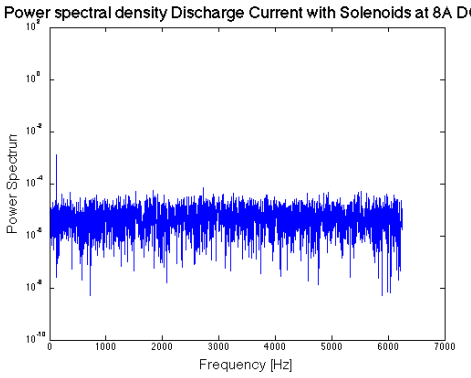

(d) Auxiliary Solenoids powered at 8 A.

Figure 5.9: *Power spectrum of the Z-70 Discharge Current with different current levels in the auxiliary solenoids.*

Two main effects are detectable. The frequency of the fluctuations increases as the solenoids current assumes a higher value and furthermore the peak of the fluctuation lowers, meaning that the RMS of the oscillations has a lower value, with the increase of the current flowing into the solenoids until the fluctuation totally disappears allowing the thruster to run in a quiescent mode. Even if this result seems to be extremely attractive it seems that the underlying reason for such behavior is connected with other kind of instabilities. Although further investigations are required, a possible explanation could involve the so-called rotating “spoke instability”. This azimuthal instability is associated with an ionization front and, as its name suggests, consists of a rotating around the symmetry axis of the thruster and seems to be associated with the enhancement of the electron cross-field transport. Rotating spoke physics is by the way still under study [24]. It could be possible that this spoke is somehow anchored near

the region were the magnetic field is intensified by the presence of the field generated by the auxiliary solenoids and this new configuration can perturb the longitudinal instability by producing a leak of current through the electron cloud. This would also justify why an increase in the mean value of the discharge current is observed even if the overall magnetic field is higher due to the presence of the solenoids. With a higher magnetic field, as already explained in the introductory section, a lower discharge current would be expected.
After the reported DC testing, some very low frequency sinusoidal signal where used to power the auxiliary solenoids; *1, 5* and *90 Hz* were considered. As in the previous test, a clear interaction is found between the thruster anode discharge current and the auxiliary magnetic field; anode voltage is affected as well. The parameters selected on the power supply were beyond the operational region of the device itself, thus the clipped pink waveform that represents the solenoid current. Discharge current is the yellow signal and anode voltage is the green one.

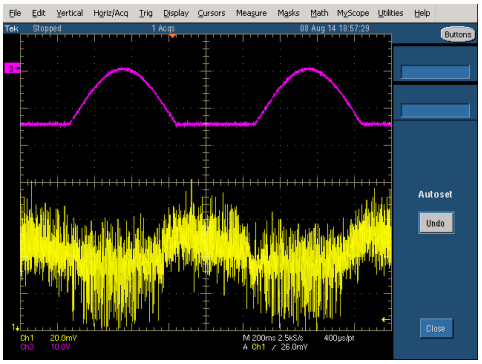

(a) 1 Hz Sinusoidal Clipped Current signal

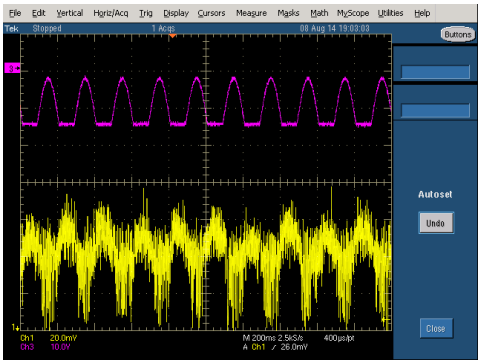

(b) 5 Hz Sinusoidal Clipped Current signal.

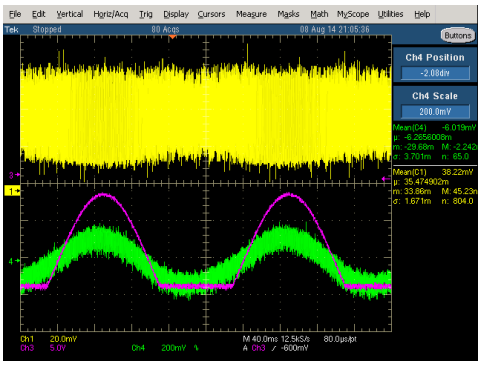

(c) 5 Hz Sinusoidal Clipped signal with. Voltage

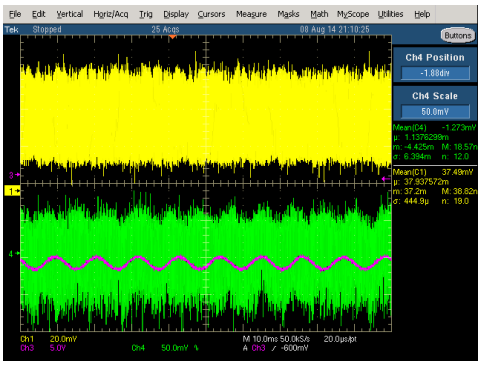

(d) 90 Hz Sinusoidal signal with Voltage.

Figure 5.10: *Auxiliary solenoids powered by very low frequency current, testing on the Z-70 thruster.*

The current flowing through the solenoids is monitored sensing the voltage across a *4 Ω*, the polarity is actually reversed so the flat part of the signal is at highest current, around *3,5 A* and the half sinus represents the lower branch of the waveform with the maximum corresponding to *0 A*.
Below the power spectrum of the discharge current during the *5 Hz* testing is reported.

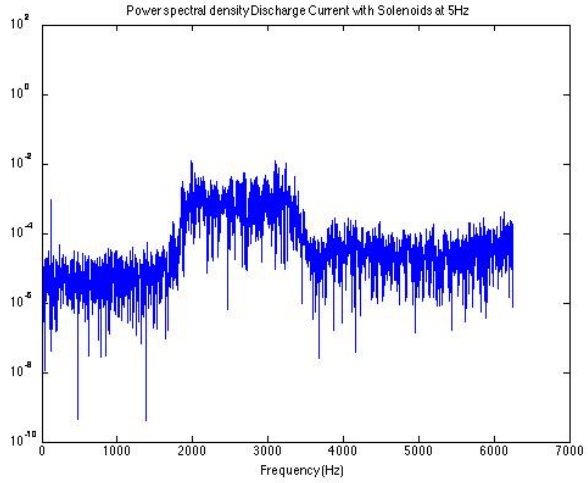

Figure 5.11: *Power spectrum of the Z-70 Discharge Current with 5 Hz current in the auxiliary solenoids.*

It is interesting how the power spectrum of the discharge current signal acquired while powering the auxiliary solenoid at *5 Hz* turn out to have a different shape compared to the ones obtained during DC testing. Considering that the frequency of the signal used in the described test (i.e.: *5 Hz*) is much smaller then the oscillation frequency, that is around *2 kHz* as already said, a more similar shape was expected. A likely explanation is that the graph shows somehow a cumulative picture of the discharge current at the different solenoid current level that are crossed during the evolution of the waveform. The predominant central frequency, thus, should be the one that corresponds to the one found during the DC test at a current level equal to the one at which the power supply was outputting a flat current that is, to all intents, similar to a DC signal with equal magnitude. Considering that the solenoid current was peaking with a flat half cycle at about *3,5 A* it is easy to see how indeed there is a good correspondence with the power spectrum computed with the discharge current trace with auxiliary solenoids at *3 A*.
Despite the quite interesting results, no further tests were performed on the Z-70 thruster, especially after the cathode was angled causing the frequency of the oscillations to rise, reaching almost *20 kHz*. Taking also advantage of the ongoing refurbishing process of another thruster, the Z-70 was no more used.

5.4 Preliminary testing using Cylindrical HET CHTr

5.4.1 Refurbished Cylindrical HET Operational Points

The CHTr has been completely reassembled and part of the components modified as already reported at the beginning of this chapter. It was thus necessary verify that the rebuilt thruster was able to run properly. Some tests have been conducted with two different cathodes, the Lab6 AFITr Cathode and the Busek cathode. Two propellants were used: argon gas has been always used during the test with the first cathode and in general during the starting process. xenon has been used with the commercial cathode during data acquisition.

AFITr Cathode, argon only

The LaB6 cathode was successfully tested on this thruster even the cathode current capability is definitely much wider compared to the needs of the thruster; the mass flow rate of the cathode was also high compared to the usual ratio between cathode and thruster mass flow rate. In order to check the proper operation of the cathode these considerations are by the way not of primary importance.

(a) CHTr running in glow mode w/o B field. (b) 40 kHz anode current oscillation.
Figure 5.12: *CHTr running on argon with AFITr Cathode*.

A preliminary analysis of the trace of the discharge current signal indicates that this system (i.e.: thruster and cathode) has an instability at about *40 kHz*. Because this value is beyond the frequency limit that the audio amplifier can handle, it was decide that this configuration was not ideal to test the interaction system. Considering by the way the importance of this test from the successful refurbishment point of view, some of the several operational points at which the thruster was tested follow. In the first table no magnetic field was applied, while in the second table a current *1,6 A* into the coils of the thruster was applied.

Argon Mass Flow Rate [sccm]	Discharge Current, mean value [A]
13,2	0,047
13,6	0,055
14,0	0,064
14,4	0,070
14,8	0,072
15,2	0,077
15,6	0,082
16,0	0,084
16,4	0,091
17,2	0,100
17,6	0,110
18,0	0,140
18,4	0,180

Figure 5.13: *CHTr Operational points with constant 1,6 A current in the thruster coil and 320 V Anode Voltage.*

Below a graph shows the trend of the data presented before. As expected the current is an increasing function of the mass flow rate. The presence of more gas decrease indeed the resistance of the plasma generated inside the thruster. It is not clear the reason for the higher derivative for high mass flow rates. Much higher chamber pressure may influence this parameter.

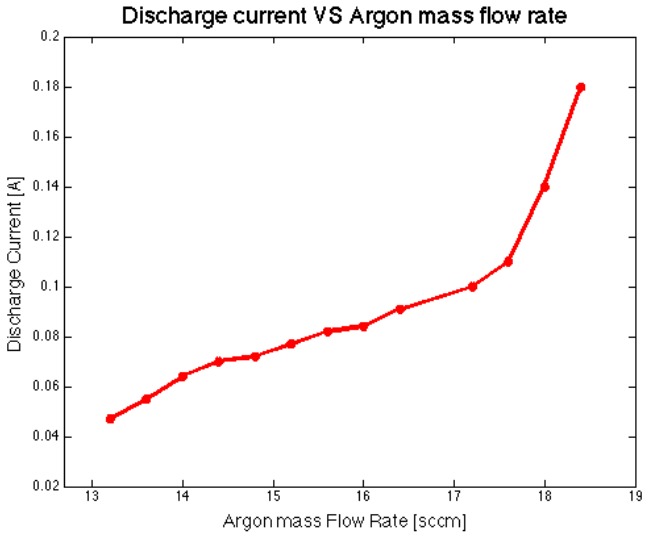

Figure 5.14: *CHTr Discharge current versus argon mass flow rate with constant anode voltage 320 V and constant electromagnet current 1,6 A.*

In the following table six different operational points are reported, constant anode voltage and magnetic field are selected. As already explained in the introductory section on the Hall Thrusters, an increase in the magnetic field results in a lower discharge current since the electrons experience a higher resistance.

Electromagnets Current [A]	Discharge Current, mean value [A]
0,5	0,430
1,0	0,210
1,2	0,180
2,0	0,131
2,2	0,129
3,0	0,117

Figure 5.15: *CHTr Operational points with constant 17,6 sccm Argon Flow and 310 V Anode Voltage.*

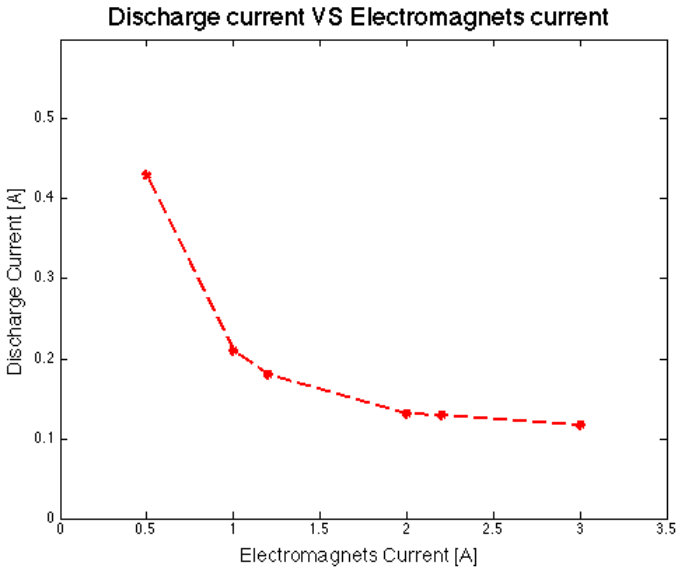

Figure 5.16: *CHTr Discharge current versus Electromagnets current with constant 17,6 sccm Argon Flow and 310 V Anode Voltage.*

After the positive result of this general testing of the rebuilt cylindrical Hall thruster, boron nitride walls were expected as well and no cracks were detected proving the good outcome of the bonding process with ceramic paste. In the following section, testing with Busek cathode and xenon propellant is described.

Testing with Busek cathode and xenon gas:

As already said, this cathode is a flight qualified one and it uses a porous tungsten hollow insert impregnated with a low work function emitter comprised of a barium and other materials mixture. Argon was used during the starting process switching then to xenon. Nominal mass flow rate in the cathode is *1,5 sccm*. All the following data were taken with an anode mass flow rate of *6 sccm*, *70 V* on the anode electrode and *0,85 A* as a mean value of the discharge current. When the electromagnets were powered, a *0,7 A* current was used to generate the magnetic field in the thruster. The visual difference between the plasma discharge obtained without and with the presence of the magnetic field is attest by the following two pictures. The different color is due to the larger ionized fraction of the injected neutral gas with the presence of the magnetic field; ionized xenon emits indeed in the light blue part of the visible spectrum compared to a more pink emission generated by the excited neutrals.

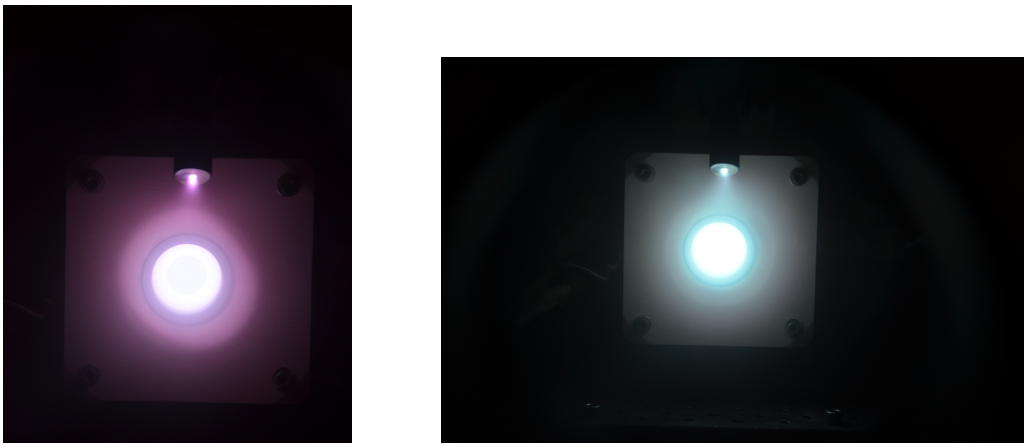

(a) CHTr running in glow mode w/o B field.

(b) CHTr running with B field.

Figure 5.17: *CHTr running on xenon with Busek Cathode*.

A brief description of the thruster behavior in the point considered follows. An analysis of the power spectral density of the discharge current signals indicates that the CHTr, in this specific configuration and operational point, presents a strong oscillation behavior, characterized by a rather low frequency that is around *3,8 kHz* as deducible from the current trace, reported below, as well.

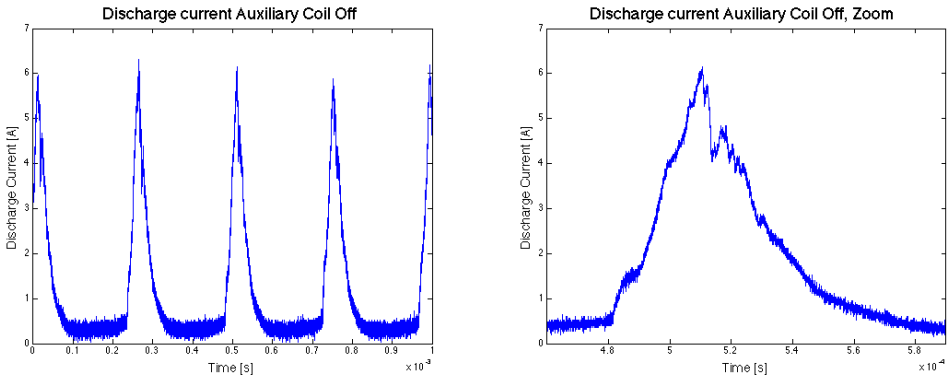

(a) Oscillations around 3,8 kHz. (b) Zoomed view: knee detail.

Figure 5.18: *CHTr with Busek Cathode, Discharge Current Trace.*

The knee on the right of the peak represents an interesting detail of the trace. Later, in the advanced testing section further data concerning this detail will be presented.
It is still not clear the physical reason behind the presence of this peak and an analysis of the behavior of the ion current through LIF technique would be interesting. Apparently two current peaks are present and one has higher intensity. The time delay between the two peaks is very regular and close to $10\,\mu s$. Qualitatively speaking, the two current peaks could be due to two different electron classes that travel inside the thruster channel with a relative delay. Once these two classes of electrons reach the anode, the peaks on the current traces are generated.

5.4.2 Preliminary testing on CHTr with auxiliary solenoid

After observing the good functioning of the thruster and its neutralizer and after characterizing the operational point chosen for the experiments, tests with the auxiliary coil started. A Faraday probe was installed as well; the reader can find some details on the used probe in chapter 5. The data presented below show how the probe properly acquires the fluctuations in the ion current produced by the thruster and how these oscillations have similar characteristics compared to the discharge current waveforms. Two pictures of the setup are presented; the one on the left show the thruster and its cathode installed on a small optical table. After all the electrical connections are properly wired and gas lines tighten the assembly is slid inside the chamber. At this point the Faraday probe is installed in front of the thruster and aligned with its axis; a *20 cm* distance from the exit plane of the thruster was used. An overall view of the complete setup is available in the picture on the right.

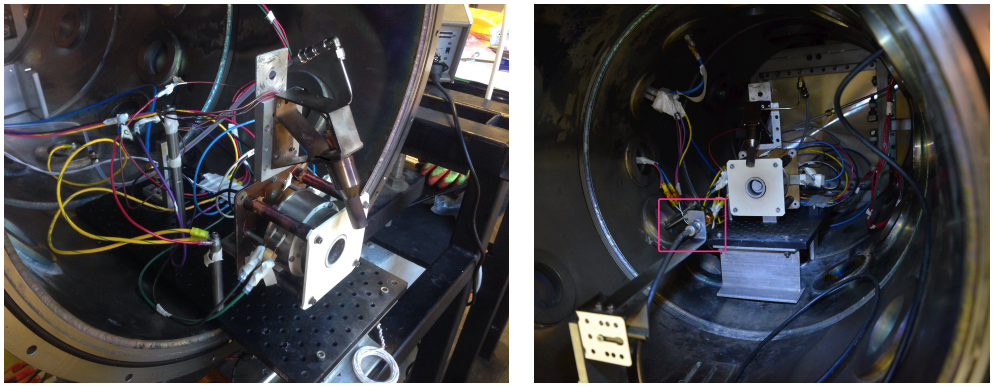

(a) Thruster assembled ready for testing. (b) Faraday probe (pink square) installed.

Figure 5.19: *CHTr with Busek Cathode and Auxiliary Solenoid.*

A trace generated by the Faraday probe and the associated power spectrum follows. The power spectrum of the discharge current of the thruster is showed as well; this allows the match of the frequency content of the two signals (i.e.: anode discharge current and ion current).

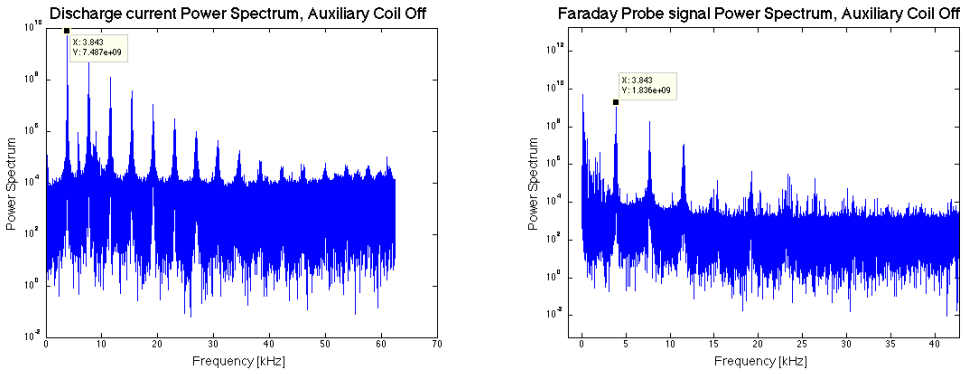

(a) Discharge current power spectrum. (b) Faraday probe signal power spectrum.

Figure 5.20: *Power spectrum comparison between CHTr Discharge Current and Faraday Probe signal, with Auxiliary Solenoid not powered.*

The discharge current power spectrum reported shows the first harmonic of the signal close to a *3,8 kHz* frequency as already pointed out, plus several harmonics at higher frequency. The very same frequency is found in the probe signal that has in addition higher energy content at *60 Hz* (i.e.: line frequency) compared to the previous signal. This is clearly visible in the non-zoomed plot of the probe signal that is presented below too. Zooming the described image, it is by the way possible to see how the low frequency oscillations affect the ion current as well.

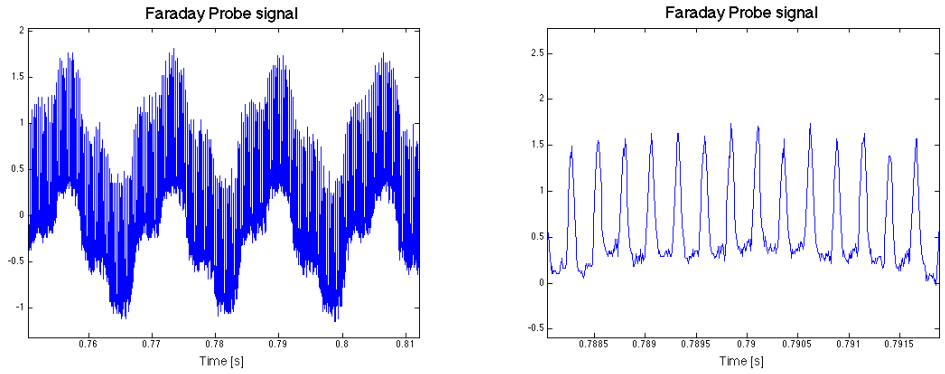

(a) Faraday probe signal, 60 Hz visible. (b) Faraday probe signal zoomed.

Figure 5.21: *Faraday Probe signal: non-zoomed and zoomed traces.*

In the following section some data acquired powering the auxiliary solenoid, installed inside the CHTr, are finally presented. The first test performed was an open loop test: a signal generator was used to produce a sinusoidal waveform that was then amplified by the audio amplifier and finally used to drive the auxiliary solenoid. In the oscilloscope screenshots reported below a signal with a frequency close to the one found in the natural oscillating mode of the thruster is used. The amplitude of the light blue signal represents the intensity of the current flowing in the auxiliary coil; a Pearson Probe with a *0,1 V/I* ratio was used so the value reported on the screen has to be multiplied by *10* in order to have the actual value of the current outputted by the amplifier. It is very interesting the difference shown in the two images. In the left screenshot the discharge current is in phase with the coil signal, while in the right image the two signals are no longer in phase, indeed they are now 180° out of phase.

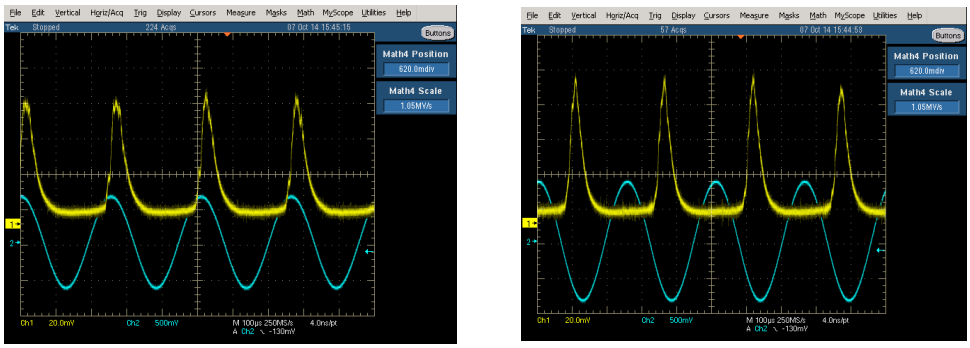

(a) Oscillations in phase with aux coil signal. (b) Oscillations out of phase with increased amplitude aux coil signal.

Figure 5.22: *Phase Shifting in Open Loop Mode. Yellow is the Discharge Current and Light Blue is the Auxiliary solenoid Current.*

In the previous comparison, the only different input parameter is the intensity of the current used to drive the solenoid: the in phase case is obtained with a *6,25 A* peak current, while the anti phase case reads a *8,75 A* peak current. Unfortunately, looking at the screenshots, it is impossible to notice something that is instead clear looking at the scope in real time: namely the thruster does not like to stay in an intermediate situation. There is a threshold of current value, in between the two reported, that leads to the sudden shift from the in-phase configuration to the anti-phase one. A further difference is present: the peak value of the discharge current is different comparing the two situations, being lower in the in-phase condition.
In the screenshot that follows, a different input was used: a sinusoidal excitation signal at *2 kHz*. With this kind of excitation signal, the discharge current waveform presents a shape strongly affected by the interaction with the auxiliary coil. Two different peaks are now present.

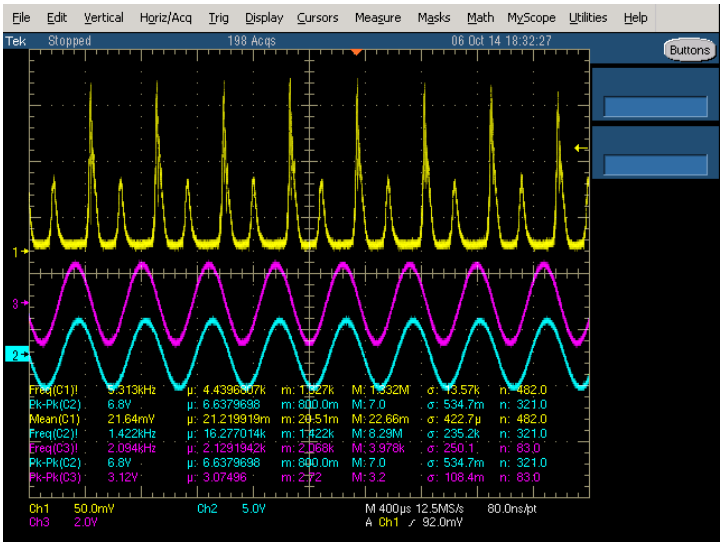

Figure 5.23: *Double-Mode behavior with system in Open Loop Mode. Yellow is Discharge Current, Pink is the signal generator and Light Blue is the Auxiliary solenoid Current.*

The amplitude ratio of these peaks is roughly speaking two as shown in the scope screenshot. A very interesting consideration is that the lower peak appears to be almost in phase with the positive half sinus of the excitation signal. A comparison with the trace of the discharge current recorded with no power in the coil shows that the amplitude of the peaks found in the natural oscillations is slightly smaller than the amplitude of the high peak into the modified signal. On the other hand the small peaks show a big reduction in their amplitude: their

peak value is indeed, roughly, half of the one found in the natural fluctuation of the thruster.

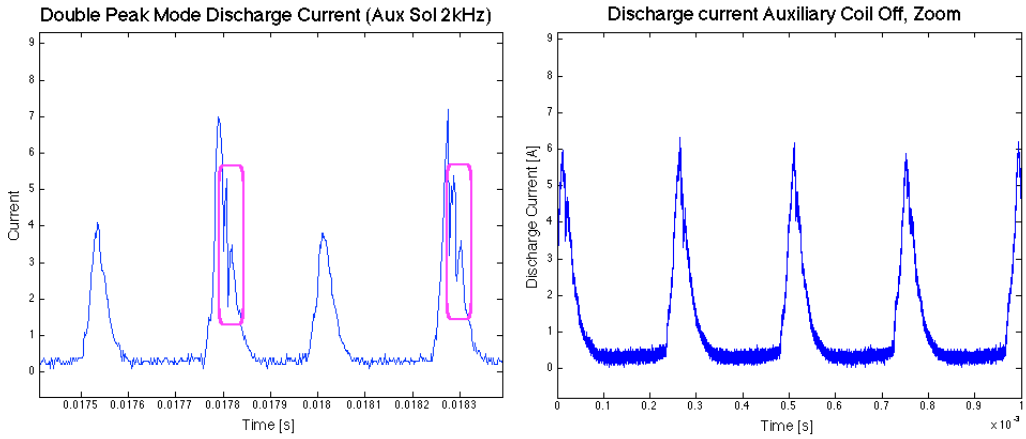

(a) Excited discharge current trace. (b) Natural discharge current trace.

Figure 5.24: *Comparison between excited and natural CHTr discharge current traces.*

Another interesting aspect of the excited current trace is the presence of an additional sub peak on the negative slope side of the big peaks, as shown in the pink box on the left side plot. The first difference with the unexcited waveform is that now, as just said, the sub peaks are no more one but two; in addition there is no sub peak in the smaller peak. It is unfortunately still not clear why this appends.

Increasing again the frequency of the excitation signal up to a value close to the natural frequency and selecting an amplitude above the threshold that is associated with the phasing of coil and discharge current traces, allows observing an interesting effect. It is indeed possible to affect the natural frequency: a small change in the frequency of the coil signal is thus able to tune the discharge current signal at the same frequency. This behavior is maintained inside a frequency range that increases with the amplitude of the excitation current as intuitively predictable.

In order to present the trend of this 'frequency locking capability' demonstrated by the auxiliary solenoid, a phase space diagram representation is used. For several frequencies the value of the excitation current is related to the corresponding value of the thruster discharge current. A three-dimensional plotting is reported for four different amplitude levels. For each value, *2-8-15-20 A*, the lower and the upper limits of the frequency range, inside which the locking mechanism is effective, are presented. In these plots the coupling between discharge current first harmonic and excitation signal of the coil is shown.

The amplitude of the sinusoidal excitation current used in the following plots is equal to *2 A* peak-to-peak. In this situation the capability of the auxiliary coil to modify the discharge current oscillation frequency works in a frequency interval ranging from 3,635 kHz to 3,726 kHz; this is roughly a 90 Hz interval.

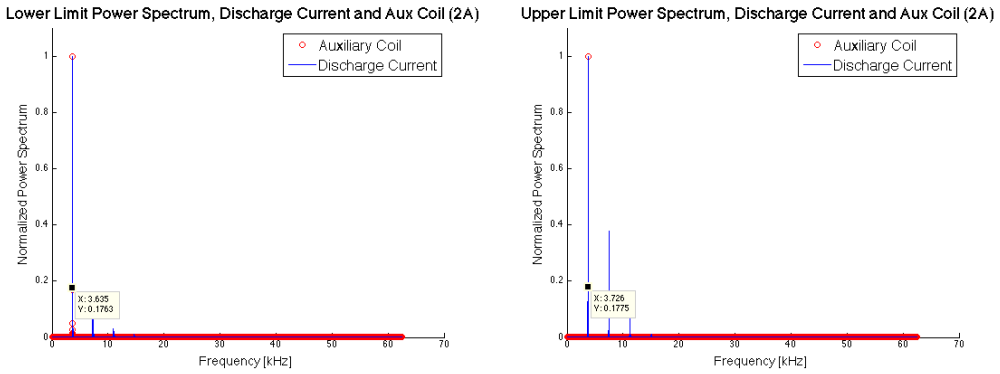

(a) Lower limit of the 2A frequency range. (b) Upper limit of the 2A frequency range.

Figure 5.25: *Comparison between lower and upper limits of the frequency range in which discharge current frequency shifts to match the coil signal (2 A) one.*

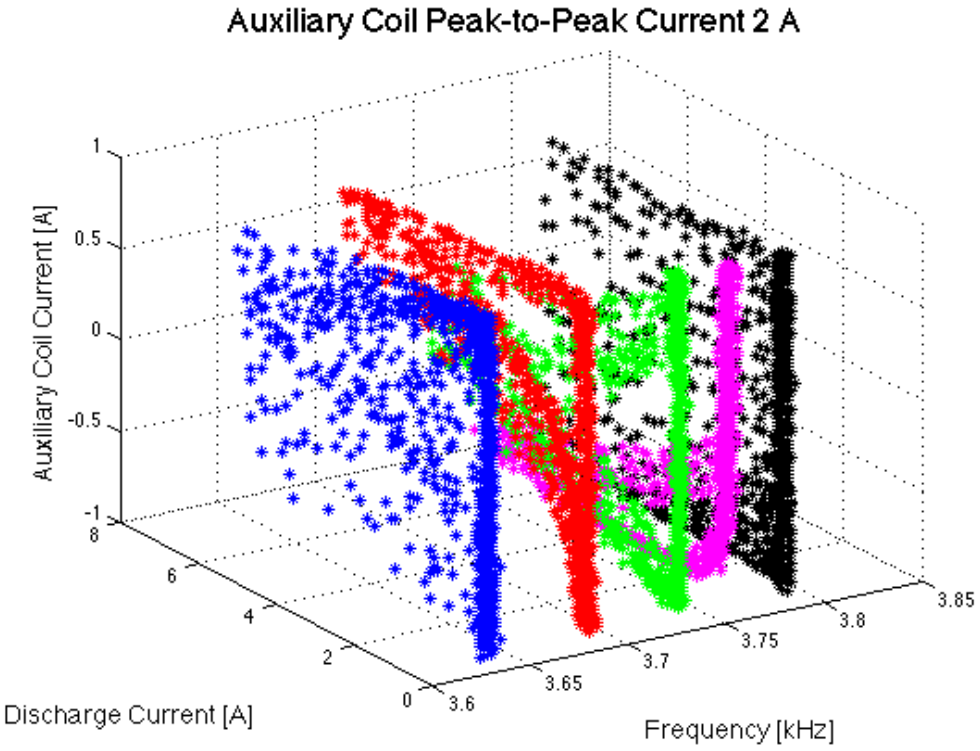

Figure 5.26: *Phase Diagram with a 2 A ptp auxiliary coil current. 90 Hz interval.*

In this test a 8 A peat-to-peak excitation current was used, resulting in a 380 Hz interval as deducible from the plots presented below.

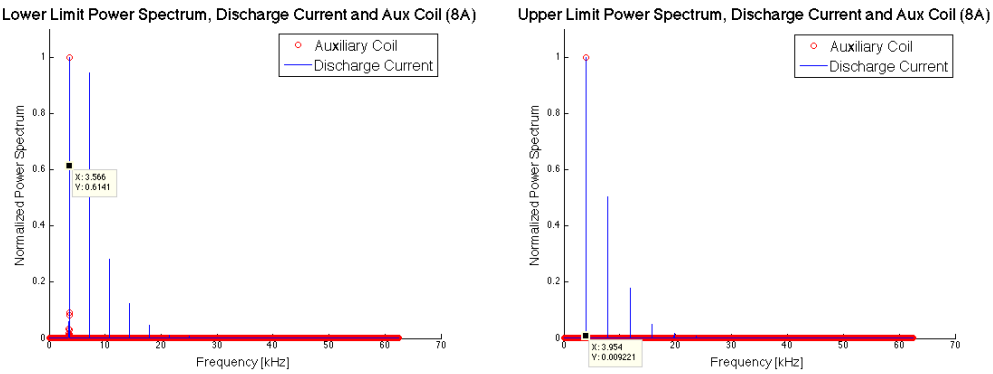

(a) Lower limit of the 8A frequency range. (b) Upper limit of the 8A frequency range.
Figure 5.27: *Comparison between lower and upper limits of the frequency range in which discharge current frequency shifts to match the coil signal (8 A) one.*

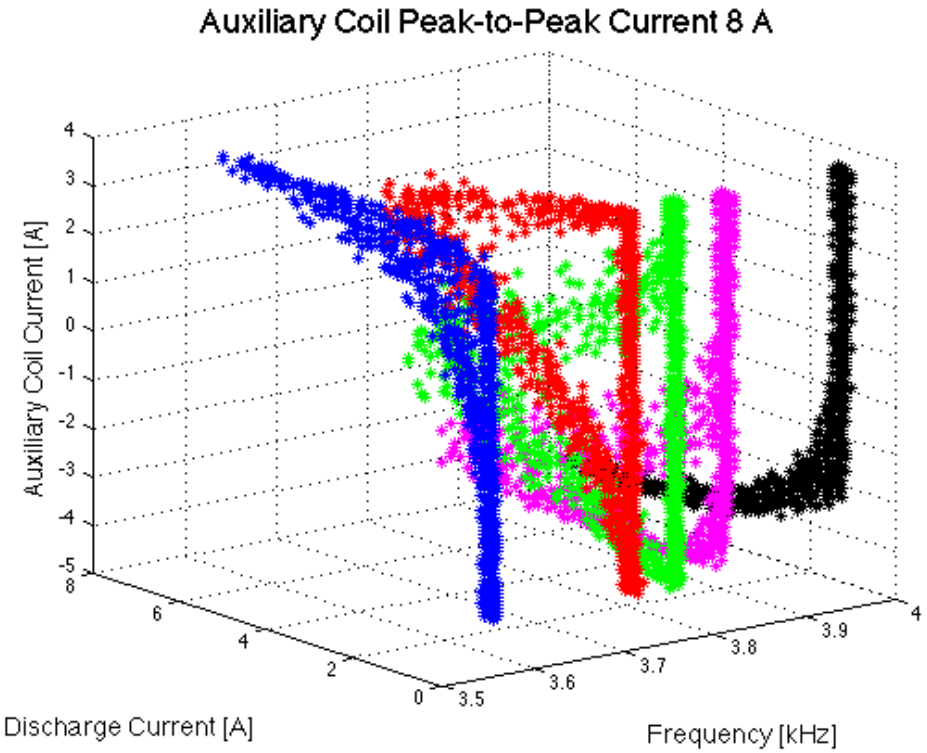

Figure 5.28: *Phase Diagram with a 8 A ptp auxiliary coil current. 380 Hz interval.*

In the third test reported, a 15 A peat-to-peak excitation current was used to power the auxiliary solenoid, resulting in a 440 Hz interval.

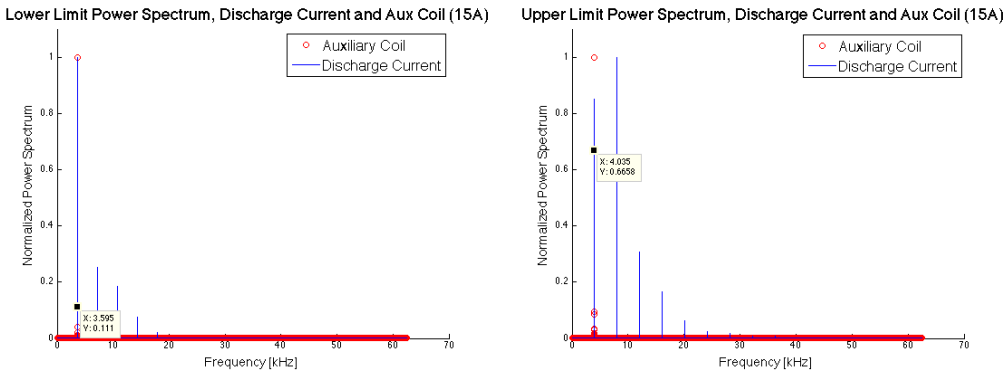

(a) Lower limit of the 15A frequency range. (b) Upper limit of the 15A frequency range.
Figure 5.29: *Comparison between lower and upper limits of the frequency range in which discharge current frequency shifts to match the coil signal (15 A) one.*

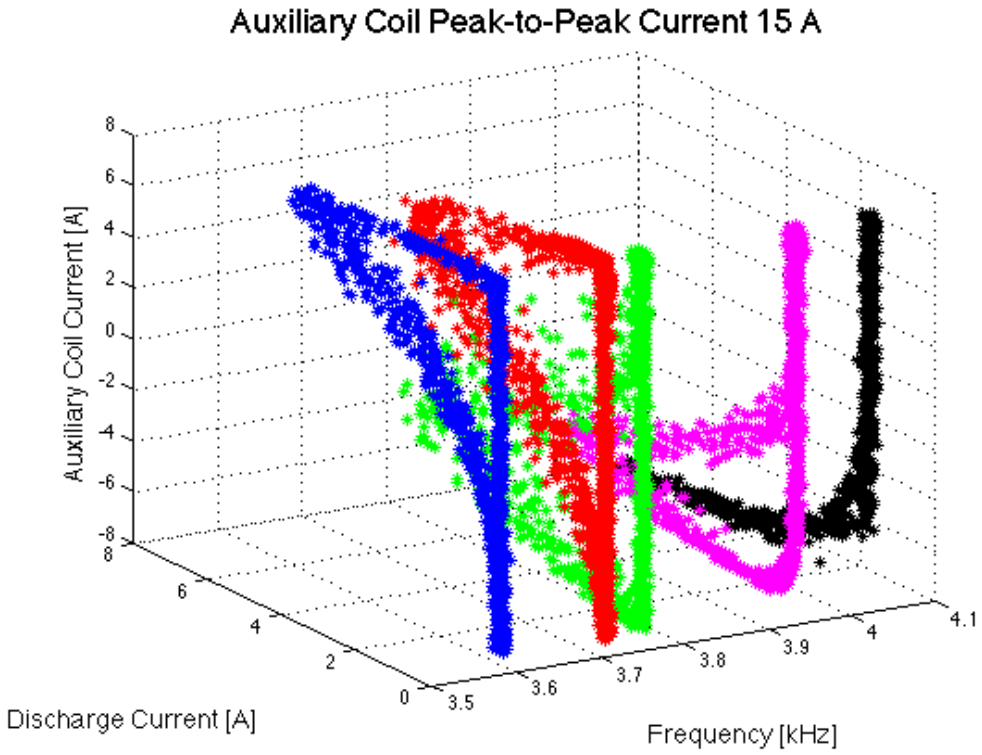

Figure 5.30: *Phase Diagram with a 15 A ptp auxiliary coil current. 440 Hz interval.*

In the last test a 20 A peat-to-peak excitation current was used, resulting in a 560 Hz interval.

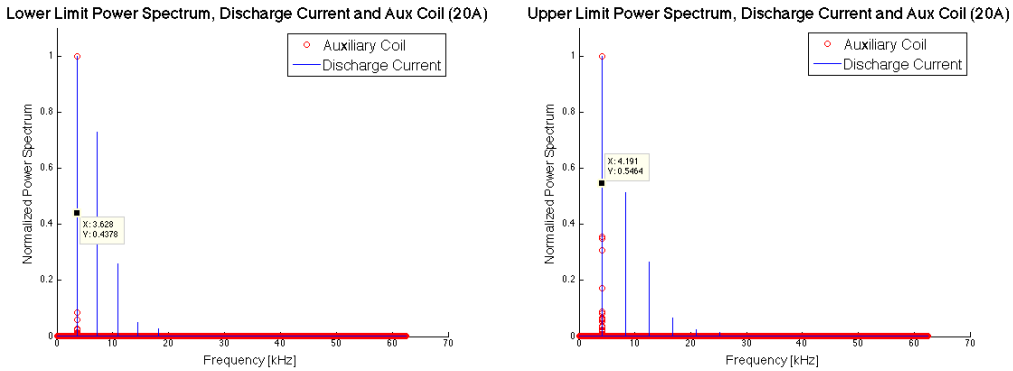

(a) Lower limit of the 20A frequency range. (b) Upper limit of the 20A frequency range.
Figure 5.31: *Comparison between lower and upper limits of the frequency range in which discharge current frequency shifts to match the coil signal (20 A) one.*

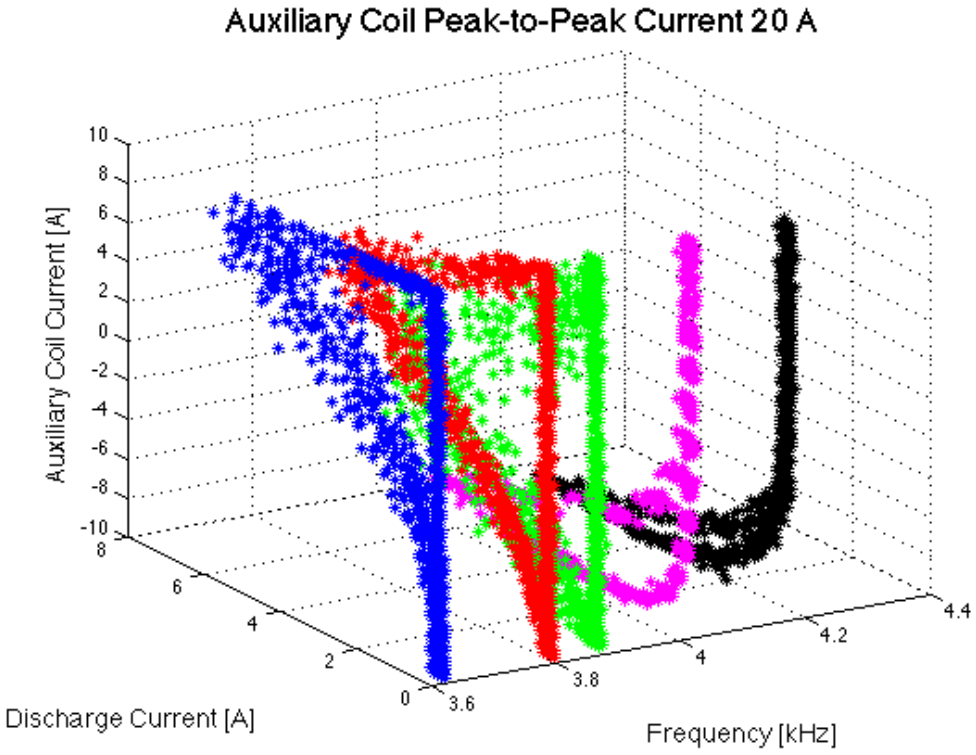

Figure 5.32: *Phase Diagram with a 20 A ptp auxiliary coil current. 560 Hz interval.*

The following table summarizes the data presented before. The trends of upper and lower limits of the frequency interval, in which the thruster adapts its fluctuations frequency to the excitation signal one, are indeed plotted as function of the auxiliary solenoid peak-to-peak current value. It is interesting to notice how the lower limit is not so affected by the increase of the power delivered to the auxiliary coil.

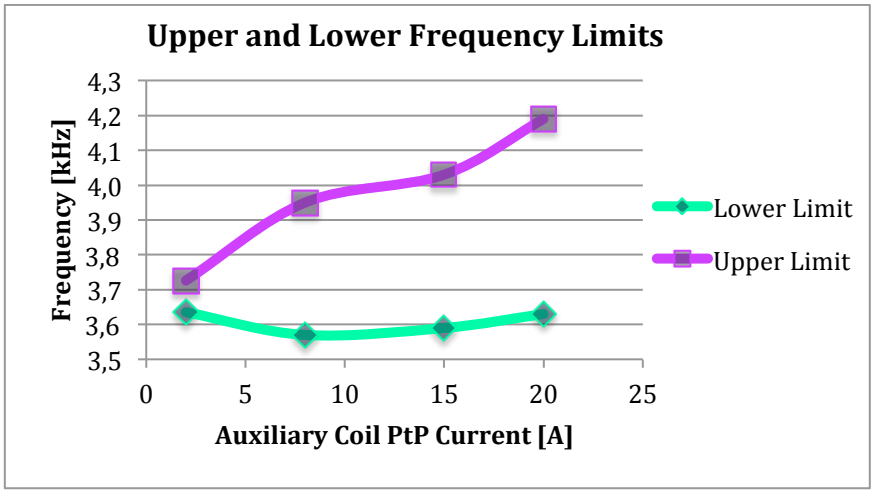

Figure 5.33: *Upper and lower limits of the frequency interval in which the thruster adapts its fluctuations frequency to the excitation signal one.*

The graph below represents the amplitude of the range as a function of the peak-to-peak coil current. Since the coil power level does not heavily affect the lower limit, as already shown in the previous graph, the shape of the curve is very close to the upper limit trend.

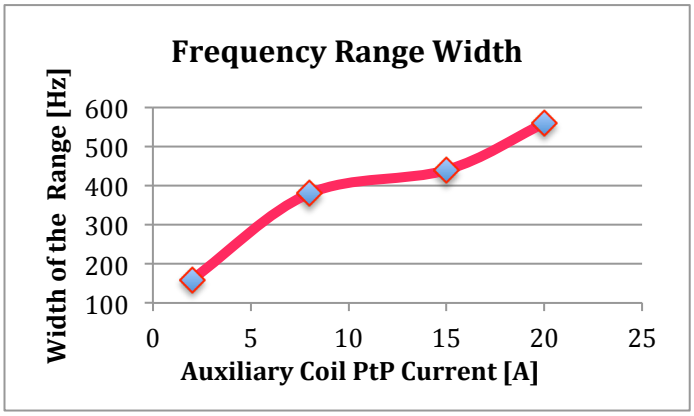

Figure 5.34: *Frequency range width as a function of the auxiliary solenoid peak-to-peak current value.*

The discharge current mean value and its route mean square parameter are discussed in the two graphs below. No very strong trend seems to be present, even if two considerations can be made. The mean value of the discharge current shows an overall increase with the power delivered to the auxiliary coil, about 1% (i.e.: 10 mA over 1100 mA). No monotonic behavior is by the way observed.

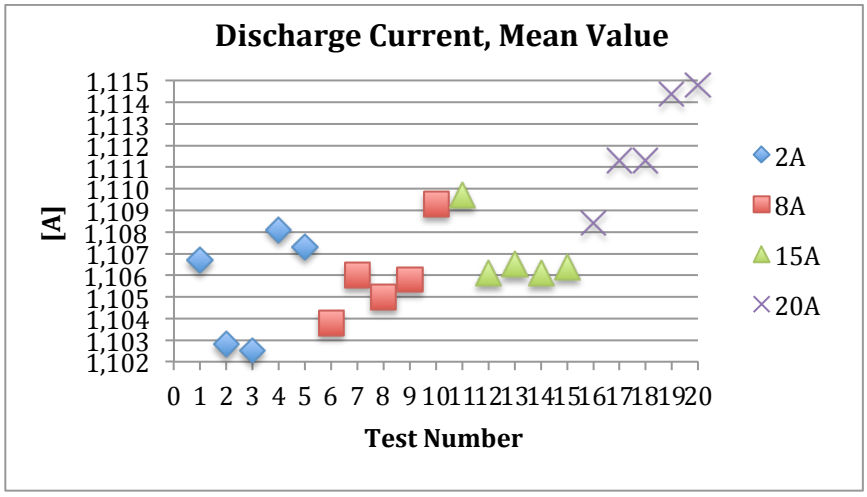

Figure 5.35: *Discharge Current Mean Value observed in the tests conducted at various powers.*

A curious behavior characterizes the RMS value of the discharge current as reported in the graph below.

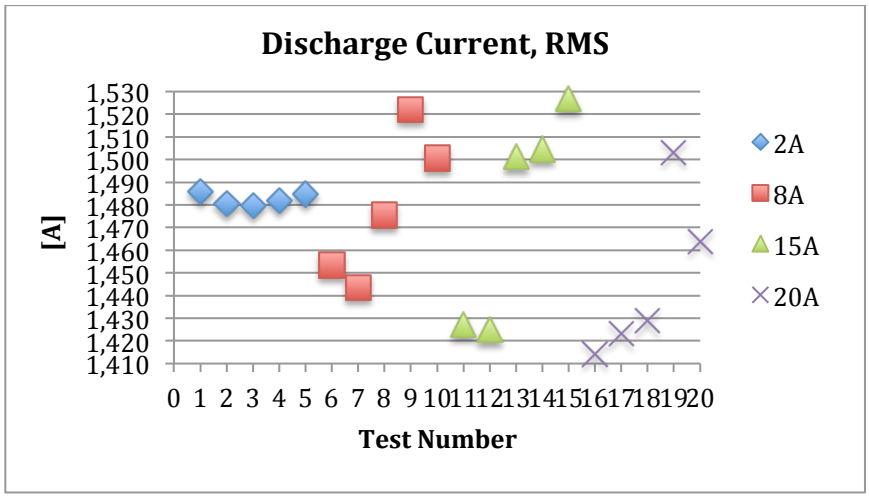

Figure 5.36: *Discharge Current RMS Value observed in the tests conducted at various powers.*

The tests conducted with a frequency lower than the central one (i.e.: the first 2-3 points of each test group) present, in general, a lower RMS. It is important to notice that the second half of the test conducted for each test group (i.e.: the last 2-3 points of each test group) are more far from the natural frequency of the oscillations, as already pointed out in the previous page. Thus it seems that a smoother discharge current can be achieved exciting the auxiliary coil with a frequency close to the natural one, but further tests are required before drawing this conclusion. The open loop testing phase revelad an interesting quantity of data.
In the next section more advane tests will be presented, including a preliminary attempt to realize a closed loop feedback system.

5.5 Advanced testing on the Cylindrical HET

After performing the reported tests in the open loop mode, the auxiliary solenoid was disconnected from the power system and plugged directly into the oscilloscope. In this configuration the solenoid acts as an antenna picking up any variation of the axial B field that takes place inside the channel of the thruster. Since during this preliminary study the relevance of the shape of the signals are more important than the absolute values, no calibration was performed. A Helmholtz coil can easily be used for the calibration of the antenna if any future experiments require that. In the graph below two traces are displayed. The light blue one shows four cycles of the discharge current oscillation, while the yellow one is the signal generated by the coil.

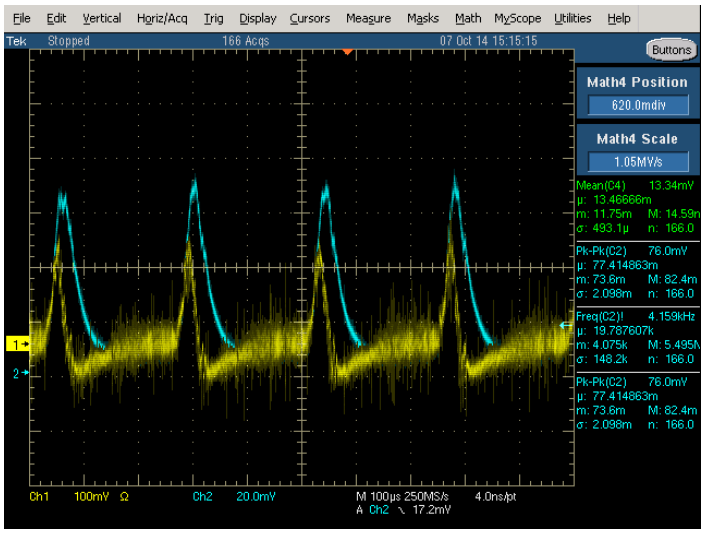

Figure 5.37: *Auxiliary solenoid signal generated by the coil in 'antenna-mode'. Light Blue is Discharge Current, Yellow is the signal picked up by the Auxiliary solenoid.*

Recalling the shape and the collocation of the auxiliary coil inside the CHTr (i.e.: a solenoid wrapped around the cylindrical channel of the thruster) and observing carefully the two traces, allows to conclude that the output of the coil is very close to the derivative of the discharge current signal. Later, it will result clear that this is an important information.
The relation between the two signals is, by the way, not so straightforward. The signal picked up by the coil is indeed the derivative of the azimuthal drift current, flowing in the *ExB* direction, which presents fluctuations as well.

$$V_{coil} = -\frac{\partial \phi(B_{axial})}{\partial t}$$

Where B_{axial} is generated by the azimuthal current j_Θ that is present in the thruster. The azimuthal current is oscillating at the same frequency of the thruster as shown in the screenshot and it is related to the axial current j_z (i.e.: the discharge current). In general there is a strong connection between azimuthal and axial oscillations as reported in past studies [26]. In particular it is experimentally seen that a constant ratio between azimuthal and axial current and its value is, very approximately, around 10; some theoretical motivation exist as well [87] being, in a quasineutral plasma, the ratio between azimuthal and axial current density equal to V_d/B where V_d is the discharge potential. In order to further justify the relation described, some basic numerical analyses are conducted on the recorded signals. In the graphs below the top two ones display measured signals while the bottom ones are numerically generated.

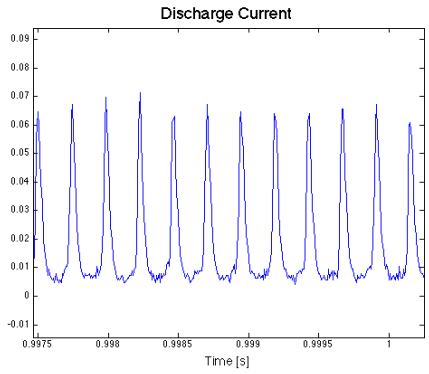

(a) Measured Discharge current trace.

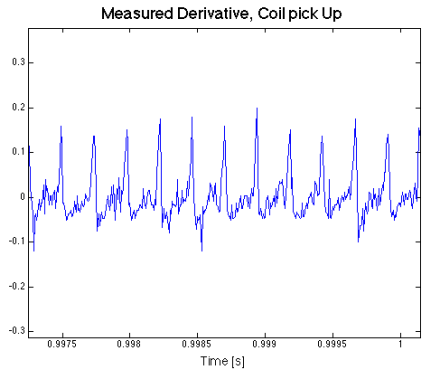

(b) Signal generated by the Auxiliary coil used as a receiving antenna.

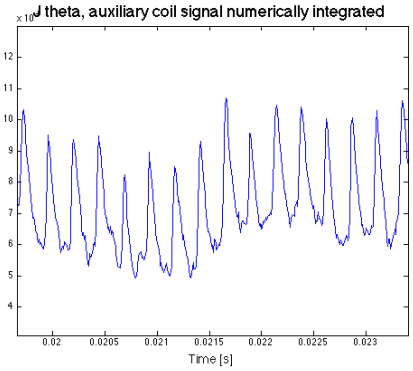

(c) Qualitative Azimuthal current waveform numerically integrated from graph b.

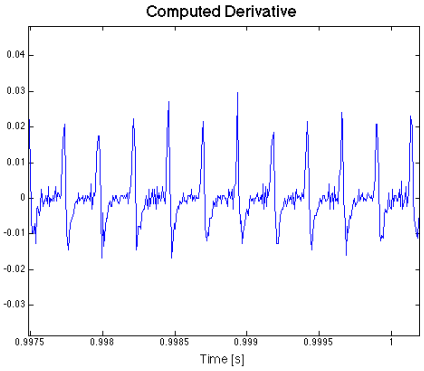

(d) Numerical Derivative of graph a.

Figure 5.38: *Comparison between experimentally acquired signals and numerically computed ones.*

There is a good agreement between experimentally sampled traces and numerically computed ones. Plot (d) represents the numerically computed derivative of trace (a) and its shape is very close to the signal shown in plot (b). Peaks are taller and the y-axis scale is different. The first difference is likely due to the absence of the non linearities intrinsically present in the physical setup, that partly mitigate the sharp peaks. With regard to the y-axis scale, two factors should be considered: no calibration of the coil was made and so no proportional factor is used and, even more important, the ratio between the azimuthal and the axial current was taken into account. Plot (b) is indeed the derivative of the azimuthal current, while plot (d) is the numeric derivative of the discharge current shown in plot (a). Plot (c) is instead the integral, numerically computed, of the signal sampled by the coil (i.e.: plot (b)). It represents then the azimuthal current. Again, no attention was paid to the y-axis scale; frequency and shape of the signal are the two main factors of interest. After having better clarified the relation that exists between the discharge current and the voltage developed at the leads of the auxiliary coil, a new component was added to the signal processing chain. The following plot is similar to the one already presented in the previous section, nevertheless two differences are present. The pink signal is indeed the output of the differentiator circuit described in chapter 5 and is in fact the inverted real time derivative of the discharge current plotted in yellow. The discharge current is then slightly less regular at the tips of the biggest peaks, hence the more 'noisy' derivative, probably because of some minor differences in the parameters of the operational point of the thruster.

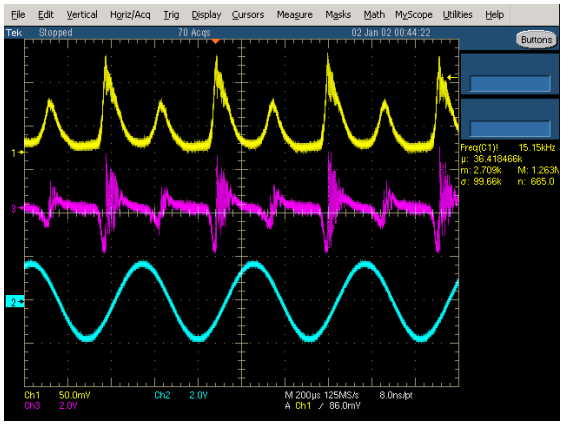

Figure 5.39: *Double-Mode behavior with system in Open Loop Mode, 2 kHz coil signal. Yellow is Discharge Current, Light Blue is the signal generator and Pink is the Auxiliary solenoid Current.*

The interesting lower peak is again present as in the previous test at the same frequency of 2 kHz as well as the asymmetry between the upward and downward sides of the discharge current peaks. In the next scope screen shot an

even more interesting interaction between the Hall Thruster and the auxiliary coil is reported. In this experiment, the frequency of the current waveform used to drive the auxiliary coil is slightly lower compared to the previous one.

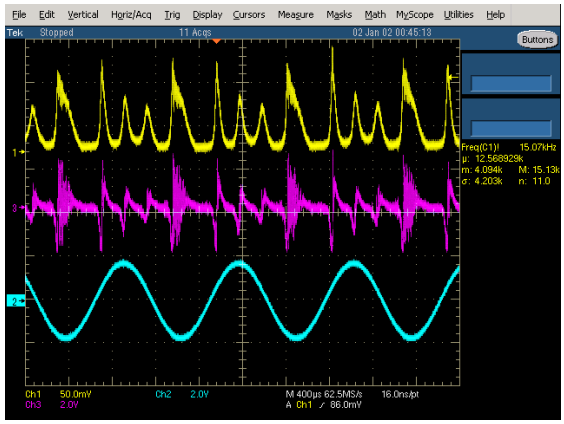

Figure 5.40: *A different behavior oh the system with a slightly lower frequency signal in the coil. Yellow is Discharge Current, Light Blue is the Auxiliary solenoid Current and Pink is the output of the differentiator circuit.*

Two new peaks are now present resulting in a four peaks periodic signal with one large peak and three narrow ones, in particular the first narrow one is much higher than the other two. Oscillations in the downward side of the wider peaks are still present as in the previous test. The last open loop test was conducted using a very different frequency of the auxiliary coil signal, 197 Hz sinusoidal signal, so much lower with respect to the frequency of the discharge current that it can be considered a DC test as well. Some interesting effects are observed.

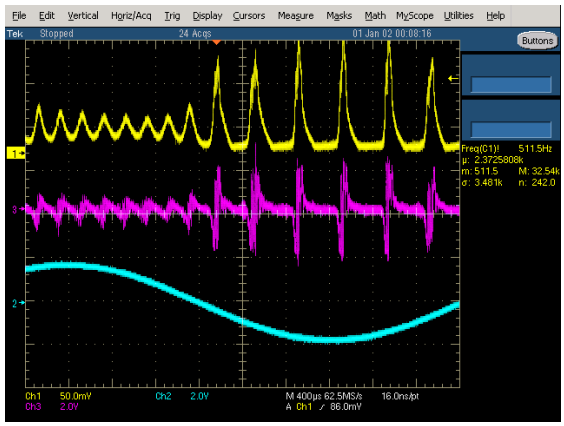

Figure 5.41: *Low frequency excitation of the auxiliary coil. Yellow is Discharge Current, Light Blue is the signal generator and Pink is the Auxiliary solenoid Current.*

Depending on the polarity of the current, the amplitude of the discharge current oscillation is much lower. Moreover, the Faraday probe waveform follows quite well the discharge current trace attesting how the effect is seen from the ions too. More cycles are shown in the plot below compared to the screenshot previously presented. Even more interesting is a detail that can be observed looking at the zoomed version of the anode current plotted in graph (b).

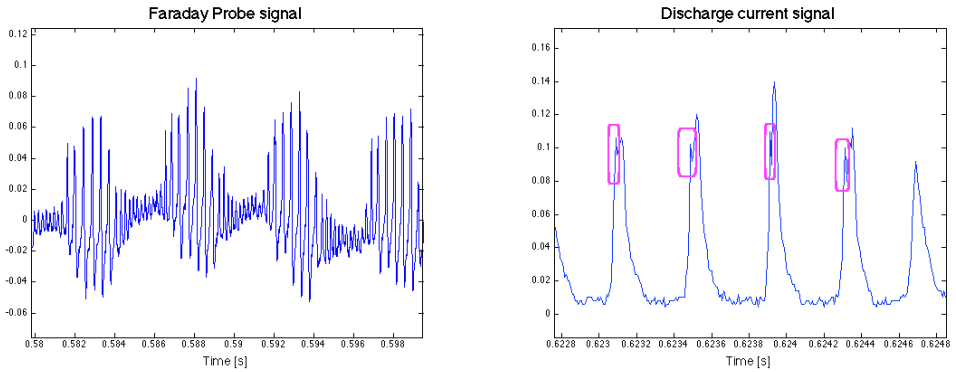

(a) Faraday probe signal. (b) Sub-peaks on the left of the tip.

Figure 5.42: *Interesting traces with a very low frequency coil signal, 197 Hz.*

The sub-oscillations observed before on the right of the tip of the peaks are now on the left as shown in the pink boxes in the graph below. An opposite position of the sub-peak (i.e.: in the downward branch of the peak) was observed in the previous open loop tests. The reason for this different is not known. After the vast open loop testing a different set of experimental trials was conducted and it is described in the following section.

Closed Loop Testing

As a last test, the signal processing system was modified in order to implement a closed loop feedback setup. The output of the differentiator circuit has been connected to the input ports of the audio amplifier resulting in the capability to inject the processed signal into the coil. This setup is equivalent to a PID controller in which the derivative constant D only is not zero. It seems to be indeed not so adequate to use a proportional or integral feedback since the signal picked up by the coil is proportional to the derivative of the discharge current, as already discussed. Two different polarities of the amplified signal were tested. Even if an interesting interaction is recorded by the scope, no strong damping effect has been observed. The left screen shot shows the closed feedback loop obtained amplifying the signal outputted by the circuit without any polarity alteration, while in the right one the polarity of the signal is inverted.

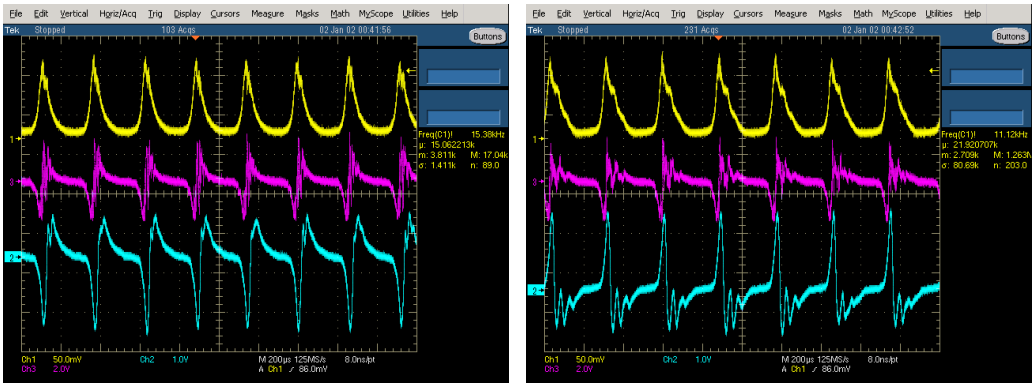

(a) Closed Loop Feedback using the inverted derivative.

(b) Closed Loop Feedback using the non inverted derivative.

Figure 5.43: *Closed Loop Testing using the discharge current derivative signal. Yellow is Discharge Current, Light Blue is the Auxiliary solenoid Current and Pink is the output of the differentiator circuit.*

Two main differences are present. The discharge current of the right configuration has a frequency slightly lower compared to the left one (3,615 kHz VS 3,892 kHz), and a maximum value slightly lower as well. The waveform is different too. In the reversed polarity test, the sub-oscillation observed in the downward side of the current trace is much more visible, as attested by the light blue trace (i.e.: waveform of the current driving the auxiliary coil) itself and by the following plots showing the anode current.

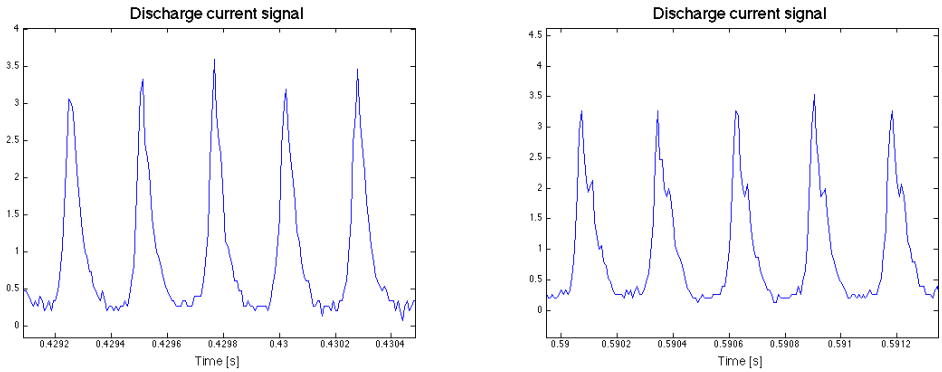

(a) Non Reversed Closed Loop.

(b) Reversed Closed Loop.

Figure 5.44: *Zoomed comparison between discharge current traces without and with inversion of the polarity.*

In order to further explain the difference in the signal processing systems used in the tests described above, the simple mathematical relation that describes the process is reported.

For the non reversed configuration of the left screenshot:

$$I_{coil}(t) = k_{amplifier}\left(-k_{derivator}\left(k_{j_\Theta j_z}\frac{\partial I_{disc}}{\partial t}\right)\right)$$

while for the reversed configuration of the right screenshot:

$$I_{coil}(t) = -k_{amplifier}\left(-k_{derivator}\left(k_{j_\Theta j_z}\frac{\partial I_{disc}}{\partial t}\right)\right)$$

where $k_{amplifier}$ is the adjustable gain of the audio amplifier, $k_{derivator}$ is the gain of the electronic circuit that takes the derivative of the signal and the minus in front of it represents its characteristic of having as an output the inverted derivative. Last, $k_{j_\Theta j_z}$ is the factor that relates the azimuthal current to the axial one as already explained. From an intuitively point of view, one could expect that the first case (i.e. amplification of the inverted derivative without further polarity inversion) would produce a damping effect. Looking at the traces recorded this is verified at least for the sub-oscillations that are instead amplified in the reversed polarity test, as intuitively predictable. Further damping is however not observed. This is likely due to the fact that a much higher power would be required in order to affect the axial current through the damping of the azimuthal current. Using a Faraday probe, more data were recorded. In this case no big difference is shown in the comparison between straight and reversed polarity of the closed loop signal.

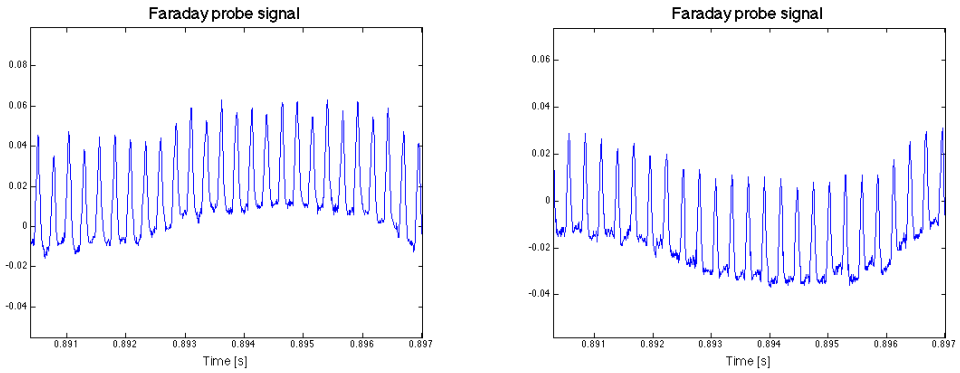

(a) Faraday probe, not reversed polarity. (b) Faraday probe, reversed polarity.

Figure 5.55: *Faraday Probe signal in closed loop, straight and reversed polarity.*

In particular no sub-peaks are detected. Further experiments are required to better understand the reason of this difference.

5.6 Operative Issues

5.6.1 Introduction

Operative issues are something normal while working in a lab. Considering that this was the first lab experience for the author, facing the large number of practical problem has been a really good training. Failures of a lot of different components generate delay and unexpected need of replacement parts. A non-properly tighten fitting in a vacuum pipeline can create a leak that is not always easy to detect and that can force to stop the pumping procedure, especially when working with high vacuum, achieved by the cryopumps. A loosen belt of the vacuum pump can overheat and brake, forcing again to interrupt the testing. Overloads in electrical lines create by current peaks frequently present when working with plasma devices can force the breaker to interrupt the power delivery shutting down all the equipment. Sometimes interference create problem as well, fluctuation of the mass flow controller due to the fluctuation of the current delivered by a nearby power supply is an example of the required mental flexibility in the research process that is often necessary in order to find the cause of the improper functioning of the device under testing. Besides that, power supplies and other electrical equipment failure played a considerable role in the troubleshooting process. The author considers worthwhile to briefly present some of the operative issues experienced during the experimental experience described in this thesis.

5.6.2 Cathodes

Cathodes are undoubtedly the most probable source of operative issues when dealing with Hall Thrusters. Two of the three cathodes used to neutralize the ion jet produced by the thrusters tested suffered major damages. The Ion Tech cathode, a barium-impregnated cathode, showed a lot of problems connected to the lifetime of the expensive insert. In the left picture below, one of the two cores burnt in few months is shown. The assembly is made up of various parts: the main ones are the tantalum heating filament with its heat shield and the emitter. The main cause of failure is probably oxygen poisoning the can easily destroy an emitter. In fact even after cathode has been used, it is important to prevent oxygen from being close to the cathode that can remain hot for hours, since in vacuum heat transfer is much lower then in air. In the right picture the refurbished cathode is shown.

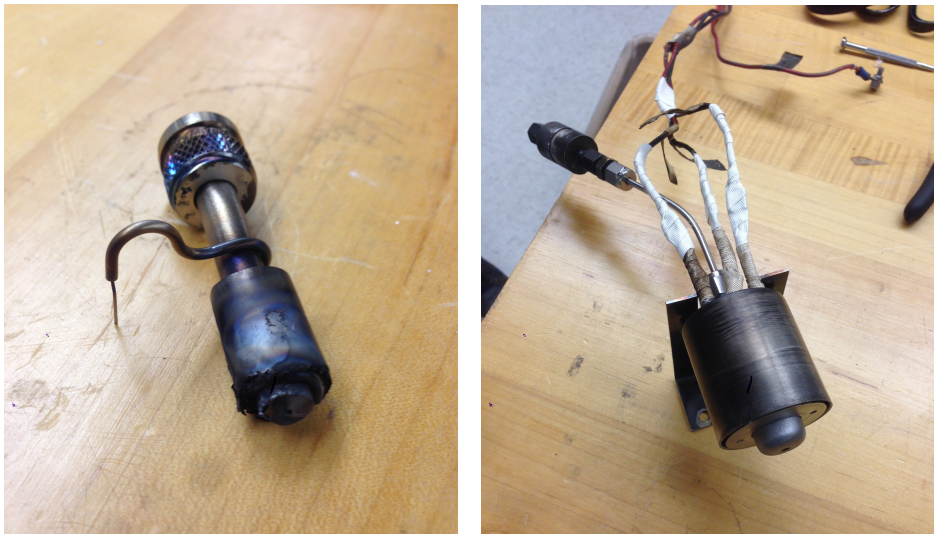

(a) Damaged Cathode Insert Assembly. (b) Ion Tech Cathode after Refurbishment.

Figure 5.56: *Ion Tech Cathode Emitter replacement*.

The emitter is by the way not the only source of problems. Relatively high voltage connections (i.e.: 600 V) to the keeper electrode require excellent insulation to prevent shorts to happen. A thin coating of the ceramic insulator of the keeper can generate a short. Usually part of these problems arise only after the cathode is warmed up because of thermal expansion and hot gas presence, forcing to stop the switch on procedure that has already taken several hours at that point.

Even more critical is the non-commercial cathode used during the laboratory testing presented in this thesis. This totally different cathode was developed by Air Force Institute of Technology; the emitter is a Lanthanum Hexaboride (LaB6) hollow cylinder. This material is definitely much easier to handle since it is less sensible to oxygen poisoning. It is also more tolerant during the conditioning procedure that allows the emitter to expel impurities before reaching the very high temperature required to generate electron emission, around 1650° C and that for traditional impregnated emitter can take double the time even if the working temperature is lower. Even if more details on this cathode are presented in Appendix A, some examples of common operative issues are described below.

The original tantalum coaxial heating filament has been replaced with a bifilar wrapping of tantalum wire passing through a series of alumina beads. Considering the new arrangement, no clear limit of the new heater was known resulting in a major failure. The heater melted after 8 hours of use. The failure

has likely promoted a short between the keeper potential and the grounded body of the cathode under the ceramic beads.

Figure 5.57: *new AFITr Cathode heater damaged.*

Keeper shorting is for sure the second most common issue while working whit this cathode. The external electrode (i.e.: the keeper) is quite close to the central body and to the heat shield wrapped around the heater. A minor misalignment can easily create a short that, again, is likely to happen after the cathode has warmed up. A more curios way of shorting the keeper is through the screws that hold it in place.

Figure 5.58: *AFITr Cathode Keeper screw and shoulder insulator damaged.*

The ceramic shoulders that prevent electrical connection between keeper and the head of the screw itself can easily get covered with sputtered material resulting in the loss of the insulation capability. If this happens and the cathode is not quickly turned off, the current established across the screw can easily melt it or causing a strong oxidation due probably to high temperature.

5.6.3 Z-70, the annular Hall thruster

In this paragraph a brief description of some of the problems encountered during the use of the Z-70 is presented. In the left picture the thruster shows a darker spot on the top left corner of the front plate. This was caused by a current leak through the metallic frame of the thruster touching the plasma after a major erosion of the wall due to a former incorrect cleaning process.

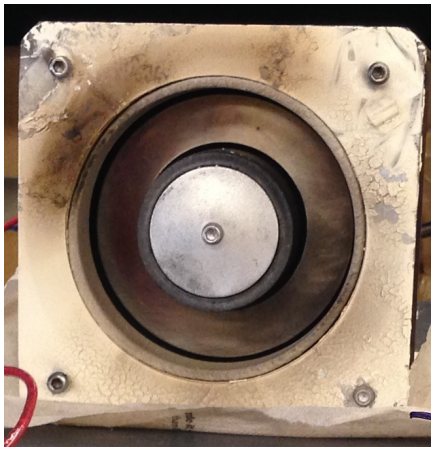

(a) Damaged wall generates current leak.

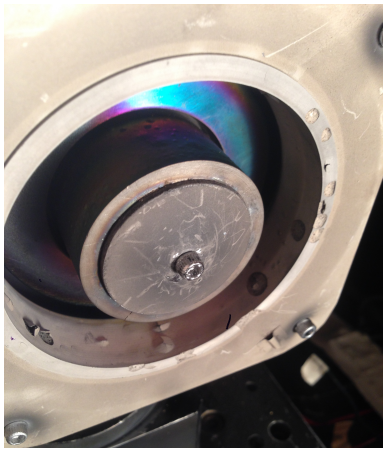

(b) BN wall damaged because of water absorption.

Figure 5.58: *Z-70 wall damaged.*

In the right picture a different operative issue is shown. After replacing the wall with new Boron Nitride component, the thruster suffered micro explosions on the surface of the new wall. This phenomenon is probably due to water absorption from the ceramic material that was then suddenly released during the exposure to high vacuum and to the strong increase of temperature following the ignition of the plasma. Luckily this damage didn't affect the testing, but it is still an interesting example that attests how much care is necessary while using these kinds of devices.

5.6.4 CHTr, the rebuilt Cylindrical Hall Thruster

This paragraph briefly describes a couple of steps of the refurbishment process of the cylindrical Hall thruster. In this case the operative issue is represented by the fact that the thruster was found completely disassemble. Some parts were missing, others even if present, did not come from the part set necessary to assemble the thruster and some others were damaged. In particular both inner and outer walls were broken. The central pole piece was cracked and split into two halves. The outer wall had part of the lower edge cracked in several parts and a small piece of ceramic was missing. High temperature ceramic paste was used to glue together and rebuild the ceramic wall, paying attention to perform a good gluing process able to survive the high temperature environment established during the thruster operation. Paste was cured for a day and the tolerances adjusted using fine sand paper. The two halves of the central pole piece were pressed together and left curing with a clamp; the junction line is visible in the image. Some pictures of the rebuilt Boron Nitride walls are presented below, the detail on the damaged outer wall prior refurbishment is missing.

(a) Glued central pole. (b) Intermediate phase. (c) Final result.

Figure 5.59: *CHTr walls gluing process instants*.

The refurbished wall was fully covered with boron nitride spray. This reveals to be not a good choice: after an hour of testing, the walls were totally covered by a fluffy black film that was then removed before testing the thruster again. This is probably due to the nitro-cellulose binder that reacts with the impact of electrons that are travelling along the magnetic field lines [80]. A comparison between the look of the thruster before and after the preliminary testing is shown in the pictures below. AFITr Cathode was used to power the thruster for the first time. Considering that back plate, external and internal coils, ceramic insulator for anode screws and some other components coming from other devices were adapted and used for the CHTr, the relatively easy start of the thruster was a great accomplishment.

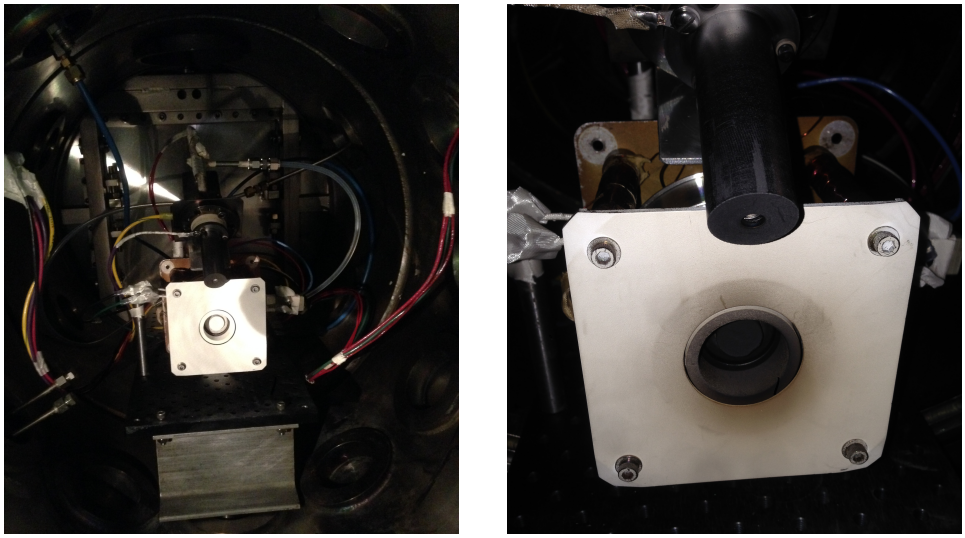

(a) Refurbished CHT before testing (b) CHTr after one hour testing

Figure 5.60: *CHTr wall blackening*.

As a last description, a curious fact is reported. After a sudden shut off of the thruster, all the setup was double-check without identify any broken or damaged component. While double-checking everything before closing the chamber to test the thruster again in order to understand if the problem was eventually a thermal one, a damaged gas line was found. The back surface of the anode gas line was indeed melted by the irradiated heat flux coming from the plasma produced by the thruster and from the cathode, as well. Replacing the pipe with a new-shielded one completely solved the issue.

Figure 5.61: *Anode gas line melted under irradiated heat flux*.

5.7 Future work and Improvements

The presented topic is strongly interdisciplinary and the improvement opportunities are incredibly numerous. Even if the technical part of the system was developed with care, further improvements are still possible.
At this point, by the way, it would probably have greater importance focusing on the theoretical aspects of the described magnetic interaction with the ionization instabilities. A lot of numerical models are available for the simulation of the Hall thruster fluctuations but they are generally not very flexible making challenging the integration of the modulation of the field, especially in the closed loop layout. Both the cases presented, the auxiliary solenoids mounted on the annular Hall thruster with their axis perpendicular to the thruster axis and the single auxiliary solenoid mounted coaxially with the channel of the cylindrical Hall thruster are characterized by a non ideal configuration of the field. In both cases the distribution of the field lines and their shapes are indeed position dependent. An accurate mapping of the field would be thus required before running any realistic simulation.
The strong impact obtained on the discharge current during the DC testing suggests that some clear physical phenomenon is having place; further experiment could better reveal the underlying mechanisms. A fast camera can be used non intrusively to check if the rotating spoke instability is effectively affected by the asymmetry introduce in the topology of the field. Some electrodes can also be placed radially close to the exit plane of the thruster to map the Hall current as a function of time and position.
More complex is the situation presented in the section about the cylindrical Hall thruster. The time varying nature of the field implies the need to update the magnetic field during the cycle of the simulation requiring an ad hoc code.
The sub-peaks showed in the discharge current traces are hint of two or three classes of electrons that are synchronized or mutually delayed by the external excitation due to the auxiliary coil, but further studies are required to better understand the physics beyond this. The open loop tests data allow then to derive a transfer function of the system: the gain can be can be computed by integrating the spectral power of the discharge current around the exciting frequency and subtracting then the spectrum of the non-excited signal. The phase can be derived by the cross-correlation between the auxiliary solenoid excitation current and the thruster discharge current [73]. Such a transfer function could be compared to the one generated by theoretical models helping in the validation process.
Phase shifting between the discharge current and the excitation signal of the auxiliary coil should also be tested in the closed loop system configuration. In this way a degree of freedom is added to the system allowing for more test

settings; commercially available or custom-built analog circuits can achieve this improvement. Cross correlation study can then help in the data analysis process.
Monitoring the output power of the amplifier and comparing that information with the time resolved parameters of the discharge current or ion current could also allow understanding how the power transmitted from the coil to the thruster varies in time and which is the relation with the speed of the ions. As already said, time resolved techniques are now available offering a powerful tool to further the unveil phenomena taking place in the creation and acceleration of the plasma in Hall thruster [2]. Such information could help understanding what is the physics behind the observed behavior during both open and closed loop experiments.
Effort should be spent trying to realize and entire magnetic circuit with material compatible with high frequency signals as explained in chapter 3. That solution offers the great advantage of a more tradition magnetic field topology reducing the numbers of the unknowns of the problem and simplifying the simulation.
In addition, a totally different interaction strategy is available as well and, until now, it remains not studied: the modulation of the propellant mass flow rate. In some different researches it was experimentally found that a bigger volume at the entrance of the gas line into the thruster could reduce the magnitude of the discharge current oscillations [74].
Moreover, a combination of the interaction strategies available could be investigated but, again, the theoretical and numerical modeling capabilities should be further developed first. A direct correlation between modulation of the magnetic field and thrust would be useful as well. Unfortunately this kind of testing requires a lot of effort in order to acquire precise data with a thrust stand.
In previous studies no clear reduction effect on the discharge current fluctuations has been observed, feeding the doubt that lowering the discharge current could be not an easy task: the magnetic field gradients affect indeed greatly the electron conductivity [25].
Of primarily importance is a theoretical in depth analysis: reproducing by numeric simulation the numerous data obtained experimentally would for sure increase the understanding of such a complex phenomena.

Chapter 6

Conclusions

The interaction with the low frequency oscillations observed in Hall thruster is achievable by different methods. In this thesis an experimental study of the effect that a time varying component of the thruster magnetic filed exercises on their typical low frequency instabilities has been carried out. Different kinds of tests were performed using two low power laboratory thrusters: an annular Hall thruster and a cylindrical Hall thruster, which was totally rebuilt and partially modified for the experimental campaign. Three different cathodes have been used; in particular one of them was refurbished and modified.

Adding the mentioned time varying part on the constant magnetic field of the thruster is definitely challenging at the frequencies of interest, namely from few kHz to some tens of kHz. Two strategies are investigated with the purpose of overcome some of the clear limits that were identified reviewing previous studies on the modulation of the magnetic field in Hall thrusters. A preliminary design of a non-traditional magnetic circuit for Hall thruster is described, but not realized because of manufacturing limitations. A different solution based on auxiliary coils, externally or internally integrated in the existing structure of the thruster, is thus conceived, design, built and tested.

Two sets of auxiliary air cored solenoids have been realized, one for each thruster. DC tests have been performed in the annular thruster, while AC tests were used to study the interaction with the instabilities in the cylindrical one. The entire power system for the high frequency auxiliary coil designated to operate in the cylindrical Hall thruster has been developed facing some of the difficulties involved in driving a coil with a broadband high current signal, roughly *0 - 40 kHz*, *0 - 30 A* peak current. A tangible improvement in the modulation of the field has been documented.

Open loop tests were thus conducted showing numerous interesting effects due to the interaction of the now achieved field modulation with the low frequency instabilities that are present in the plasma. These effects have been studied sampling the trace of the thruster discharge current that was monitored with an oscilloscope and some additional electronic components.

Ion current has been sampled as well using a Faraday probe.

Furthermore, preliminary closed loop tests on the cylindrical thruster were performed using, in this case, the derivative of the discharge current computed in real time as a feedback signal. A physical motivation that supports this choice is proposed and a technical description of the equipment used is provided.
Interesting phenomena, probably due to the asymmetry of the magnetic field, have been observed in the annular thruster while even more curious effect was detected in the cylindrical one. The hint of the presence of two or more classes of electrons travelling in the thruster channel is showed by the discharge current traces acquired. Depending on the powering configuration of the system, different effects on these electrons are obtained.
In order to fully understand the intriguing phenomena documented and reported in this thesis, a deeper theoretical analysis should be undertaken and some numerical simulations performed. Moreover, a number of different and more complex experimental techniques is also accessible, as already explained in the previous section. Among them, non intrusive time resolved measurements can be carried out and the power coupling between the auxiliary coil and the plasma can be related to that measurements, hopefully helping to further explain the interaction observed during the preliminary testing of the new born system. Fast camera imaging can be use to monitor low frequency azimuthal instabilities and relate possible effects with the longitudinal fluctuations of the plasma jet as well. New insight on the physics of the Hall thrusters could be derived from such a study and some improvements in their design and in the on board circuitry possibly achieved.

Bibliography

[1] A. Lucca Fabris, "*Traveling Magnetic Field Plasma Accelerator"*, IEPC-2013-86.

[2] C. Young, A. Lucca Fabris, N. Gascon, M. Cappelli. *"Experimental Characterization of the Time-Averaged and Oscillatory Behavior of a Hall Plasma Discharge"*. 67th Annual Gaseous Electronics Conference. 2014.

[3] Goebel D. and Katz I., "Fundamentals of Electric Propulsion: Ion and Hall Thrusters", Wiley, Hoboken N.J., 2008.

[4] http://www.engineeringtoolbox.com/awg-wire-gauge-d_731.html

[5] John E. Rotter, Lieutenant Commander, USN, *"An analysis of multiple configurations of next-generation cathodes in a low power hall thruster*". Air Force Institute Of Technology, thesis.

[6] http://www.edfagan.com

[7] N. Gascon, M. Dudeck, S. Barral, "*Wall Material Effects* in *Stationary Plasma Thrusters. Parametric studies of an SPT-100"*, Physics of Plasmas, Vol. 10, No. 10, 2003.

[8] A. I. Morozov, Kurchatov Institute Moscow Russia, "*Stationary plasma thruster (SPT) development steps and future perspectives"*, IEPC 93 101.

[9] Christopher D. Vineski, "*Experimental Analysis of Dampened Breathing Mode Oscillation on Hall Thruster Performance"*, Capt, USAF AFIT-ENY-13-M-39, thesis.

[10] David Liu, "*Two-Dimensional Time-Dependant Plasma Structures of a Hall E_ect Thruster"*. PhD thesis, Air Force Institute of Technology, September 2011.

[11] M. K. Tikhonravov, editor, "*Works on Rocket Technology"* by E. K. Tsiolkovsky. Publishing House of the Defense Ministry, Moscow, 1947.

[12] R. H. Goddard, "*Method and means for producing electrified jets of gas*", December 1920.

[13] Artsimovich L. A. and et al., "*Development of the stationary plasma thruster (SPT) and its test on Meteor satellite*", Vol. 7, No. 3, pp. 451-468, 1974.

[14] Busek Co. Inc., http://www.busek.com/flightprograms__ts2.htm

[15] E. Y. Choueiri, *"Plasma oscillations in Hall thrusters"*, Physics of Plasmas, vol.8, pp. 1411-1426, Apr. 2001.

[16] S. Barral, E. Ahedo, *"Theoretical study of the breathing mode in Hall thrusters"*. In Proceedings of the 42nd AIAA Joint Propulsion Conference, page 5172. American Institute of Aeronautics and Astronautics, 2006.

[17] Plasma Accelerators Group, Poland, http://pag.ipplm.pl/?id=hall

[18] A. W. Smith, *"Field structure and electron transport in the near-field of coaxial hall thrusters"*, PhD thesis, Stanford University. 2010.

[19] S. Barral, J. Miedzik, E. Ahedo, *"A model for the active control of low frequency oscillations in Hall thruster"*, 44th AIAA/ASME/SAE/ASEE Joint Propulsion Conference & Exhibit 21 - 23 July 2008, Hartford, CT.

[20] R. Hofer, *"Development and Characterization of High-Efficiency, High-Specific Impulse Xenon Hall Thrusters"*. PhD thesis, The University of Michigan, 2004.

[21] J. Linnell and A. Gallimore, *"Efficiency analysis of a hall thruster operating with krypton and xenon"*. Journal of Propulsion and Power, 22(6), November-December 2006.

[22] D. H. Manzella and J. M. Sankovic, *"Hall thruster ion beam characterization"*, in Proceedings of the 31st Joint Propulsion Conference and Exhibit, San Diego, CA, 1995. AIAA/ASME/SAE/ASEE**.**

[23] L. T. De Luca, *"Problemi energetici in propulsione aerospaziale"*, Politecnico di Milano, 2007.

[24] J. P. Boeuf, B. Chaudhury, *"Rotating Instability in Low-Temperature Magnetized Plasmas*", Physical review letters 111 (15), 155005.

[25] M. S. McDonald and D. Gallimore, A, *"Parametric Investigation of the Rotating Spoke Instability in Hall Thrusters",* in Proceedings of the 32nd International Electric Propulsion Conference*,* 2011.

[26] D. Escobar, E. Ahedo *"Global stability analysis of azimuthal oscillations in Hall Thrusters",* IEPC-2013-304.

[27] V. I. Baranov, Yu. S. Nazarenko, V. A. Petrosov, A. I. Vasin, Yu. M. Yashonov, *"Theory of Oscillations and Conductivity for Hall Thruster",* AIAA Paper 96-3192*,* July 1996.

[28] Baranov V. I., Nazarenko Yu. S., Petrosov V. A., Vasin A. I., and Yashonov Yu. M., *"The Ionization Oscillations Mechanism in ACD"*, Pro- ceedings of the 24th International Electric Propulsion Conference, IEPC, Paper 95-059, Sept. 1995.

[29] Fife J. M., Martinez-Sanchez M., and Szabo J., *"A Numerical Study of Low-Frequency Discharge Oscillations in Hall Thrusters",* AIAA Paper 97-3052, July 1997.

[30] Boeuf J. P., and Garrigues L., *"Low Frequency Oscillation in a Stationary Plasma Thruster"*, Journal of Applied Physics, Vol. 84, No. 7, pp. 3541–3554 (1998).

[31] Naoji Yamamoto, Kimiya Komurasaki and Yoshihiro Arakawa, *"Discharge Current Oscillation in Hall Thrusters"*, Journal Of Propulsion And Power Vol. 21, No. 5, September–October 2005.

[32] R. Clarke, Surrey University, *"Power losses in wound components"*. 2008.

[33] Marian K. Kazimierczuk, *"High-Frequency Magnetic Components"*. 2014.

[34] N. Bower, *"Frequency-dependence of relative permeability in steel"*, Iowa state University Center for Nondestructive Evaluation, Applied Sciences Complex II, 1915 Scholl Road, Ames, IA 50011, USA, 2006.

[35] Busek Co. Inc., http://www.busek.com/halleffect.html

[36] Magnetic Metals corporation, Catalog Magnetic Material, http://www.magmet.com/catalogs.php

[37] Multimedia university, ECT1026 Field Theory Chapter 4: Magnetic Circuit. Updated - June2006

[38] Online Coil inductance calculator. http://www.66pacific.com/calculators/coil_calc.aspx

[39] Angara, Raghavendra, *"High Frequency High Amplitude Magnetic Field Driving System For Magnetostrictive Actuators"*, Ph.D., University of Maryland, Baltimore County, 2009.

[40] D. Mazza, *"Materiali per l'elettrotecnica"*, Dipartimento di Scienza dei Materiali e Ingegneria Chimica, Politecnico di Torino.

[41] New England Wire Technology Corporation, http://www.newenglandwire.com/products/litz-wire-and-formed-cables/types-and-constructions

[42] New England Wire Technology Corporation http://www.litzwire.com/litz_fiber_tape.htm

[43] Proto Laminations Inc. http://www.protolam.com/page7.html

[44] R. Conversano, "*Magnetically Shielded Miniature Hall Thruster: Development and Initial Testing*", IEPC-2013-201.

[45] Lobbia R.B. and A.D. Gallimore, *"Evaluation and Active Control of Clustered Hall Thruster Discharge Oscillations"*. 41st AIAA Joint Propulsion Conference and Exhibit, Tucson, Arizona,, 2005. AIAA-2005-3679.

[46] Xi Nan and C. R. Sullivan, *"Simplified High-Accuracy Calculation of Eddy-Current Losses in Round-Wire Windings"*, IEEE Power Electronics Specialists Conference, June 2004, pp. 873 - 879.

[47] W. G. Hurley, W. H. Wölfle, *"Transformers and inductors for power electronics"*. 2013.

[48] Lobbia R. B., and Gallimore A. D., *"Dynamic Electromagnetic Field Measurements of Clustered Hall Thrusters"*, AIAA paper 2006-4996, 2006.

[49] Wai-Kai Chen and P. Hammond, *"Theory and Design of Broadband Matching Networks"*, 1976.

[50] MathWorks, documentation centre on line, http://www.mathworks.com/help/rf/examples/designing-broadband-matching-networks-part-1-antenna.html

[51] Magnetic resonance imaging online documentation, http://mri-q.com/gradient-coils.html

[52] J. Sabate, L. Garces, P. Szczesny, Q. Li, and W. F. Wirth, "*High-bandwidth high-power gradient driver for magnetic resonance imaging with digital control*", APEC 2005, pp. 1087-1091, Feb. 2005.

[53] Crown Audio Inc, http://www.crownaudio.com/media/pdf/amps/137234.pdf

[54] Rod Elliott, measuring Louspeaker Parameters, http://sound.westhost.com/tsp.htm

[55] Analog Devices Inc. website material, http://www.analog.com/static/importedfiles/application_notes/236037846AN_843.pdf

[56] David Darling, Encyclopedya of alternative energy, http://www.daviddarling.info/encyclopedia/H/Halleffectthruster.html

[57] Goebel D. M. and Watkins D. M., *"LaB6 Hollow Cathodes for Ion and Hall Thrusters"*, AIAA-2005-4239, 41st Joint Propulsion Conference, Tucson, AZ, Jul 2005.

[58] Dustin J. Warner, *"Advanced cathodes for next generation electric propulsion technology"*. Air Force Institute Of Technology, thesis. 2008.

[59] Beiting E., Garrett M., Pollard J., Pezet B. and Gouvernayre P., "*Spectral Characteristics of Radiated Emission from SPT-100 Hall Thrusters*", IEPC-2005-221, 29th International Electric Propulsion Conference, Princeton University, New Jersey, 2005.

[60] Zhurin V., Kahn J., Kaufman H., Kozubsky K., and Day M.*,"Dynamic Characteristics of Closed Drift Thrusters",* IEPC-93-095, 23rd International Electric Propulsion Conference, Seattle, WA, 1993.

[61] J. Brophy, R. Gershman, N. Strange, D. Landau, R. Merrill and T. Kerslake, "*300-kW Solar Electric Propulsion System Configuration for Human Exploration of Near-Earth Asteroids*", in AIAA-2011-551, 47th AIAA Joint Propulsion Conference, San Diego, California, July 31-3, 2011.

[62] Florenz R., et.al., "*First Firing of a 100-kW Nested-channel Hall Thruster*", IEPC-2013-394, 33rd International Electric Propulsion Conference, Washington, D.C., October 6-10, 2013.

[63] Strange, N. et al., *"Human Missions to Phobos and Deimos Using Combined Chemical and Solar Electric Propulsion"*, AIAA/ASME/SAE/ASEE Joint Propulsion Conference, Paper AIAA-5663, Aug. 2011.

[64] Manzella D., Jankovsky R., and Hofer R., *"Laboratory Model 50 kW Hall Thruster"*, AIAA paper 2002-3676, 2002.

[65] Zurbach S., Cornu N., Lasgorceix P., "*Performance Evaluation of a 20 kW Hall Effect Thruster*", Proceedings of the 32nd International Electric Propulsion Conference, 2011.

[66] J. M. Fife, *"Hybrid PIC modeling and electrostatic probe survey of Hall thrustr"*, Ph.D. Thesis, MIT, Cambridge MA, 1998.

[67] Barral S., Ahedo E., Hartfuss H.-J., Dudeck M., Musielok J., and Sadowski M. J., *"On the Origin of Low Frequency Oscillations in Hall Thrusters"*, Vol. 993, 2008, pp. 439–442.

[68] Lobbia R. B., "*A Time-resolved Investigation of the Hall Thruster Breathing Mode*", Ph.D. Dissertation, University of Michigan, 2010.

[69] D. Meeker. *Finite Element Method Magnetics*, version 4.0. Software Package, 2004.

[70] S. Barral and J. Miedzik, *"Numerical investigation of closed-loop control for Hall accelerators",* J. Appl. Phys. 109, 013302 (2011).

[71] Wei Liqiu, Han Ke, Wang Chunsheng, Li Hong, Zhang ChaoHai and Yu Daren, *"Study on breathing mode oscillation suppression of self-excited Hall thrusters",* J. Vac. Sci. Technol. A 30, 061304 (2012).

[72] S. Barral, J. Kaczmarczyk, J. Kurzyna, M. Dudeck, *"Closed-loop control of ionization oscillations in Hall accelerators"*. Physics of Plasmas; Vol. 18 Issue 8, p083504, 2011.

[73] S. Barral, J. Kaczmarczyk, J. Kurzyna, M. Dudeck, *"Active Control and Excitation of Breathing Oscillations in a Hall Thruster with a Fast Digital Signal Processor"*. Proceedings of the 33nd International Electric Propulsion Conference, 2013.

[74] Bruce Pote, Rachel Tedrake, *"Performance of a High Specific Impulse Hall Thruster",* 27 International Electric Propulsion Conference, Pasadena, CA, 2001.

[75] Day M., Kim V., and Popov G., *"Investigation of the Possibility to Reduce SPT Plume Divergence by Optimization of the Magnetic Field Topology in the Accelerating Channel",* 25th International Electric Propulsion Conference, IEPC- 2001-015, Pasadena, CA, 2001.

[76] Duchemin O., Saverdi M., and Estublier, D., *"Performance and Lifetime Assessment of a Thrust Steering Device for PPS®1350 Hall-Effect Plasma Thruster",* Paper No. 49, ESA SP-658, May 2008.

[78] Sonato P., et al., *"Machine modification for active MHD control in RFX",* Fus. Eng. and Des. 66-68 (2003), 161-168.

[79] S. Barral, *"Theoretical Analysis of the Influence of the Power Supply on Breathing Oscillations in HallThrusters",* in Proc. 30th International Electric Propulsion Conference, 07-261, The Electric Rocket Propulsion Society, Worthington, OH, Florence (Italy), 2007.

[80] William A. Hargus, Jr. *"Investigation of the plasma acceleration mechanism within a coaxial hall thruster"*, PhD Thesis, Stanford University, 2001.

[81] J. Dickens, M. Kristiansen, *"Development of A "Smart" Power Processing Unit for Hall Effect Thrusters"*, IEPC-99-066.

[82] Christopher D. Vineski, *"Experimental Analysis of Dampened Breathing Mode Oscillation on Hall Thruster Performance"*. Thesis. Air Force Of Technology.

[83] Scharfe M. K., Thomas C. A., Scharfe D. B., Gascon N., Cappelli M. A. et al., "*Shear-Based Model for Electron Transport in Hybrid Hall Thruster Simulations*", IEEE Transactions on Plasma Science (accepted for publication, 2008).

[84] M. E. Griswold, C. L. Ellison, Y. Raitses, and N. J. Fisch, *"Feedback control of an azimuthal oscillation in the E 3 B discharge of Hall thrusters"*. *Phys. Plasmas* 19, 053506 (2012).

[85] M. Kapulkin and V. F. Prisnyakov, *"Feedback Stabilization of Plasma Instability in Stationary Plasma Thrusters"*, IEPC-99-085, 1999.

[86] Raitses Y., and Fisch N. J., "*Parametric Investigations of a Nonconventional Hall Thruster*", Phys. Plasmas, Vol. 8, No. 5, May 2001, pp. 2579-2586.

[87] V. V. Zhurin, H. R. Kaufman, "*Physics of Closed Drift Thrusters*" Plasma Sources Sci. Technology 8, R1-R20, 1999.

[88] Hofer R. R., Jorns B. A., Polk J. E., Mikellides I. G., and Snyder J. S., "*Wear Test of a Magnetically Shielded Hall Thruster at 3000 Seconds Specific Impulse*", Presented at the 33rd International Electric Propulsion Conference, IEPC-2013-033, Washington, DC, Oct 6-10, 2013.

APPENDIX A

Hollow Cathode Refurbishment

Appendix A, Contents

Appendix A, List of Figures

APPENDIX A

Hollow Cathode Refurbishment

A.1 LaB6 Hollow Cathode and refurbishment process

Most hollow cathodes for space propulsion in use today utilize a tungsten-based impregnated emitter. This kind of material is highly susceptible to poisoning: water vapor or oxygen can seriously degrade the performance of these types of emitters. Their lifetime is another limiting factor for these cathodes, as our laboratory experience confirms, being governed by the rate at which the impregnate evaporates that is a function of the temperature of the insert that increases with the current demanding [57]. In a high-current application, the lifetime of a tungsten-based impregnated emitter is thus considerably shorter than in low-current applications. Cerium Hexaboride (CeB_6) and Lanthanum Hexaboride (LaB_6) are viable alternatives to impregnated tungsten as a cathode emitter material. A wide range of current can be obtained using this emitter ranging from few Amps to hundreds of Amps. In the last ten years LaB_6 cathodes have been used with Hall thruster extensively.
In this appendix the refurbishment process of an existing LaB_6 hollow cathode, the AFIT Cathode, is reported and some modifications explained, hence the name AFITr, revisited. A detailed description of this cathode can be found in [58]. A brief description of some the parts of the mentioned hollow cathode is now provided. The core component of the cathode is the emitter. In the case of a hollow cathode, neutral gas flows into the cathode tube and passes through the emitter resulting in an ionization process due to the electrons emitted by the insert. A heater filament is wrapped around the tube that contains the insert; when current flows through that, the emitter is heated up to a temperature sufficient for electron emission. A coaxial tantalum heater wire with Al_2O_3-insulation between the core and the outer sheet was originally used to bring the emitter to ignition temperature required, approximately 1650° C [57]. Later the different architecture used to modify the cathode will be reported.

An electric field extracts electrons from the plasma generating a current flowing through the cathode orifice. An external anode is usually used to set the electric field but an embedded electrode is sometimes enough. The keeper encloses the cathode and acts as an electrode, as mentioned before, facilitating in this way the starting of the cathode itself, in fact it brings a positive high voltage (in the order of 500-600V) close to the emitter that is right behind the orifice. It also acts as a shield preventing heavy ion bombardment from thruster's plasma and cathode plume wearing the cathode itself [3]. Once the cathode starts, the keeper is biased at a lower voltage, between the thruster's anode one and the cathode one, the latter being grounded in our setup. In the case of the described cathode, the keeper was made of graphite, a high temperature proof and conductive material. This material is quite fragile and during an attempt to run the cathode, this component was broken. A more detailed description of the machining processes is later reported.
The first step of the refurbishment process involves the cleaning of the sputtered surfaces, in particular ceramic insulators. Sand paper or and a sandblaster have been used to remove the layer of sputtered material from the ceramic component that act as an insulating support for the keeper electrode. Their cleaning is important to prevent the risk of a conduction path through the graphite layer.

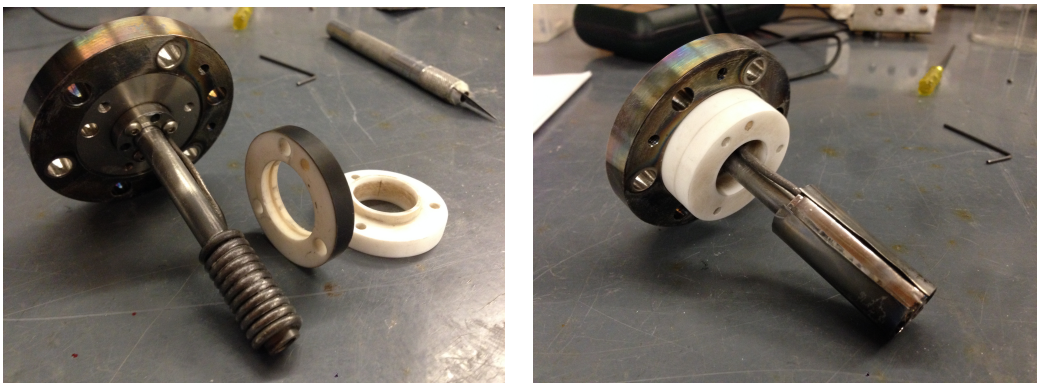

(a) Coated ceramic insulating elements, with original heating filament.

(b) Ceramics after cleaning (with heat shielding mounted).

Figure A.1: *AFIT Cathode during the ordinary cleaning process.*

The heater was then checked.
The heater filament is made out of tantalum. This metal has good thermal conductivity, and is used is in the manufacture of heating elements, vacuum tubes and other high temperature parts, as well as in capacitors and electronic components in general. Tantalum is also known for its resistance to corrosion by acids, and it is for this reason largely used in surgical implants and instruments. A properties table of this material follows.

Tantalum Physical Properties		
Density	lb/in^3	0.60
	gm/cm^3	16.60
Melting Point	°F	5425
	°C	2996
Thermal Conductivity	$Cal/cm^2/cm°C/sec$	0.13
Specific Heat	Cal/gm/°C	0.036
Coefficient of Linear Thermal Expansion	micro-in/°F x 10^{-6}	6.50
	micro-in/°C x 10^{-6}	3.60
Electrical Resistivity	micro-ohm-cm	12.40

Figure A.2: *Tantalum physical properties table [6].*

During the inspection process, resistance value of the heater filament was find to be not consistent with the one reported on the cathode's documentation and even more important the connection between inner and outer tantalum parts at the hot end of the wire was no more present resulting in an improper electrical scheme. Nevertheless the measured heater resistance was not infinite; the most likely solution is that the ceramic sleeve positioned inside the coaxial wire was broken in some point resulting in a conduction path for the current. For these reasons it was decided to replace it.

Considering the high cost of the alumina-insulated tantalum filament used before and the brittleness of the unsheathed part of the cold end of the wire, a completely different arrangement for the heater was choose. Following previous research in cathodes a 'necklace like' configuration was adopted: a single tantalum wire was covered with alumina beads shaped with a conical surface at the ends allowing, in this way, to create a curved line. For sake of reliability and maintenance easiness the author relied on a floating configuration for the new heater filament: both ends of the wire stick out the back plate and are connected to the leads of the power supply. The winding is thus bifilar and an additional trough hole in the circular back plate of the cathode was required. The two leads of the heater are then insulated wit alumina rod and connected to the power supply line at a distance of about 5 cm behind the back plate of the cathode taking advantage of the gas line pipe that was used as a support for the wiring. Two bolts were used to connect the leads of the thin and flexible tantalum wire with the wire terminals crimped on the power supply line.

The following two pictures show the new architecture adopted for the new heater assembly. The left one shows the heater still uncovered by the heat shield. In the right picture the shield in installed and the two insulated electrical leads of the heater winding can be barely distinguished.

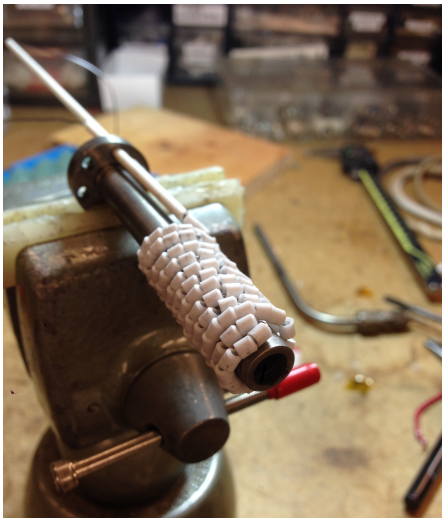

(a) Heating Filament assembling.

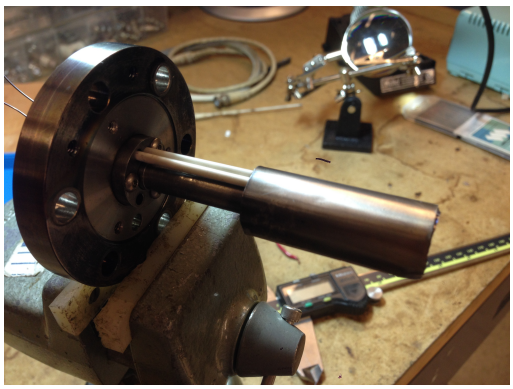

(b) AFITr with heat shielding mounted.

Figure A.3: *AFITr Cathode refurbishment: building the heater*.

As already mentioned, during the refurbishment process a new keeper was realized after the existing one was broken in an attempt of testing the cathode. Thus, a new part has been machined out of a solid bar of graphite using the equipment of the laboratory machine shop.
A three-dimensional model of the part was realized as well using the geometrical parameters available in the documentation of the cathode to help building the part in some of the necessary steps.
A special thanks to Mike Carter for the indispensable help he offered in this process.

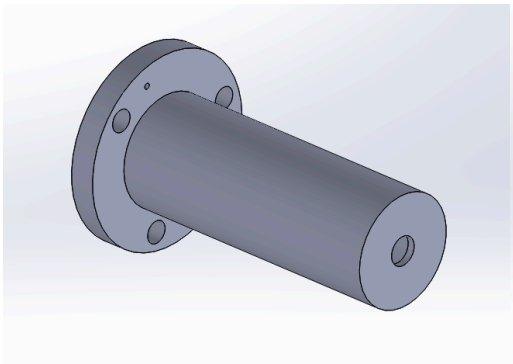

(a) Front view of the hollow keeper.

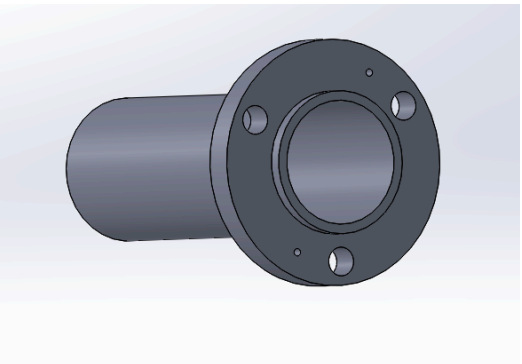

(b) Back view of the hollow keeper.

Figure A.4: *AFITr Cathode Graphite Keeper three-dimensional model*.

After an analysis of the available room, a higher thickness of the wall was decided as an attempt to have a slightly less delicate component. The inner diameter was not reducible, the heat shielding was indeed grounded in the original heater configuration and a contact between the latter and the keeper would produce a short circuit. Even if, as already explained, the new version of the heater makes the heat shield floating, it is still preferred not to have the risk of contact between it and the keeper, resulting in raising the potential to the keeper one. In the new version of the keeper the distance between the heat shield and the inner surface of the keeper results thus slightly increased. The bigger thickness of the keeper wall has been thus achieved increasing the external diameter, which was constrained by the presence of the three holes required to hold the keeper in place. Despite this the thickness of the wall was increased of about 20%.

The machining process was organized on the basis of the following order of operations:
- Cut the graphite bar at the proper length: keeper length plus 3 cm in order to have enough length to hold it properly on the lathe.
- Smooth the surface of the face facing the tool.
- Drill a pass through hole with the diameter of the keeper orifice.
- Machine outer diameter of part until the flange.

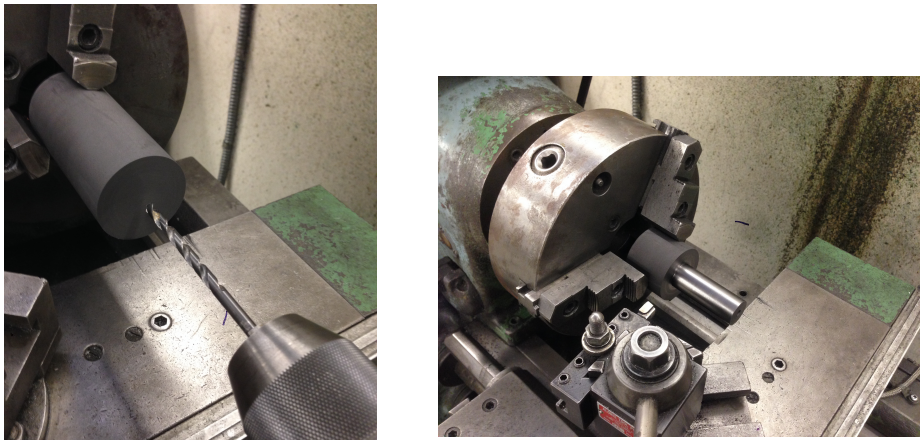

(a) Drilling a pass t through hole. (b) Machining part of the outer diameter.

Figure A.5: *AFITr keeper machining, part 1.*

- Rotate the part and roughly reduce the length of the part to the desired value.
- Drill the four outer holes, keeper support screws and electrical connection, using the SPPL CNC machine.
- Machine outer diameter of flange.

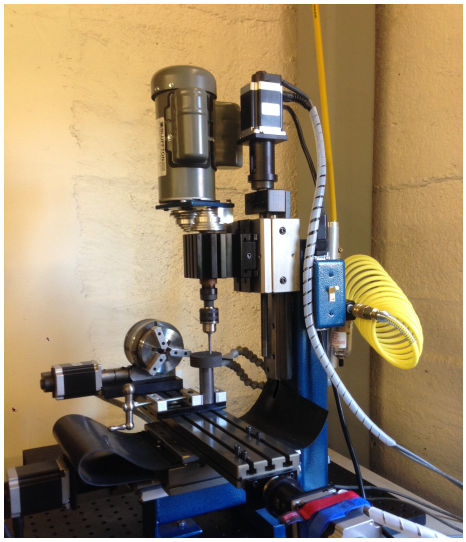
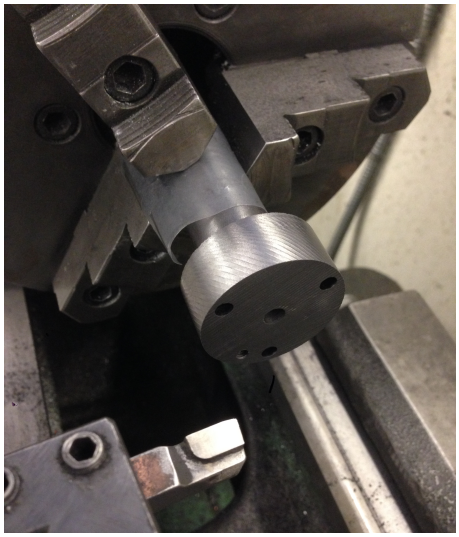

(a) Drilling outer holes with the SPPL CNC. (b) Machine outer diameter of flange.
Figure A.6: *AFITr keeper* machining, *part 2*.

- Refine the face of the part preparing the step too.
- Enlarge gradually the inner central hole.

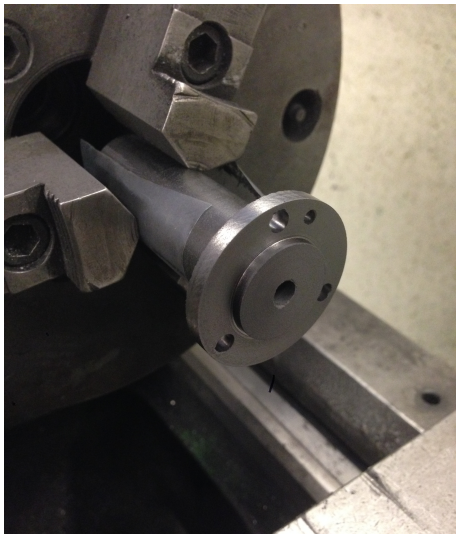
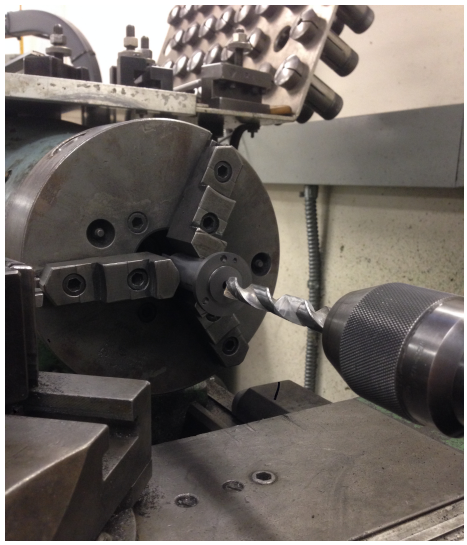

(a) Refine the face of the part. (b) Enlarge gradually the inner central hole.
Figure A.7: *AFITr keeper* machining, *part 3*.

- Threading the keeper wire terminal hole and checking all the dimensions.
- Final check of the thickness and dimensions.

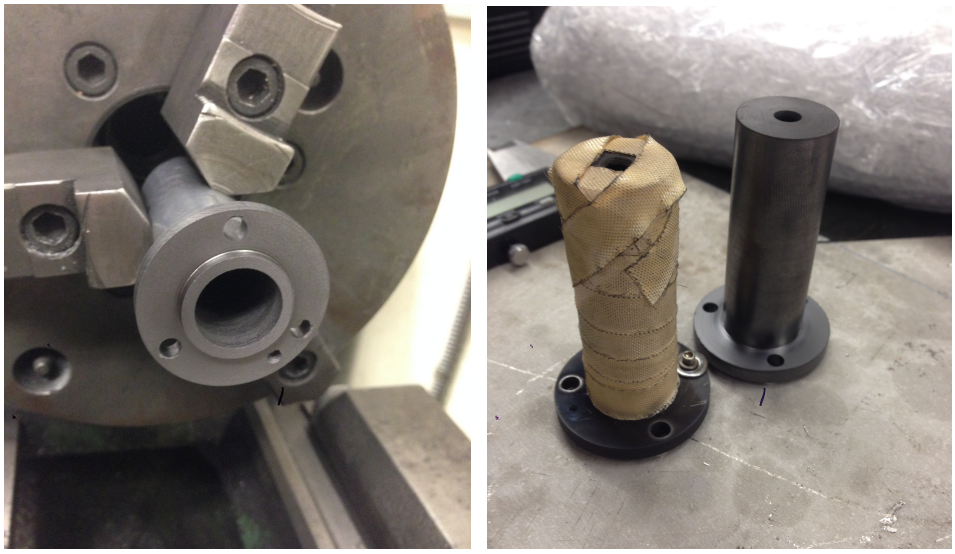

(a) Final enlargement of the inner hole. (b) Comparing the old and the new parts.

Figure A.8: *AFITr keeper* machining, *part 4*.

The component perfectly fit the cathode and it was successfully tested.

A.2 AFITr Cathode Testing

After some testing attempt the proper power level of the heater was found: 8,5 A at almost 24 V were necessary to reach the ignition temperature of the cathode. In the reported test, the cathode run on argon gas, even if xenon is more typical of hollow cathodes used in EP devices; indeed, although more expensive, in order not to have double reservoirs and feeding line system, use of xenon for cathodes feeding is preferred. Some operation points were tested resulting in different color of the plume. The next three tables summarize some of the points.

Testing at 6sccm HEATER OFF

Keeper A set	Keeper V	Notes
0,2	190	violet
0,3	150	pink
0,5	120	yellowish
0,75	90	bright
1	75	brighter

Testing at 7,2sccm HEATER OFF

Keeper A set	Keeper V	Notes
0,2	220	violet
0,5	120	pink
0,8	80	yellowish
1	70	bright

Testing at 8sccm HEATER OFF

Keeper A set	Keeper V	Notes
0,2	240	violet
0,5	120	pink
0,8	80	yellowish
1	70	bright

Figure A.9: *AFITr Cathode operational points, current limit mode on keeper.*

The same data are rearranged in the following graph.

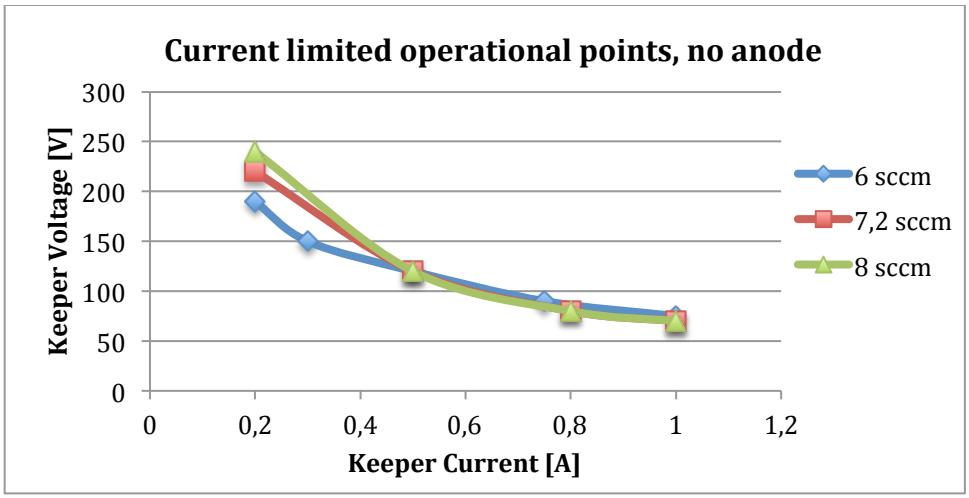

Figure A.10: *AFITr Cathode operational points, current limit mode on keeper.*

A different set of data is reported below; setting the current value on the keeper power supply, mass flow rate is scanned and the voltage on the keeper recorded. Even if the trend is not totally regular, it can be seen how decreasing the gas

flow rate results in the increase of the voltage. The effect was expected, being the resistance of the plasma increased when less mass flow is selected.

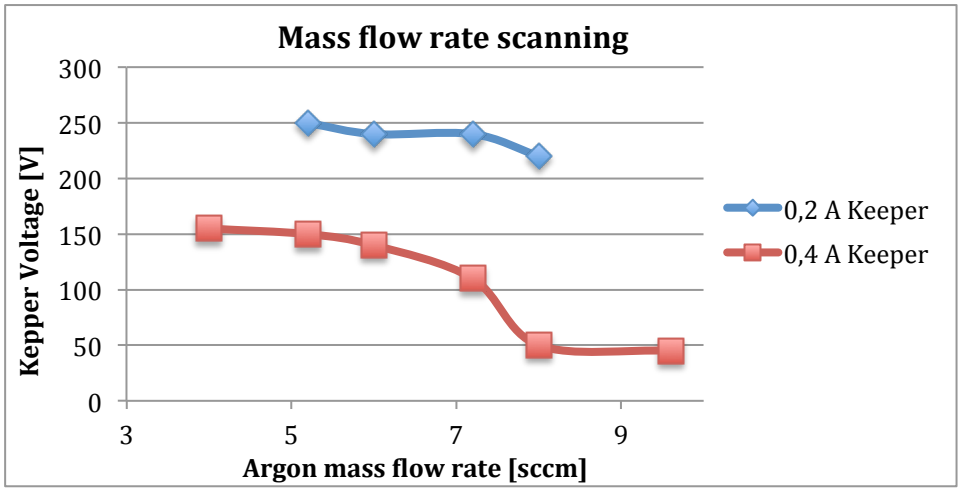

Figure A.11: *AFITr Cathode operational points, xenon mass flow rate scan.*

In order to further characterize the cathode and better investigate the emitter health condition further test using Langmuir probe, Faraday probe or ExB probe can be conduct following the vast literature on topic [58].

The next two pictures, taken in two different operational points and from two different chamber windows, show the cathode running for the first time after the refurbishment on September 16th 2014 in the small vacuum chamber of the Stanford Plasma Physics Laboratory.

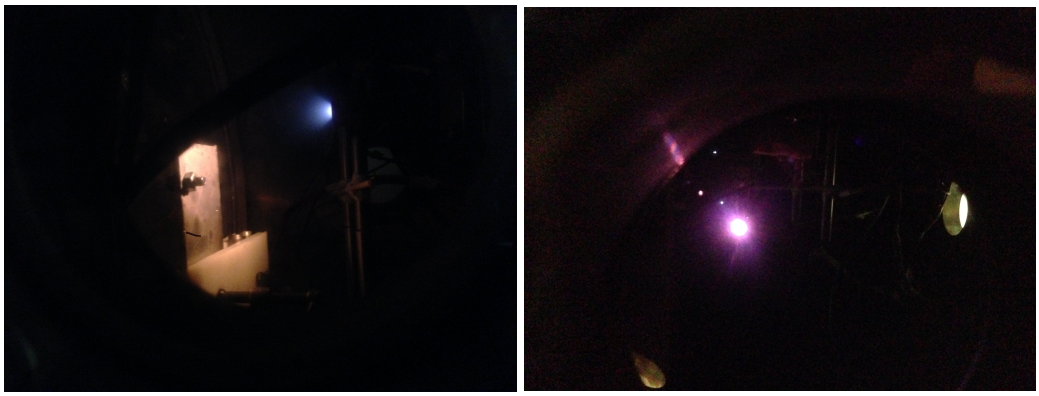

(a) Side view. (b) Front view.

Figure A.12: *AFITr Cathode first test, running on argon.*

Appendix A, Bibliography

[3] Goebel D. and Katz I., "Fundamentals of Electric Propulsion: Ion and Hall Thrusters", Wiley, Hoboken N.J., 2008.

[6] http://www.edfagan.com

[57] Goebel D. M. and Watkins D. M., *"LaB6 Hollow Cathodes for Ion and Hall Thrusters"*, AIAA-2005-4239, 41st Joint Propulsion Conference, Tucson, AZ, Jul 2005.

[58] Dustin J. Warner, *"Advanced cathodes for next generation electric propulsion technology"*. Air Force Institute Of Technology, thesis. 2008.

Acknowledgments – Ringraziamenti

Ringraziamenti (Italian Version)

Il primo pensiero di queste pagine è rivolto a mio papà, colui che ha reso possibile la mia intera carriera universitaria, compreso il privilegio di trascorrere otto mesi in una delle università più belle del mondo; senza questa esperienza non avrei mai potuto stravolgere l'idea di ingegneria e soprattutto di ricerca che aveva, ahimè, ormai preso forma in me. Non solo, contemporaneamente a tutto ciò mi hai sempre concesso di inseguire le mie passioni che hanno fortemente contribuito a rendermi ciò che oggi sono, donandomi soddisfazioni sicuramente al di là del comune. Grazie per rendere i miei sogni realtà.

Grazie mamma, mi hai sempre sostenuto, anchequando non lo meritavo, facendomi acquisire quella sicurezza in me stesso che mi ha consentito di non arrendermi anche quando la strada per arrivare alla meta sembrava puntare nella direzione contraria. So che non sono capace di dimostrarlo abbastanza, ma credo tu sia una mamma davvero speciale.

Nonostante non manchino le volte in cui non ci capiamo a causa probabilmente della mia caparbietà o della mia scarsa propensione allo spiegare le mie intenzioni, l'avervi accanto è stato sicuramente una fonte di insostituibile sostegno, grazie.

Un abbraccio gigante alla nonna Franca che mi ha cresciuto tenendomi per mano e sopportando i miei mille capricci, dispetti e scherzi che ancora mi fanno ridere quando li rivivo accarezzandoli con la memoria, compreso il mattone tirato sul piede. Ti voglio bene!

Pur non essendo più qua, un grazie unico va al nonno Renato che mi ha donato la passione per le applicazioni pratiche e la capacità di lavoro manuale che tanto mi hanno aiutato in laboratorio durante questa esperienza di tesi; è come se parte della ricerca che ho portato avanti qua a Stanford l'avessi fatta tu. Sei senza dubbio tu ad essere stato il mio primo *Advisor ("guida")* che mi accompagnato crescendomi e stuzzicando le mie passioni, cercando sempre di assecondare la mia voglia e curiosità di inventare, smontare e costruire, proprio come è stato qua in questi mesi. Sei il miglior nonno di sempre.

Un pensiero affettuoso va alla nonna Gilda e alle sue abilità culinarie, vale la pena citare le lasagne al forno, gli gnocchi alla romana, la torta pasqualina ed i muscoli ripieni, ma soprattutto il petto di pollo che prepari sempre per la mia ragazza. Ricordo sempre con piacere le cene a Lerici quando ero piccolo, spesso con annesso dolce della pasticceria sotto casa, durante le quali lo zio Lamberto mi faceva da 'ascensore'; mi avrebbe fatto piacere avere l'opportunità di trascorrere più tempo insieme.
Grazie a tutto il paese di Marciaso. Purtroppo la maggior parte di voi non è più qua, ma ciascuno mi ha lasciato un insegnamento o un ricordo che spesso mi fa sorridere, anche quando qualcosa non va per il verso giusto: mi accompagneranno per sempre e voi con loro.
Un pensiero particolare per Laila e Sandro che mi perdoneranno per non essere riuscito a partecipare al loro matrimonio ma che, speranzosamente, avranno presto l'onore (e l'onere!) di prepararmi la mia pasta all'amatriciana preferita.
Un caro grazie a Luisa e Gianni per gli innumerevoli dolci che mi hanno accompagnato durante le colazioni a Milano in cui ho vissuto due tra i più begl'anni di sempre.
Un abbraccio a tutta la famiglia della mia ragazza, in questi anni mi avete trasmesso più di quanto forse pensiate; anche se a volte alcune riflessioni non si affrontano facilmente, molte di loro sono diventate un pezzo della mia vita.
Grazie a Bruno per i tanti messaggi divertenti e per avermi aiutato a realizzare un acquario da sogno, che dopo quasi dieci anni di impegno ha saputo lasciarmi senza parole; e grazie per essermi stato vicino quando ahimè ho dovuto separarmene.
Grazie al gruppo delle Frecce Azzurre per avermi insegnato a volare con gli aeromodelli e a vedere finalmente un'applicazione pratica dell'aerodinamica e della dinamica del volo che troppo teoricamente ho studiato all'università.
Grazie al prof. Luigi De Luca per aver accettato il ruolo di relatore dandomi di conseguenza la possibilità di vivere questa esperienza di tesi, ma soprattutto per le belle lezioni di propulsione spaziale che hanno saputo alimentare la mia passione in materia presentatami per la prima volta dal prof. Daniele Pavarin presso l'Università di Padova. A lui anche va un caro ringraziamento per avermi aiutato in modo essenziale a organizzare questa esperienza di ricerca.
Un sorriso va a tutto il mio gruppo di amici del Politecnico di Milano col quale ho condiviso gli anni della laurea magistrale; siete troppi per citarvi tutti! E' stato davvero bello il tempo trascorso insieme a voi anche se ciò ci tengo a dire: so che tanti di voi sono sempre molto occupati, credo però valga la pena ritagliare un po' del proprio tempo per scrivere, di tanto in tanto, due righe ai vecchi, ma pur sempre amici.
Un simile messaggio va ai pochi compagni di corso, incontrati durante gli anni della triennale all'università di Padova, che sporadicamente manifestano il loro essere ancora in vita, proprio come i vecchi amici del liceo.

Grazie anche a te Andrea, il tuo appartamento a Milano è stato la più bella cornice a questo quadro che mai avessi potuto desiderare, davvero.
Grazie al mio omonimo, Fabiozzo! Il mio coinquilino preferito di sempre, e anche l'unico per la verità (ti piace vincere facile eh!). I due anni e mezzo passati insieme a Milano sono stati davvero spettacolari; il loro ricordo non smetterà mai di farmi sorridere. Sei una persona davvero speciale e sono fiero di avere un amico come te; ovviamente non considerando per un attimo la tua scarsa attenzione alle date di scadenza dei cibi all'interno del frigo in particolare, ma non solo (ti ricordi la torta nel forno?)!
Jack: abbiamo vissuto la stessa laurea triennale a qualche fila di banco di distanza ma, chi l'avrebbe mai detto, non avevo capito proprio niente di te: soltanto gli anni della laurea magistrale mi hanno dato davvero questa possibilità. Il tuo mix di scherzosità e serietà tuttora mi crea difficoltà nel capire quando stai scherzando e quando no. Non so come tu abbia superato la mia caparbietà nell'andare forse oltre il richiesto livello di comprensione durante le tante ore di studio passate insieme. Grazie a te ho pure quasi imparato ad usare il computer e…la Wi-Fi! Si può dire che hai aggiunto una passione alle esistenti. Sei un ragazzo in gamba, ad eccezione del numero di Vodka Tonic che mi hai preparato: danno dipendenza!
Paoluccia e Claudio, grazie per le tante risate e le cene insieme che ho avuto il piacere di vivere, per essermi venuti a trovare a Milano e per farvi sentire spesso, vi voglio bene! Un grazie anche ad un amico storico, Mattia: grazie per avermi fatto scoprire la salsiccia in crosta, ma anche per non essere mai venuto a trovarmi a Milano, non te lo perdonerò facilmente, anzi, probabilmente non te lo perdonerò mai! Un caro pensiero ad Emanuele e Federica per le proficue discussioni sull'estero durante le buone pizze di Vicenza e per condividere la passione per le piante carnivore e l'amore per le cose ben fatte. Grazie a Michela e Lorenzo per gli innumerevoli consigli che mi hanno aiutato nella pianificazione della mia tesi all'estero e a Federico per tutte le informazioni sulla scelta dell'alloggio e per l'entusiasmo che mi trasmesso ancor prima di approdare a Stanford, avevi ragione, questo posto è magico.
Sue, sei stata una tra le persone più speciali che ho incontrato nei meravigliosi mesi passati in California, tornare a casa la sera (…o la mattina!) è sempre stato meraviglioso, la tua ospitalità è un dono non comune. Spero ci incontreremo presto in Italia, grazie di cuore per avermi accudito e trattato come un figlio, sei stata fondamentale.
Un ringraziamento speciale va alle persone che ho conosciuto a Stanford: il gruppo di fisica dei plasmi del SPPL. E' stato un privilegio ed un onore lavorare con ciascuno di voi. Grazie ragazzi per aver condiviso questi mesi con me, non ce l'avrei fatta senza di voi. Grazie a Perry per l'instancabile aiuto nel gestire la mia sconfinata ignoranza in materia di burocrazia e per aver sempre pazientemente risposto alle mie decine e decine di email. Queste parole sono per

te LaMarr, sei davvero un bravo ragazzo, credo non sia facile trovare un sorriso sincero come il tuo. Grazie per il tempo passato insieme (compreso quando pensavo stesse andando a fuoco il bagno pubblico di fronte al mio ufficio!) e per tutte le volte che mi hai aiutato con le stampanti (parecchie ad essere sinceri!).
Andre, sei stato un insostituibile maestro; sei stato il mio fratello maggiore durante questa intera esperienza condividendo con me l'amore che hai per la ricerca e la scienza applicata. Grazie per avermi insegnato a vivere il laboratorio, dall'accendere un oscilloscopio, all'usare le pompe da vuoto. Anche se ultimamente il numero di domande sull'impedenza è sceso stai allerta che non si sa mai! Senza di te non avrei nemmeno iniziato a scrivere queste righe, ti sarò per sempre grato.
Chris, mi hai aiutato un sacco di volte negli ambiti più disparati con una professionalità davvero invidiabile, ma hai saputo trasmettermi qualcosa anche da un punto di vista umano che non ho trovato altrove frequentemente ad essere sincero. Sono fiero di averti avuto come compagno di ufficio nel nostro vecchio edificio, grazie per aver sopportato il mio monopattino sempre parcheggiato lì; un abbraccio ad Holly! Keith, ecco l'altro vecchio compagno di ufficio! La tua capacità di descrivere le cose con minuzia e termini degni di rivista scientifica mi ha sempre affascinato. Grazie per le numerose discussioni su circuiti contenenti induttori e grazie per avermi fatto scoprire Femm (e scusa se quando me l'hai nominato pensavo ti riferissi all'analisi agli elementi finiti!). Grazie anche per aver spaventato a morte me e Ben con un fulmine (due per la verità) da 6.5 kV in laboratorio; non mi ero accorto che tra i mille progetti che abbiamo ci fosse anche fare ricerca in campo meteorologico! Ben, anche tu mi hai aiutato davvero molto, grazie per esserti occupato di tutti gli ordini del materiale che ho utilizzato. Spero un giorno di far volare qualche aeromodello con te. David, quante volte mi hai spiegato come funzionano le Matching Network? Sai che non sono ancora sicuro di averle capite bene?! Grazie anche per avermi introdotto al club di Wine Tasting di Stanford ed avermi fatto stupire davanti ad una bottiglia di Vermentino tra i vini da degustare; queste sono cose che non ci si aspettano di certo! Eunsun, grazie per avermi pazientemente spiegato come usare il codice di calcolo per i motori Hall, considerato che la mia capacità di interazione con la simulazione numerica è trascurabile, sei stata davvero brava. Bob, grazie per l'aiuto sul progetto riguardante l'utilizzo del laser, mai avrei pensato di poter generare degli spot di plasma in aria con un laser e un paio di lenti, spero di incontrarti verso Natale quando vieni in Italia! Nic la tua presenza durante le giornate in cui abbiamo acceso i motori e relativi catodi è stata davvero utile; considerando che non sapevo cosa fosse un *sccm*, se adesso sono quasi in grado di gestire un motore è anche grazie alla tua esperienza. Jack, abbiamo passato un sacco di tempo insieme. Grazie per l'aiuto con LabVIEW che ha segnato penso entrambi per la vita! Grazie per l'aiuto con alcuni file CAD il cui risultato è indubbiamente di molto superiore al precedente citato,

grazie anche per aver perso il conto del numero di spire di filo mentre stavamo avvolgendo un solenoide e per avermi preparato una cena degna di *piatto del buon ricordo* a La Jolla! …ma soprattutto grazie per tutte le risate durante le innumerevoli cene a base di panini di *CoHo* e gli innumerevoli *mocha* da *Starbucks*, è stato davvero divertente.
Un grazie a tutti gli studenti estivi dai cui progetti ho stupefacentemente scoperto un sacco di cose curiose e la cui dinamicità mentale mi ha veramente colpito; sappiate che vi invidio moltissimo e che siete davvero fortunati ad avere questo genere di occasioni. Un grazie particolare a Hiroshi e Mike per l'aiuto con i nostri amati catodi! Chiara, sei tornata in Italia troppo presto! E' stato bello averti accanto nel nuovo ufficio e ridere insieme come piace a noi. Sei la miglior organizzatrice di viaggi di sempre, grazie per tutti i consigli che mi hai dato per il mitico *road trip*, io se fossi in te scriverei una guida! Un grazie anche a Martina e Gherardo che per un paio di mesi mi hanno fatto compagnia nella bella casa di Palo Alto. Ricordo con piacere le numerose lezioni serali di fisica delle particelle, spesso accompagnate da eccellenti bistecche e pure qualche mojito sapientemente preparato. Tante sono le persone che ho incontrato e a tutte coloro con le quali ho condiviso parte di questa esperienza va un pensiero.
Mark, non ci sono parole per descrivere la gratitudine che provo per te, sei stato un'inestimabile guida. Grazie per le innumerevoli ore che mi hai dedicato, durante le quali mi hai insegnato cose di cui nemmeno sospettavo l'esistenza, trasmettendomi una passione sconfinata, fuori dal comune. Nel nostro laboratorio sono finalmente riuscito a vedere e toccare ciò che ho studiato per anni, realizzando così il mio sogno di fare ricerca e non semplicemente di leggerla sui libri. La tua capacità di moltiplicare idee tra loro non smetterà mai di affascinarmi. Ma la tua *mentorship* si è spinta ben oltre; il sorriso che porti negli occhi sa trasmettere mille parole in un solo sguardo. In questi mesi sei stato per me una guida fondamentale ed insostituibile, portandomi per mano, nel mio progetto di tesi ma soprattutto nella vita quotidiana. Non avrei mai potuto immaginare di incontrare una persona come te, in particolare durante il mio percorso universitario, specie in un progetto di tesi a 9000km da casa. Grazie.
A concludere queste forse fin troppo lunghe pagine, il mio più grande e speciale ringraziamento: a Francesca, la mia ragazza. Sei stata la ragione che più di tutto il resto mi ha spinto in questi anni facendomi approdare in moli dove ho trovato luoghi, opportunità e persone uniche e dove ho collezionato ricordi meravigliosi che sono, e saranno, le fondamenta per il futuro. Grazie per riuscire a farmi amare così tanto il mondo. Sei la mia torcia, che ha il potere di illuminare e far brillare ciò che ho attorno, proprio come una torcia per un subacqueo, senza la quale egli non sarebbe in grado di apprezzare i meravigliosi colori di pesci e coralli che lo circondano: tutto gli apparirebbe di un indistinto blu, ma non lo è. Grazie per essermi stata accanto in questa incredibile immersione; ora è tempo di caricare le bombole per quelle future, non vedo l'ora!

Acknowledgments (English Version)

The very first thought of these pages addresses my dad, the one who made possible my entire university carrier, including the privilege of spending eight months in one of the most beautiful universities in the world. Without this experience I couldn't have radically change the picture of engineering and research that were wrongly shaped in my mind. Even more: at the same time you always let me pursuing my passions that are now part of me and experiencing a, certainly not common, satisfaction. Thank you for making my dreams true.

Thank you mom, you have always supported me, even when I didn't deserve it; in that way I gained the self-confidence that allows me not to give up even when the path seemed to head in the wrong direction. I'm not good in making you feel that I really believe you are a very special mom.

Even if sometimes we don't get along probably because of my stubbornness and because of my inclination not to express my intention, both of you have been a source of unique support, thank you.

A huge hug is dedicated to my grandma Franca who brought me up hand in hand bearing my temper tantrum, my pranks and jokes. They still make me laugh when I go back in time remembering them, including the brick I throw on your foot. I love you!

Although no longer on hearth, a very special thanks goes to my grandpa Renato who made me falling in love with practical applications developing, in this way, the capability of working with my hands that helped me so much in the lab during this experience, you did part of my research here at Stanford. Without any doubt you have been my first advisor who supported me while I was growing up, encouraging my passions, trying to satisfy my curiosity of creating, disassembling and building, in the very same way I did here during these months. You are the best grandpa ever.

I extend an affectionate greeting to my grandma Gilda; you really are a good chef! I have to mention *lasagne, gnocchi alla romana, Pasqualina* pie and stuffed mussels, but in particular the chicken breast you prepare for my girlfriend. I still remember with joy the when we used to have dinner together at your place in Lerici when I was a kid; we used to have a cake, bought in the close by bakery, and my uncle Lamberto used to lift me up making me laugh. I wish we spent more time together.

Thanks to all the people from the little hamlet, Marciaso. Unfortunately the vast majority of you passed away; each of you taught me something or donated me a memory that often make me smile even when I'm sad for some reason. You will be forever with me.

A special thought to Laila and Sandro. Please forgive me not to be at your wedding. Hopefully you'll have the honor (and the responsibility!) to cook my favorite *amatriciana* pasta for me!
A dear thanks to Luisa and Gianni for the multitude of cakes associated with my breakfast in Milan where I spent two of the best years of my life.
This thank you is for my girlfriend's family: during these years you gave me more than you think. Some lessons were not easy but they are now part of my life.
Thanks to Bruno for the many funny messages and for helping me realizing my dream aquarium, which left me breathtaking after almost ten years of commitment; thanks for being close to me when I sadly had to part from it.
Thanks to the *Frecce Azzurre* group. You taught me how to operate the radio controlled planes making me experiencing a practical application of aerodynamics and flight mechanics that I studied at university too much theoretically.
Thanks to my Professor Luigi de Luca for being my supervisor so that I could have the opportunity to enjoy this thesis experience; thank you especially for the brilliant space propulsion classes, which fed my passion on the field that has been presented to me for the first time by Professor Daniele Pavarin at University of Padua.
Warm greetings to all my friends of Politecnico of Milano I shared the Master's years with; you are too many to be mentioned! I did really enjoy the time spent with you guys. There is by the way something I want to tell you and to all my old friends from Padua, both the Bachelor's ones or the ones from high school: I know that the majority of you is often very busy, but I believe that cropping some of your time, occasionally, to text to an old friend would be nice!
Thank you Andrea, your flat in Milano was the best frame for this picture I could have ever asked for.
Thank you to my homonym, Fabiozzo! You are my best housemate ever and, to be honest, the only one I have ever had (it is easy to win in this case, isn't it?). The two and a half years we lived together in Milano have been wonderful; that memory will never stop to make me smile. You are a very special person and I am grateful to have you as a friend; all this without of course considering your poor attention to food's use by date: especially those in the fridge but not only (do you remember the pie you forgot inside the oven?).
Jack: we attended the Bachelor Degree at the same university and we were just few seats away. Who would have thought I haven't understood anything about you? Only during the Master's Degree I had the opportunity to know you deeply. Your mix of jokes and seriousness is still giving me a lot of trouble to get whether you are joking or not. I don't know how you were able to exceed my stubbornness in trying to go beyond the requested level of understanding during the many hours of study we spent together. Thanks to you I have almost learnt

how to use the computer…and the Wi-Fi! You add a passion to those I already had. You are such a good guy, except the many Vodka-Tonics you prepared to me: they give addiction!
Paoluccia and Claudio, thank you for all the laughs and the dinners I had the pleasure to share with you, for coming to visit me in Milan and for keeping in touch; I love you.
Thank you to an old friend, Mattia: thanks for making me discover "*salsiccia in crosta*" and also for never coming to visit me in Milan; you won't be forgiven so easily. Actually I'll probably never forgive you.
A kind thought to Emanuele and Federica for the fruitful chats about the idea of moving to another country we had while eating good pizzas in Vicenza. Thank you also for sharing the passion for carnivorous plants and the love for details.
Thank you to Michela and Lorenzo for giving me a ton of tips which helped me planning my thesis abroad.
Thanks also to Federico for sharing with me all the precious information about the accommodation and for passing me on a lot of enthusiasm even before I could arrive at Stanford; you were right, this place is magical.
Sue, you are one of the most special people I met during the wonderful months I spent in California: It has always been amazing to come back home in the evening (or even in the morning!); your hospitality is an unusual attribute. I wish to meet you in Italy soon. Thank you so much for looking after me as a son, you have been essential.
Special thanks you to all the people I met at Stanford: the SPPL group. It was a privilege and an honor to work with all of you. Thank you guys for sharing this experience with me. I couldn't have done it without you.
Thanks to Perry for your tireless help in managing my ignorance about bureaucracy and for always replying patiently to my countless emails.
These words are for you, LaMarr: you are such a good guy; I believe it is not easy to find such an honest smile. Thank you for the time together (included when I thought the public WC in front of my office was going up in flames) and for helping me with the printers (in a lot of occasions to be honest!).
Andre, you have been a unique guide, you have been my elder brother during this experience sharing with me your love for research and applied science. Thank you for teaching me how to enjoy the laboratory, starting from turning on an oscilloscope to how to use vacuum pumps. Even if I am not bothering you any more with questions about impedance, you still have to be aware…you never know! I couldn't have started writing these lines without you, I will always be grateful to you.
Chris, you helped me a billion of times with an enviable competence on a variety of fields. You were also able to pass me on something emotional, and I think this is an attitude not easy to find. I am pride I had you as an office mate in the old building; thanks for standing my scooter always parked there. Give a hug

from me to Holly! Keith, here you are, my other old office mate! I have always been fascinated by your capability in describing things with details and technical terms which could belong to a scientific magazine. Thank you for the many conversations about inductors and for introducing me to Femm (I am sorry if the first time you mentioned them I tough you were speaking about the finite elements analysis). Thanks also for frightened to death Ben and me with a 6.5kV lightning in the laboratory (two of them to be honest); I haven't realized that one of the projects we are working on is about meteorology!
Ben, you helped me a lot, thanks for ordering all the materials I needed for my experiment. I wish one day we could play together with some remote-control planes. David, how many times did you explain to me how a Matching Network works? You know, I am not totally sure I got it! Thanks for introducing me to the Stanford Wine Tasting Society and for letting me surprising whit a Vermentino wine, I was really not expecting it! Eunsun, thank you for explaining me how to use the computation code for Hall thrusters; you were really good explaining that to me considering that I do not like numerical simulations at all! Bob, thank you for helping me with the project about lasers, I have never thought that it was possible to produce plasma spots in air with a laser and some lenses. I hope to see you around Christmas in Italy!
Nic, you have been very helpful being around when we were running the thrusters and the cathodes. I didn't know what a *sccm* was; if now I am able to manage a thruster is thanks to your experience as well.
Jack, we spent a lot of time together. Thanks for the help with LabVIEW; that experience scared us forever! Thank you for helping me with some CAD files whose result was certainly better than the one mentioned before. Thank you for losing count of the wire turns while winding the solenoid; thanks also for cooking to me and to my girlfriend a gorgeous dinner in La Jolla. That dinner deserves the award of "*Piatto del buon ricordo*"! Thanks especially for all the laughs during the many dinners at *CoHo* and for the uncountable mochas at *Starbucks*, I had a great time. I would like to thanks all the summer students. From your projects guys I have learnt a lot. I was really surprised by your openness; I envy you so much, you are so lucky for having that kind of opportunity. A special thank you to Hiroshi and Mike for helping me with our beloved cathodes!
Chiara, you went back to Italy too early! It was lovely to share with you the new office and to laugh together in the way we love to. You are the best travel agent ever, thank you for tips about the road trip; if I were you I would write a guide!
Thanks also to Martina and Gherardo who were my housemates in Palo Alto for two months. I remember with pleasure the evening lessons about particle physics that were often matched with excellent steaks and mojitos skillfully made.
Thanks to all the people I met during this amazing experience.

Mark, no words can describe the gratitude I feel for you; you have been an invaluable guide. Thanks for the countless hours you spent with me, teaching me things that I barely knew they existed, with boundless passion that is out of the common. In our lab I finally experienced what I studied for years, transforming into reality my dream of doing research, not only reading about it. Your capability to create new ideas from a previous one will never stop to fascinate me. Your mentorship went much beyond that. The smile that you carry in your eyes can express thousands of words with a single glimpse. During these months you have been for me an essential and unique guide, you hold my hand during my thesis project and, above all, in my every day life. I was definitely not expecting to meet someone like you, in particular during my university path, in a 5600 miles far from home project. Thank you.

After these too long pages, there is my biggest and most special thanks, to Francesca, my girlfriend. You have been the reason that, more than everything else, kept me going during these years. Thanks to you I arrived to lands where I experienced places, situations, opportunities and people that were more than unique, building in this way wonderful memories that are now the pillars for the future. Thanks for making me love the world so much. You are my flashlight that is able to light up and make shining all I have around, in the very same way a torch does for a scuba diver. He would not be able to enjoy the colors of fishes and corals that are around him; all of them would look vaguely blue, but they aren't. Thank you for being my buddy in this diving, it was incredible; now it's time to fill the scuba tanks for the next ones, I can't wait!

Fabio Righetti
Stanford, CA
November 2014